JOURNAL OF TELECOMMUNICATIONS AND INFORMATION TECHNOLOGY

Preface

The first 2007 issue is constituted of papers dealing with the subject of modern trends in the development of microwave techniques, antenna and satellite technology. The significant cluster of papers covers the field of smart, ring and phased array antennas and their applications and equipment, as well as issues connected with satellites and radars.

The future wireless systems have to be equipped with multiband and wideband smart antennas in order to provide high speed data transmission and avoid undesired interference. The beamforming techniques used in the narrowband systems are unsuitable for wideband counterparts as they cause such adverse effects as main beam squinting and null shifting. The use of the radar adapting wideband beam and null steering methods is unattractive for communication systems because of both, high complexity and the cost of the systems. In order to overcome this obstacle, the fully spatial wideband beam forming techniques can be applied in designing of the wideband smart antennas. In the paper by M. Uthansakul and M. E. Bialkowski, a smart array antenna with the capability of beam steering in azimuth over a wide frequency band using only spatial signal processing, is presented. In this array, only constant real-value weighting coefficients, realized using amplifier or attenuator, are used to form a desired radiation pattern. Another solution to increase the amount of data to be transferred as well as the increase of bit rates is presented in the paper by S. Kozłowski *et al*. The results of simulation of a MIMO system comprising phased array antennas in all receiving branches are shown in this paper. Bit error rate (BER) of two systems using different detection methods was examined in order to determine phased array antennas applicability. It has been shown that using the phase array can significantly improve the communication system performance.

Example of compact planar antenna for multiband system, among others, for WLAN, is presented in the paper by A. Miskiewicz and M. Kitliński. The designed antenna is matched in the bands of HiperLAN1/2 and IEEE 802.11b/g standards. Due to the application of the new feeding technique, it is possible to design and implement antennas which could operate in multi-standard terminals. The paper by M. Hornik *et al.*, presents the results of an optimization into patch antenna elements that would be capable of providing good circular polarization not only in the broadside direction, but also over a wide range of elevation angles. The optimized patches are to be used mostly in space communications, polarimetric measurements and in radio interface of wireless services. The paper by M. Khruslov and V. Pazynin presents the novel coaxial monopole antenna with additional element as a second metal screen. It was found that the different conical radiation patterns can be

formed by variations of both, the distance between these screens and the additional screen dimensions. This kind of antenna can be considered as a promising candidate for various practical applications, e.g., as a single radiator or an array composite element.

Another important area, where modern microwave antennas are used, is the radar technology. Radars can be used in many security applications to detect and track intruders and also in the remote sensing applications to create high resolution images of the Earth, the Moon and other planets' surface. The paper by R. Rytel-Andrianik describes the use of classical continuous wave radar to estimate not only the target position and velocity but also the target acceleration. The paper by B. Dawidowicz and K. Kulpa covers combinely two hot topics: space technology and radar technology. This paper presents the possibility of designing and manufacturing of cheap space-borne synthetic aperture radar for 3D mapping of the Moon surface. The radar was designed for student satellite under SSETI-ESMO project.

The space research and space technology are the subjects of the next few papers. The student's involvement with space technology is described in the paper on SSETI Express satellite misssion by K. Kardach and D. Wydymus. The Express satellite was the first students' satellite ever launched. The satellite was constructed and financed entirely by students groups cooperating in SSETI initiatives. The problem of constructing the cheap satellite is also described in the paper *Technologies for low costs small satellites*. The times when the budget for huge satellites was almost unlimited, are over. Now, it is necessary to work out cheap, but reliable technology for satellite missions, especially if formation flight is a required feature. The formation satellite flights are required for both, optical and microwave interferometer missions, for creating precise 2D and 3D images of the Earth surface and also for deep-space exploration. The problem of the precise controlling over the formation flights is the subject of the paper by R. Wawrzaszek and M. Banaszkiewicz. In order to glimpse the results of satellite experiments, remotely taken images and collect other data it is necessary to construct the radio-links networks covering almost the whole planet. Building the professional radio-station for satellite communication is a difficult, time- and money-consuming task. The paper by M. Stolarski and W. Winiecki presents the concept of cheap radio amateur net for communication with satellites. The final paper in the space field deals with the problem of "proper disposal" of old satellites – which is, their interception. This process is described in the paper *Interception of a free-rotating satellite: an autonomous rendezvous scenario*.

Rapid technological progress in the field of SiGe HBT technology has also found its reflection in the areas of interests of the authors, as it allows to rethink and apply silicon technology also for the millimeter wave applications. With its use, M. Krčmar *et al.* proposed a wideband amplifier achieving more than 10 dB gain over 20–50 GHz band with noise lower than 9 dB and acceptable power consumption. It is the highest gain-bandwidth product ever reported for monolithic SiGe HBT amplifier. Another hot area is still MEMS technologies, which are presented in the first paper providing information on the new type of an RF MEMS capacitors with dual-gap height architecture for continuous tuning with low-resisting loss and a large tuning range at 30 GHz. The paper by A. Shutko *et al.*, covering the subject of remote sensing microwave technology for monitoring and emergency mapping of areas of water seepage and high groundwaters, deserves particular attention. The passive microwave radiometry (PMR) is based on spectral measurements and is the only technology which takes these measurements under the earth's surface. This noteworthy method, proposed by the authors, helps to monitor water seepage and undergrounds waters fast and reliably.

The guest editor would like to take this opportunity and express his thanks to the authors and reviewers who made efforts to delve into various issues of technological interests and presented the results of their research in terms of practical application.

Józef Modelski
Guest Editor

Paper

Performance and operation of stressed dual gap RF MEMS varactors

Greg McFeetors and Michal Okoniewski

Abstract— The design, fabrication and measurement of a continuously tunable RF MEMS capacitor is described. The capacitor's dual gap height architecture allows for electrostatic tuning with low resistive loss and a large tuning range. A new dual tuning scheme is introduced for use with two voltage sources. This dual tuning, coupled with a stress-induced bridge, is used to reach further device tuning. Measurements indicate a continuously tunable capacitance range of 6.2:1 with a quality factor over 50 at 30 GHz for 310 fF.

Keywords— electromechanical systems (MEMS), varactors, capacitors, Q factor.

1. Introduction

Microelectromechanical systems (MEMS) have demonstrated excellent characteristics as microwave circuit components. In particular, switches and capacitors have proven to have excellent radio frequency (RF) specifications due to the low loss and inherent mechanical tunability of MEMS structures [1]. While most MEMS variable capacitors reported have been developed as digitally-switched capacitors, continuously tunable capacitors are often benificial where high tuning range is required. Analog MEMS varactors can possibly offer an integration-friendly, low-loss replacement for diode varactors, however, until recently, MEMS varactors have suffered from poorer tuning range than their diode counterparts.

Quite recently, a number of RF MEMS varactors have been designed and fabricated for use at RF with excellent quality factors at frequencies up to 40 GHz. A summary of recently reported analog MEMS varactors is shown in Table 1, along with the results of this work. As quality factor is dependant on frequency and capacitance, the notable metric columns are tuning range and equivalent series resistance (ESR).

Table 1
High-Q RF MEMS varactor comparison

Device	Frequency [GHz]	Q	Tuning	Value	ESR [Ω]
Dussopt [2]	34	95	1.5:1	80 fF	0.6
Borwick [3]	3	25	8.4:1	1.5 pF	1.42
Chen [4]	5	30	1.7:1	60 fF	17
Dec [5]	1	20	1.87:1	2.05 pF	3
Peroulis [6]	40	80	3:1	168 fF	0.3
This work	30	52	6.2:1	310 fF	0.34

2. Design

Electrostatic actuation of MEMS beams is easily amenable to a tunable parallel plate capacitor design. While both cantilever (single-fixed) and bridge (fixed-fixed) beam designs have been utilized for MEMS capacitors, the bridge design presents higher stable continuous tuning in its simplest form [7] and is used as a basis for this work.

The stable continuous tuning range is limited in all simple electrostatic beam actuator designs. A flat, fixed beam, with force applied at the center can only obtain a continuous tuning range of 1.5:1, or 50%, before pull-in. However, electrode placement can effect the pull-in deflection, both by increasing the "beam stretching" [8] and using "beam leveraging" [9]. This is done by placing the bottom DC electrodes at the ends of the beam, rather than the center. This alteration can increase the deflection at the beam center to beyond 50% of the initial beam height.

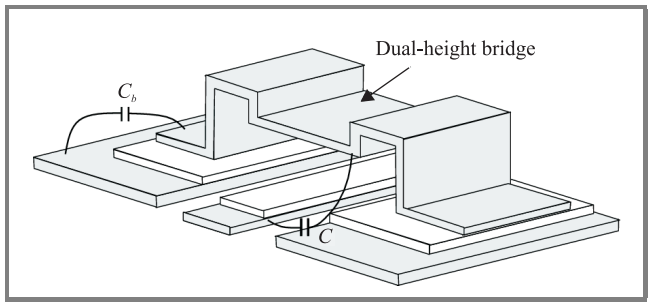

Fig. 1. Planar MEMS bridge geometry isometric view.

A method for greater tuning has been implemented by the authors in [10] using a two-layered bridge with dual gap heights, shown in Fig. 1. This architecture avoids the pull-in limitation by separating the capacitance plate gap (d_c) from the electrostatic electrode gap (d_e), as shown in Fig. 2. Therefore, the pull-in deflection at the electrodes corresponds to a larger deflection ratio at the capacitor. Electrostatic electrodes at the ends of the beam also create the leveraging and stretching effects. However, the tuning of this device is still limited to 4:1 due to the compressive beam stress and beam curvature under deflection, as discussed in Section 3.

This has led to a dual-tuning concept, which removes much of the tuning limitation caused by the beam stress and nonplanarity, and in fact takes advantage of beam stress to increase tuning range. The device, as fabricated, is shown in Fig. 2. This figure also shows the adaptation of this design to a coplanar waveguide shunt-ground configuration variable capacitor. The signal conductor forms the bottom

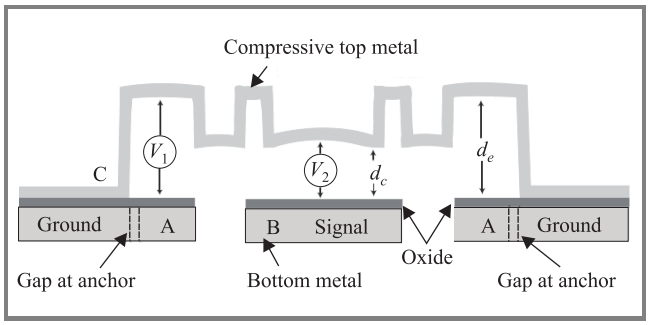

Fig. 2. High tuning dual-height stressed bridge capacitor profile.

plate of the capacitor, while the ground conductors are used as the bottom electrodes for electrostatic actuation.

Actuation is controlled in two stages: the first stage is controlled by applying a DC voltage from electrodes A to C, with a common voltage on B and C to avoid attraction between these electrodes. The second stage then additionally adds potential difference between electrodes B and C to fully tune the device. Chrome silicide resistive lines can be used to connect DC voltages to B and C, as they supply RF isolation. A thin layer of oxide is used to insulate the top and bottom electrodes, as well as create an RF short, C_b, between the large top metal anchors and the bottom ground conductor. The design of the capacitor must ensure that the outer electrode length, oxide height, and bridge gap heights are such that the bridge deflection allows for full tuning and bridge center contact before pull-in. These design details are verified using an electromechanical simulator, as discussed in the following section. Furthermore, this design allows for secondary tuning, as also discussed more fully in Section 3.

As shown in Fig. 2, reliability is increased by introducing a small gap in the bottom A electrode at the bridge anchor. This removes the attractive force at the anchor and decreases the bridge deflection at the anchor corner, preventing the bridge from weakening or failing after repeated cycles.

3. Modeling and simulation

Dynamic 3D modeling of the MEMS device is performed using the commercial software Coventorware. This allows for simulation of the mechanical and electrical properties of MEMS structures based on the stress, load, and electrostatic forces. Based on the device layout and the measured stress of the thin films, the movement of the bridge can be predicted for various actuation voltages. The geometry of the device and the bridge stress has warranted the need for software simulation of the varactor operation, as closed-form equation modeling has proven inaccurate.

Figure 3 shows the bridge geometry and deflections for 0 V, 30 V, 40 V and 50 V cases. For illustrative purposes, the z-dimension has been scaled by a factor of 10. In this figure, conductor A is grounded, while voltage is applied to conductors B and C (with RF isolation between them).

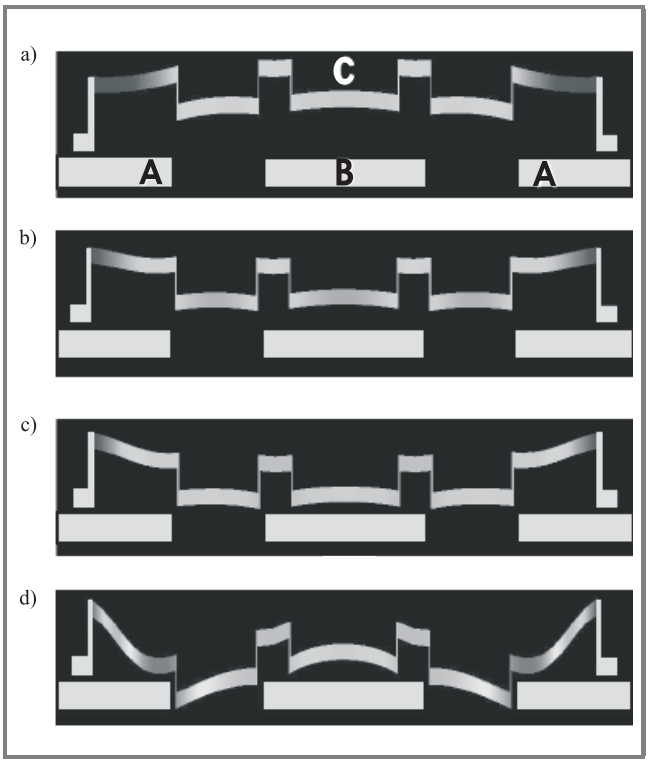

Fig. 3. Stage 1 tuning: (a) $V_{AC} = 0$ V; (b) $V_{AC} = 30$ V; (c) $V_{AC} = 40$ V; (d) $V_{AC} = 50$ V. For all cases $V_{BC} = 0$ V.

The 30 V case shows mid-range tuning of the device. The 40 V case shows the point at which the bridge comes in contact with the oxide layer. Increasing the voltage further causes the bridge to reach pull-in, as seen by the 50 V case. Interestingly, this causes the beam to lift off the bottom center plate in the middle, due to the intrinsic beam stress and the force caused by the outer electrodes, and hence lowers the capacitance.

The primary continuous tuning range of the capacitor in this configuration is exhausted by varying the voltage on the outer electrodes from 0 V to 40 V. The beam curvature due to stress and deflection curls the top electrode to prevent further tuning, as shown in Figs. 3c and 3d. Thus, a new dual-tuning scheme is then introduced by applying

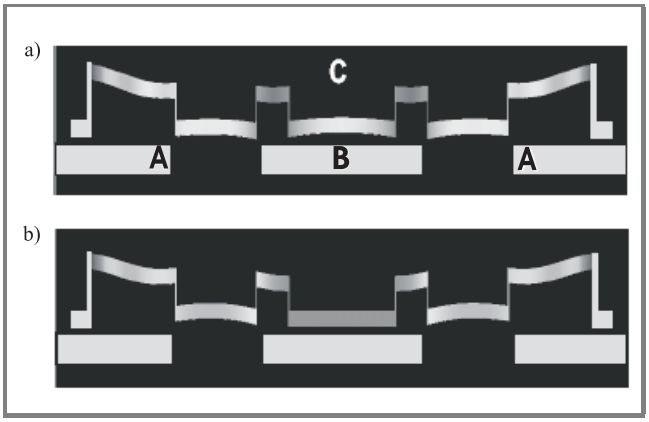

Fig. 4. Stage 2 tuning: (a) $V_{CB} = 10$ V; (b) $V_{CB} = 25$ V. For both cases $V_{AC} = 40$ V.

additional voltage between electrodes B and C, which pulls the bridge into the bottom capacitor plate, shown by Fig. 4. The deformation of the bridge due to the outer electrodes produces a nonlinear spring restoration force, allowing the bridge to be significantly flattened before final pull-in.

This two-stage bridge deflection allows for a large tuning range from a relatively simple capacitor structure. Also note that the tuning range of the first stage can be further increased by enlarging the gap height, d_e, at the consequence of increased actuation voltage.

4. Fabrication

The fabrication process used in this project is a modified custom process previously developed by the authors for the fabrication of MEMS RF phase-shifters [10]. The devices are built on a fused silica substrate using surface micromachining. Copper, with its high bulk conductivity, is ideal for forming base conductors of a CPW layer and is deposited, along with titanium adhesion layers and a gold oxidation barrier, using DC magnetron sputtering. The copper lines are then covered in 300 nm of PECVD oxide that serves two purposes: it insulates the signal conductors from the bridge, thus preventing a short-circuit at full bridge deflection, and creates a dielectric layer for a large capacitance between the ground lines and the bridge anchor (C_b). This oxide must be carefully processed to avoid dielectric breakdown during actuation. Optional $CrSi_2$ resistive lines can then be deposited and patterned, using a sputtering lift-off process.

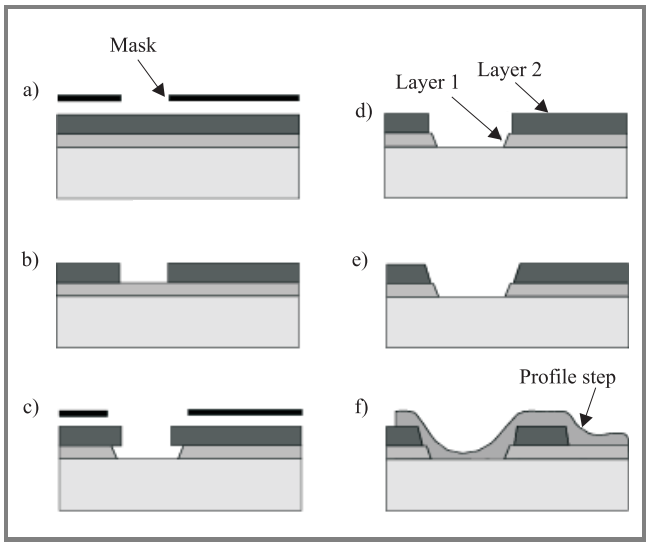

Fig. 5. Dual sacrificial layer height process: (a) expose top resist; (b) develop top resist; (c) develop bottom resist and expose top resist; (d) develop top resist; (e) develop sidewalls of top resist; (f) deposit and pattern metal beam.

The bridge requires micromachining with two consecutive sacrificial layers to obtain two different heights. The resulting bridge has a height of 950 nm over the center electrode and oxide, and 2.5 μm over the side electrodes and oxide. This unique process, as shown in Fig. 5, is critical to obtain varactors with desirable tuning characteristics.

Aluminum is then deposited at low temperature and low stress (< 50 MPa) to form the bridge metal. Figure 6 is an SEM picture of a single gap height bridge, demonstrating the near-planar low compressive stress deposition

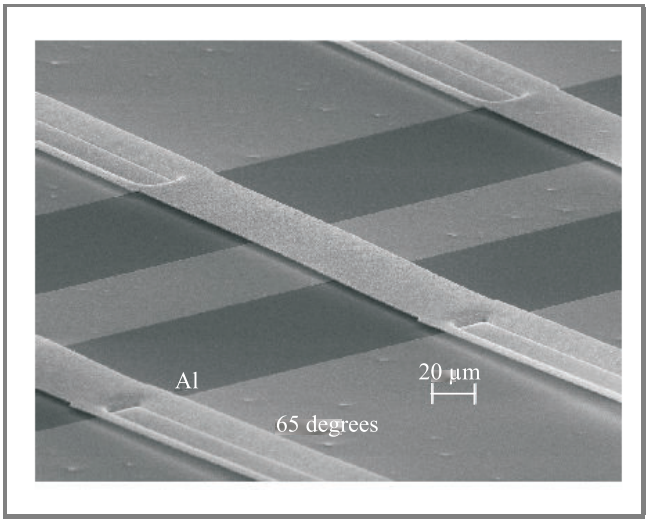

Fig. 6. SEM photograph of planar bridge.

technique. To increase the limits of elastic deformation, molybdenum or copper is alloyed with the aluminum to increase the hardness of the metal, minimizing the bridge damage due to plastic deformations. The stress of this film can then be manipulated by controlling the deposition vacuum and temperature, sputtering power, and post-deposition annealing time and temperature. To complete the device, the bridge is released and the structure is critically dried. The final released structure is shown in Fig. 7.

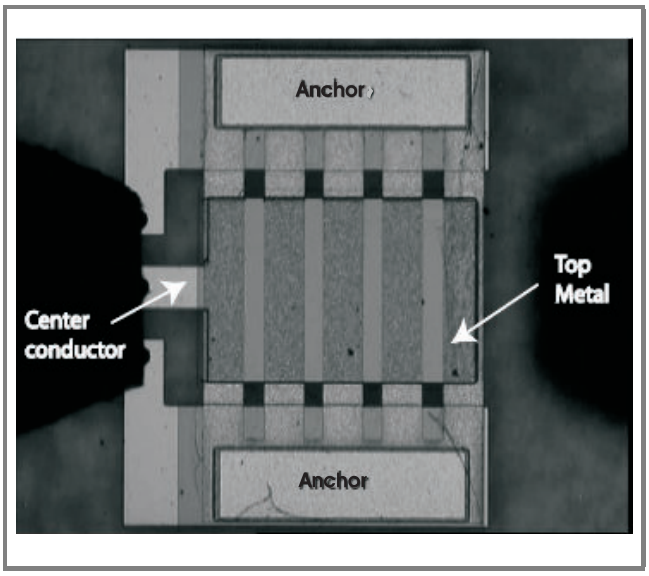

Fig. 7. Optical photograph of fabricated capacitor.

An alternative bridge material using electroplated copper has also been fabricated. Near zero stress is possible us-

ing this deposition method (< 10 MPa tensile), allowing for measurement comparison to the aluminum-molybdenum bridges.

All fabrication work was performed by the authors at the Advanced Microfabrication Integration Facility (AMIF) at the University of Calgary and at the Nanofab facility at the University of Alberta.

5. Measurements

Measurements have been performed using an E8364A Agilent precision network analyzer (PNA) with the capacitors in shunt-ground configuration. Due to the tolerances of this equipment at lower frequencies and small capacitances, Q values approaching and greater than 100 cannot be determined with sufficient accuracy. The result of the measurements of the capacitance versus tuning voltage is shown in Fig. 8. The capacitance at 0 V is 310 fF, while 45 V gives 1.4 pF. Utilization of the second tuning stage increases the capacitance to 1.93 pF by changing voltage B by 25 V, to either 20 V or 70 V.

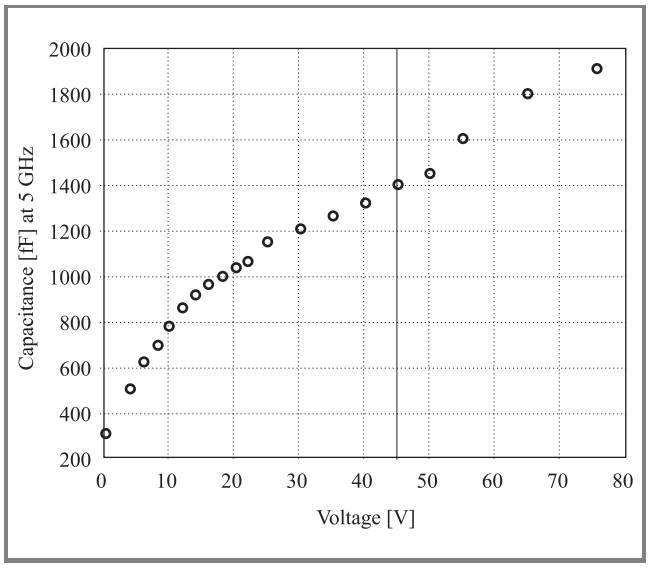

Fig. 8. Capacitance versus voltage with two tuning stages.

This shows a 4.5:1 tuning range using the 1st tuning stage, and 6.2:1 total continuous and repeatable tuning range. The 0 V case gives C = 310 fF and Q = 50 and the 45 V case gives C = 1.4 pF and Q = 10.6 at 30 GHz. This corresponds to ESR = 0.34 Ω at 30 GHz for 0 V, and 0.36 Ω at a 45 V deflection potential.

This two-stage tuning demonstrates an additional 37% device capacitance tuning in the second tuning stage. To demonstrate the dependence on bridge compressive stress, these measurements were compared to near zero-stress bridges of electroplated copper. The electroplated copper devices showed similar tuning in the first stage, however, only an additional 7% tuning could be achieved in the second tuning stage.

6. Conclusion

The successful design and custom fabrication of a high tuning RF MEMS varactor utilizing a relatively simple structure has been described. Simulations have also been presented to explain the mechanical properties of the device. Measurements of this device indicate a quality factor of 50 at 30 GHz, with an ESR below 0.4 Ω and large continuous analog tuning range of 6.2:1 (Fig. 9). To our knowledge, this demonstrates the largest tuning range of any sub-1 Ω ESR varactor reported to date.

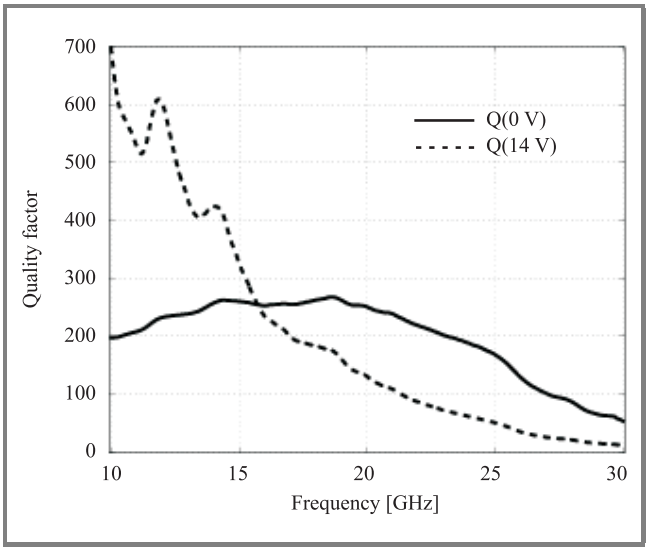

Fig. 9. Q-factor measurements.

This varactor may be useful in any application where a low loss, large tuning varactor is required. Especially where large resolution tuning is required, analog MEMS varactors may be preferable to digitally switched MEMS variable capacitors, as digital capacitor network can quickly become large and lossy when high capacitance resolution is required. Specifically, this varactor is suitable for applications such as voltage controlled oscillators, phase shifters [10], phased array and tunable reflect-array antennas [11], and high-Q filters.

Acknowledgment

The authors wish to acknowledge the assistance and support of the National Science and Engineering Research Council of Canada, the Alberta Ingenuity Fund and TR-Labs Calgary.

References

[1] S. Lucyszyn, "Review of radio frequency microelectromechanical systems technology", *IEE Proc. Sci. Meas. Technol.*, vol. 151, no. 2, pp. 93–103, 2004.

[2] L. Dussopt and G. Rebeiz, "High-Q millimeter-wave MEMS varactors: extended tuning range and discrete-position designs", in *IEEE MTT-S Int. Microw. Symp. Dig.*, Seattle, USA, 2002, pp. 1205–1208.

[3] R. L. Borwick *et al*., "A high Q large tuning range MEMS capacitor for RF filter systems", *Sens. Actuat. A: Phys.*, vol. 103, no. 1, pp. 33–41, 2003.

[4] J. Chen *et al*., "Design and modeling of a micromachined high-Q tunable capacitor with large tuning range and a vertical planar spiral inductor", *IEEE Trans. Electron Dev.*, vol. 30, no. 3, pp. 730–739, 2003.

[5] A. Dec and K. Suyama, "Micromachined varactors with wide tuning range", *IEEE Trans. Microw. Theory Techn.*, vol. 46, pp. 2587–2596, 1998.

[6] D. Peroulis, S. Mohammadi, and L. P. B. Katehi, "Electrostatically-tunable analog RF MEMS varactors with measured capacitance range of 300%", in *IEEE MTT-S Int. Microw. Symp. Dig.*, Philadelphia, USA, 2003, vol. 3, pp. 1793–1796.

[7] G. M. Rebeiz, *RF MEMS Theory, Design, and Technology*. Hoboken: Wiley, 2003.

[8] E. K. Chan *et al*., "Design and fabrication of a novel two-dimension MEMS-based tunable capacitor", *IEEE Int. Conf. Commun., Circ. Syst.*, Chengdu, China, 2002, vol. 2, pp. 1766–1769.

[9] E. S. Hung and S. D. Senturia, "Extending the travel range of analog-tuned electrostatic actuators", *J. Micromech. Syst.*, vol. 8, no. 8, pp. 497–505, 1999.

[10] G. McFeetors and M. Okoniewski, "Distributed MEMS analog phase shifter with enhanced tuning", *IEEE Microw. Wirel. Compon. Lett.*, vol. 16, no. 1, pp. 34–36, 2006.

[11] S. V. Hum, G. McFeetors, and M. Okoniewski, "Integrated MEMS reflectarray elements", in *1st Eur. Conf. Anten. Propagat.*, Nice, France, 2006.

Greg McFeetors received the B.Sc. degree from the University of Manitoba and the M.Sc. degree from the University of Calgary in 2000 and 2004, respectively. He is currently a Ph.D. student at the University of Calgary. His current research interests lie in RF MEMS systems design, fabrication, and applications, including varactors, inductors, antenna systems, filters, and various applications of MEMS into communications circuits. He is also affiliated with TR-Labs Calgary.

e-mail: geomcfee@ucalgary.ca
Department of Electrical and Computer Engineering
University of Calgary
2500 University Drive N.W.
Calgary, Alberta, T2J 1K5, Canada

Michal Okoniewski is a Professor and Canada Research Chair with the Department of Electrical and Computer Engineering, University of Calgary. He is also affiliated with TR-Labs Calgary. Doctor Okoniewski received the M.Sc. and Ph.D. degrees from the Gdańsk University of Technology, Poland. He is a Senior Member of IEEE, Associate Editor for "IEEE Transactions on Antennas and Propagation" and member of IEEE Standard Groups. Doctor Okoniewski is interested in many aspects of applied electromagnetics, ranging from computational electrodynamics, to reflectarrays and self configuring antennas, RF MEMS, and re-configurable computational hardware for electromagnetics applications. He is also actively involved in bio-electromagnetics, where he works on tissue spectroscopy and cancer detection.

e-mail: michal@enel.ucalgary.ca
Department of Electrical and Computer Engineering
University of Calgary
2500 University Drive N.W.
Calgary, Alberta, T2J 1K5, Canada

Paper

SiGe HBT wideband amplifier for millimeter wave applications

Marko Krčmar, Nils Noether, and Georg Boeck

Abstract— A wideband amplifier up to 50 GHz has been implemented in a 0.25 μm, 200 GHz f_t SiGe BiCMOS technology. Die size was 0.7×0.73 mm^2. The two-stage design achieves more than 11 dB gain over the whole 20 to 50 GHz band. Gain maximum was 14.2 dB at 47.5 GHz. Noise figure was lower than 9 dB up to 34 GHz and a current of 30 mA was drawn from a 4 V supply. To the author's best knowledge this is the highest gain bandwidth product of a monolithic SiGe HBT amplifier ever reported.

Keywords— wideband amplifier, HBT, SiGe, millimeter wave, bipolar integrated circuits.

1. Introduction

Up to now compound semiconductors dominate the applications in the millimeter wave range. Rapid technological progress in the field of SiGe HBT technology [1] allows to re-think and to apply silicon technologies also for millimeter wave applications. The SiGe BiCMOS technologies allow integration of analog and digital parts, provide high integration densities and save cost. The main purpose of this work is the demonstration of the millimeter wave capabilities of SiGe BiCMOS technologies. A broadband amplifier has been chosen for this reason. The main goal was a gain greater than 10 dB up to 50 GHz and a bandwidth as high as possible. Compared with narrow band designs, the difficulties grow up significantly because of broadband matching circuits and the lossy silicon substrate decreases the overall performance. Because of these reasons only less comparable work has been published so far. To our knowledge SiGe HBT wideband amplifiers have been published just in [2] (bandwidth = 10 GHz) and [3] (1–15 GHz).

2. Device technology

The circuit was fabricated in a commercially available SiGe BiCMOS technology with $f_t = f_{\max} = 200$ GHz [4, 5].

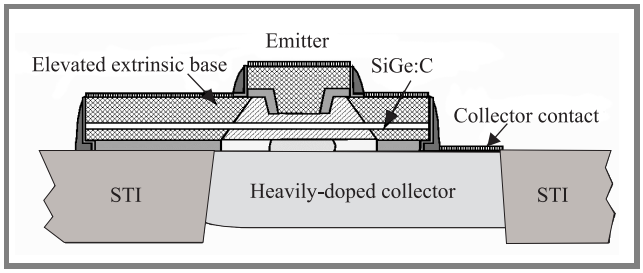

Fig. 1. Schematic cross section of an HBT with elevated extrinsic base.

The HBTs were designed for high performance at low cost. The cross section of the structure is illustrated in Fig. 1. Key features of the device technology are:

- elevated extrinsic base regions self-aligned to the emitter window resulting in low base resistance;
- formation of the whole HBT structure in one active area without shallow trench isolation between emitter and collector contact resulting in low collector resistance and small collector-substrate junction areas;
- device isolation without deep trenches resulting in reduced process complexity and improved heat dissipation.

The HBT module was fabricated in a BiCMOS process after gate patterning and gate spacer formation. During HBT fabrication, CMOS regions are protected with a layer stack that is opened over HBT regions. The HBT fabrication begins with the formation of the collector wells by high-dose ion implantation. The collector wells are laterally confined by shallow trench regions. Next, the active collector region is defined by depositing and patterning on oxide layer. A Si buffer layer, the SiGe:C base layer, and a Si cap layer are grown in one epitaxial step. After epitaxy, a sacrificial layer is deposited, and emitter windows are structured. An additional inside spacer is formed before depositing and structuring the As-doped emitter. Next, spacers are formed at the emitter and the sacrificial layer is removed by wet etching, followed by the self-aligned selective growth of the B-doped extrinsic base. In a reference process without the elevated base, the extrinsic base is formed by ion implantation after emitter structuring as described in [4]. This HBT structure provides low-capacitance isolation from the substrate and low collector resistances.

3. Circuit design

Figure 2 shows the two-stage amplifier, implemented with two cascode stages [6, 7]. Among different architectures this topology has been found to be the best trade-off with respect to gain and bandwidth. The first stage was implemented with the goal of best noise performances. The second one was designed for maximum power gain. Both cascode stages are biased with $V_{CC} = 4$ V and $I_C = 10$ mA and 20 mA, respectively.

Figure 3 shows a photograph of the realized chip. Input/output signal pads are on the left and right side, re-

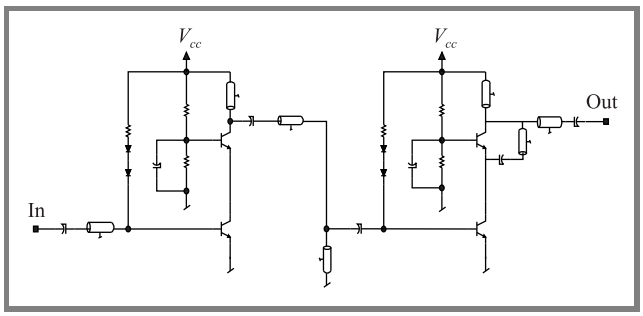

Fig. 2. Simplified schematic of the wideband amplifier.

spectively. The pad structure has been designed for standard GSG on-wafer probing. The three top pads provide the biasing for the whole amplifier in a ground-V_{CC}-ground structure. The identical structure at the bottom side allows the monitoring of the bias voltage. All DC-lines are RF-shorted to ground wherever possible, in order to provide a low ohmic ground for RF-signals. For example, the relatively wide microstrip line in the middle of the chip is a short circuited stub.

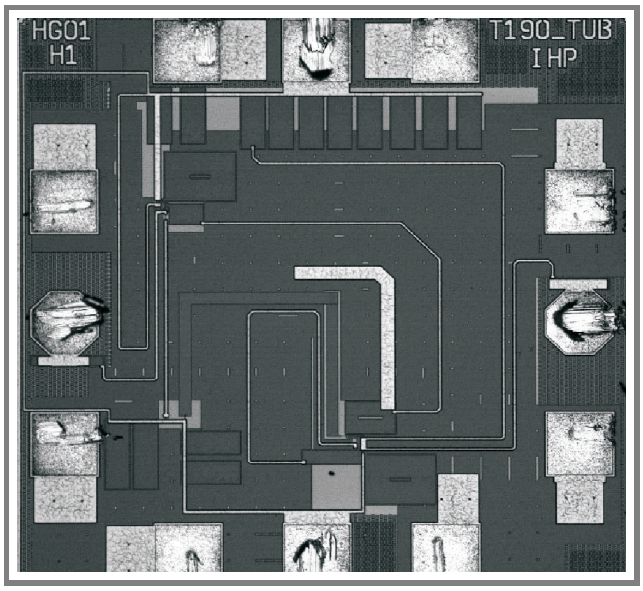

Fig. 3. The photograph of the realized chip.

Because the input impedance of a bipolar transistor shows a dominant real part with week frequency dependence a simple microstrip line was adequate to achieve acceptable 50 Ω-input matching over 20–50 GHz. On the contrary, the output impedance of a bipolar transistor is strongly capacitive and broadband matching is complicated. The solution for this problem was a compensation microstrip line connected in parallel to the output transistor (see Fig. 2). It works as a resonator with a low Q factor and a high bandwidth, neutralizing the parasitic capacitances of the transistor and allowing us to achieve a satisfying 50 Ω-output matching in the 20–50 GHz band. This compensation line not only allows for wideband output matching, but also improves the stability of the amplifier at higher frequencies. A short circuited stub was introduced between the two stages in order to tune the gain flatness, because at the beginning of the design process the gain at the low frequency end of the band was significantly higher. Theoretically this stub is an open circuit for $30 < f < 50$ GHz. Besides of decreasing the gain below 20 GHz we automatically reduced also the risk of instabilities at low frequencies. Once again, microstrip lines were used instead of inductors [8], which were not available, for DC-RF-decoupling. All microstrip lines were realized on the same metal level in order to avoid the coupling between the lines as much as possible [8]. We chose hexagon-shaped signal pads in order to reduce the capacitive coupling between pads and substrate. The die size is 0.7×0.73 mm^2. For the biasing of the cascode transistors a fixed potential provided by a simple voltage divider has been used whereas the common emitter transistors were fed by a diode/resistor combination providing a constant base current. This solution saves chip size and provides at the same time satisfying temperature stability, too.

Wherever possible, the first metal plane, used as ground, was connected with the substrate by p-taps.

Thus, substrate coupling effects are effectively suppressed. This p-taps behave like low ohmic conductors at high frequencies. RF losses are minimized by this way.

4. Results

Seven chips have been characterized from the first wafer run so far with respect to its RF performance. Power supply values and ambient temperature were in all cases 4 V, 30 mA and 25°C, respectively. Figure 4 shows the S_{21} graphs of the ensemble of 7 dies. Besides of one curve we can conclude to a remarkable uniformity and reliability of the semiconductor process technology.

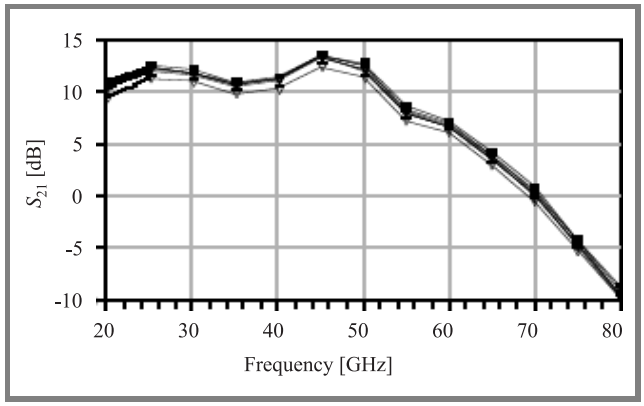

Fig. 4. Measured S_{21} of seven chips ($V_{CC} = 4$ V).

Figures 5a to 5c represent both, measured (squares) and simulated S-parameters. The maximum measured S_{21} achieved is 14.2 dB at 47.5 GHz and more than 11 dB were measured between 20 and 50 GHz (Fig. 5a). Gain flatness

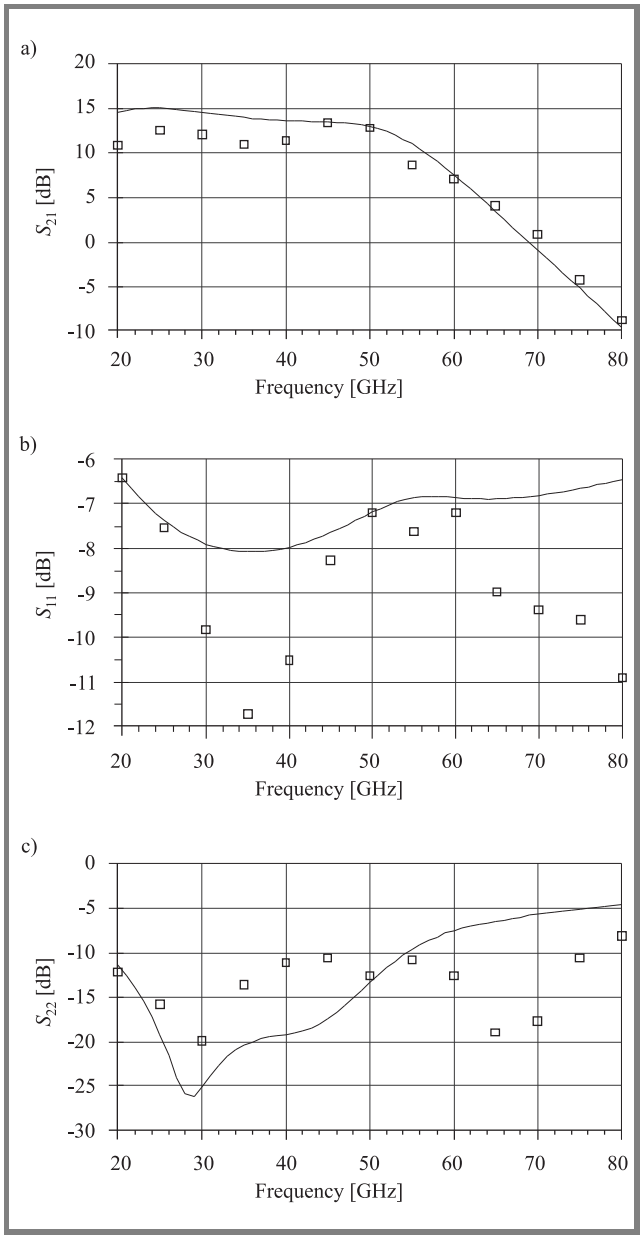

Fig. 5. Simulated and measured: (a) power gain ($V_{CC} = 4$ V); (b) input return loss; (c) output return loss.

within the whole frequency band is about ± 1.6 dB. At the same time, the reverse isolation (not shown) is more than 40 dB from 20–50 GHz. Measured input (Fig. 5b) and output (Fig. 5c) return losses are lower than 6.5 dB and 10 dB, respectively, from 20 to 50 GHz.

4.1. Noise

Noise behavior was measured between 30 and 34 GHz. The band limitation was given by the measurement equipment. Table 1 shows the results. From simulations a *NF* of at least 1 dB lower was expected at these frequencies. According to our simulations best noise values should occur between 40 and 50 GHz in correlation with gain maximum. In that range we expect experimental *NF* values in the order of 7 to 7.5 dB corresponding to simulation results of about 6 dB.

Table 1
Measured noise figure

Frequency [GHz]	*NF* [dB]
30	8.9
31	8.8
33	9.0
34	8.7

4.2. Gain compression

Gain compression was measured and biasing was $V_{CC} = 4$ V and $I_C = 10$ mA and 20 mA, again. The measurements were performed at 47.5 GHz, and an input 1 dB compression point of –10 dBm (Fig. 6) was found corresponding to +3 dBm at the output. This value is slightly higher as predicted by the simulations.

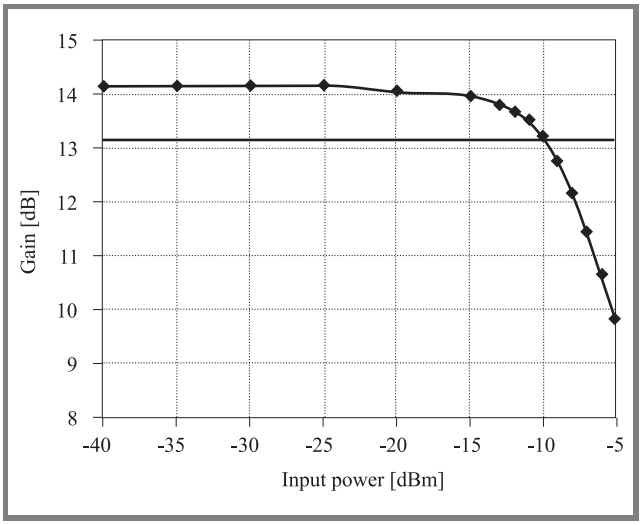

Fig. 6. Gain compression at 47.5 GHz.

The observed discrepancies between measured and simulated results are mainly due to not sufficiently adequate models for the used passive structures in a silicon environment in the millimeter wave region. Verification work at some microstrip discontinuities, transmission lines, vias and substrate coupling effects based on 3D EM simulations showed us considerable discrepancies with circuit simulator based results.
To overcome these problems we are working towards experimental investigation of a passive element library. Based on the characterization of these structures we will establish

a design library containing the models of all passive elements. Using this library we will then re-design the whole amplifier with respect to enhanced performance. Especially with respect to gain, noise and bandwidth we expect considerable improvements.

5. Conclusion

In this work a monolithic wideband amplifier using a SiGe HBT technology has been presented. The chip has been realized on a very low silicon area of 0.7×0.73 mm^2. The main design goals, high bandwidth, more than 10 dB gain within this band and acceptable noise figure and power consumption have been achieved. To the best knowledge of the authors this is the highest gain-bandwidth product ever reported for a monolithic SiGe HBT amplifier. A comparison with state of the art work is given in Table 2.

Table 2
Comparison of state of the art work

Parameter	This work	3–10 GHz LNA [9]
3 dB-frequency range	20–50 GHz	3.1–17.6 GHz
Max. gain	14.2 dB @ 47.5 GHz	22 dB @ 10 GHz
NF	ca. 8 dB	2.7–3.9 dB

Nevertheless, the achieved performance should be improvable if more reliable models for the passive elements are available for the design process. In this case we expect a considerable performance enhancement especially with respect to gain, noise and bandwidth. In case of low power applications the power consumption should be considerably reducible, too.

Acknowledgment

We would like to thank Dr. P. Heymann from Ferdinand-Braun-Institut Berlin for valuable discussions and support concerning the noise measurements.

References

[1] J. D. Cressler, "SiGe HBT technology: a new contender for Si-based RF and microwave circuit applications", *IEEE Trans. Microw. Theory Techn.*, vol. 46, issue 5, pp. 572–589, 1998.

[2] L. Jongsoo and J. D. Cressler, "A 3–10 GHz SiGe resistive feedback low noise amplifier for UWB applications", in *Symp. Radio Freq. Integr. Circ. RFIC*, Long Beach, USA, 2005, pp. 545–548.

[3] H. Knapp, D. Zoschg, T. Meister, K. Aufinger, S. Boguth, and L. Treitinger, "15 GHz wideband amplifier with 2.8 dB noise figure in SiGe bipolar technology", in *Symp. Radio Freq. Integr. Circ. RFIC*, Phoenix, USA, 2001, pp. 287–290.

[4] B. Heinemann *et al.*, "Novel collector design for high-speed SiGe:C HBTs", in *IEEE Int. Electron Dev. Meet. IEDM*, San Francisco, USA, 2002, p. 775.

[5] H. Rücker *et al.*, "SiGe:C BiCMOS technology with 3.6 ps gate delay", in *IEEE Int. Electron Dev. Meet. IEDM*, Washington, USA, 2003, p. 121.

[6] M. Gordon and S. P. Voinigescu, "An inductor-based 52-GHz 0.18 μm SiGe HBT cascode LNA with 22 dB gain", in *Solid-State Circ. Conf. ESSCIRC*, Leuven, Belgium, 2004, pp. 287–290.

[7] Q. Liang, G. Niu, J. D. Cressler, S. Taylor, and D. L. Harame, "Geometry and bias current optimization for SiGe HBT cascode low-noise amplifiers", in *IEEE MTT-S Int. Microw. Symp. Dig.*, Seattle, USA, 2002, vol. 1, pp. 517–520.

[8] G. E. Ponchak, E .M. Tentzeris, and J. Papapolymerou, "Coupling between microstrip lines embedded in polyimide layers for 3D-MMICs on Si", in *IEE Proc. Microw. Anten. Propagat.*, vol. 150, issue 5, pp. 344–350, 2003.

[9] N. Shiramizu, T. Masuda, M. Tanabe, and K. Washio, "A 3–10 GHz bandwidth low-noise and low-power amplifier for full-band UWB communications in 0.25-pm SiGe BiCMOS technology", in *Symp. Radio Freq. Integr. Circ. RFIC*, Long Beach, USA, 2005, pp. 39–42.

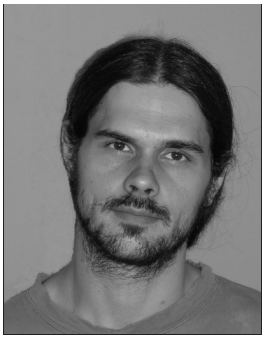

Marko Krčmar was born in Sarajevo, Bosnia Herzegovina, in 1981. He received the B.Sc. and M.Sc. degree from the Politecnico di Milano, Italy, in 2003 and 2005, respectively. During his thesis work he studied SiGe HBT's behavioural at very high frequencies. He is currently pursuing the Ph.D. degree at Technische Universität Berlin, Germany. His main research interests are in the field of wireless frontend and local positioning.
e-mail: krcmar@mwt.ee.tu-berlin.de
Technische Universität Berlin
Microwave Engineering Lab
Sekr. HFT 5-1, Einsteinufer 25
10587 Berlin, Germany

Nils Noether was born in Berlin, Germany, in 1978. He has studied electrical engineering at Technische Universität Berlin with focus on microwave technology and photonics and received his Dipl.-Ing. degree in 2006. Currently he is with the Federal Institute for Materials Research and Testing (BAM), working towards the Ph.D. degree. His field of research is in fibre optic sensors for structural monitoring.
e-mail: nils.noether@bam.de
Technische Universität Berlin
Microwave Engineering Lab
Sekr. HFT 5-1, Einsteinufer 25
10587 Berlin, Germany

Georg Boeck received the Dr.-Ing, degree in electrical engineering from the Technische Universität Berlin, Germany, in 1984. In 1984, he joined the Siemens Research Labs in Munich, Germany, where his research areas were fiber optics and GaAs electronics. Since 1991, he has been the Chair of the Microwave Engineering Lab at the Technische Universität Berlin. His main areas of research are characterization, modeling and design of microwave semiconductor devices, MICs, and MMICs up to the 100 GHz regime. His special interest during the last years has been the development of RF-CMOS integrated circuits for wireless communications. Professor Boeck is a worldwide IEEE Distinguished Microwave Lecturer for the years 2006–2008 in the field of "Design of RF CMOS Integrated Circuits".

e-mail: boeck@tu-berlin.de
Technische Universität Berlin
Microwave Engineering Lab
Sekr. HFT 5-1, Einsteinufer 25
10587 Berlin, Germany

Paper

A wideband smart antenna employing spatial signal processing

Monthippa Uthansakul and Marek E. Bialkowski

Abstract— A smart antenna with capability of beam steering in azimuth over a wide frequency band using only spatial signal processing is presented. Filters and tapped-delay networks employed in conventional wideband linear arrays are avoided by using a two-dimensional rectangular array structure. In this array, only constant real-valued weighting coefficients, realized with amplifiers or attenuators, are used to form a desired radiation pattern. In order to estimate direction of arrival of a wideband signal, the MUSIC algorithm in conjunction with an interpolated array technique is applied. In the interpolated array technique, a composite covariance matrix is generated, which is a simple addition of covariance matrices of narrowband virtual arrays, being stretched or compressed versions of a nominal array. A working prototype of this wideband array is presented. Its operation is assessed via full EM simulations and measurements.

Keywords— direction estimation, null steering, wideband beamforming, wideband smart antenna, wideband antenna.

1. Introduction

It has been recently envisaged that in order to meet high speed data transmission while avoiding undesired interference, future wireless systems have to utilize wideband smart antennas [1].

Until to date, most of the works on smart antennas have concerned narrow band communication systems that are characterized by a fractional bandwidth in the order of one to a few percents. The beamforming techniques used in these narrowband systems are unsuitable for wideband counterparts because they cause such adverse effects as main beam squinting and null shifting [2]. In turn, adapting wideband beam and null steering used in radar are unattractive to communication systems because of the use of a large number of filters or tapped delay networks [2, 3] which add to complexity and cost of the system. In order to overcome this hurdle fully spatial wideband beam forming techniques have been suggested for use in wideband smart antennas.

In the present paper, we design and develop a wideband smart antenna employing only spatial signal processing. The working principle of this array antenna has been introduced in [4]. It has been demonstrated by assuming a large number of antenna elements all in the form of point sources. The use of large number of elements was required for the proper functioning of beam steering algorithm, which involved an inverse district Fourier transform (IDFT) applied to an assumed radiation pattern. The effect of mutual coupling on performance of this wideband beamformer has not been considered. Another issue, which has not been addressed in [4], concerns direction of arrival (DOA) estimation of a wideband signal.

The present paper covers the above shortfalls and provides the following new contributions. It describes a refinement to the beam and null steering algorithm making it valid for small and large size wideband arrays. The modified algorithm neglects mutual coupling effects in the array, similarly as in the original algorithm [4]. However, its impact is assessed by performing full EM simulations and measurements on the array with real antenna elements. In order to overcome problems associated with increased sidelobe levels due to mutual coupling the following remedy is recommended. Using the modified beamforming algorithm (which neglects mutual coupling) an array with low sidelobes is initially designed. As a result of this strategy, when the mutual coupling is present the sidelobe level becomes acceptable. In order to obtain a DOA estimation algorithm which preserves spatial signal processing, an interpolated array technique initially demonstrated for a one-dimensional wideband linear array in [5] and [6], is adapted.

2. Design

2.1. Configuration

The configuration of a wideband smart antenna that employs a fully spatial signal processing for beam and null steering in the azimuth direction is shown in Fig. 1. It is constituted by $N_1 \times N_2$ wideband antennas arranged in a rectangular lattice. Amplifiers or attenuators connected to individual array elements produce weighting coefficients. The signal is combined by a summing network. In Fig. 1, d_1 and d_2 represent array spacing in two orthogonal directions and are usually chosen as half-wavelength at the highest frequency of a given frequency band of operation. Antenna elements are denoted by indices m_1 and m_2, where $-M_1 \leq m_1 \leq M_1$ and $-M_2 \leq m_2 \leq M_2$. The relation between N and M is $M_i = (N_i - 1)/2$. The purpose of using a 2D instead of 1D array is explained as follows. As the signal is assumed to arrive from the direction not perpendicular to the array's plane, the array's elements receive the signal's replicas with different phases. This results in a set of signals, which can be used for processing both in frequency and angular domains. If a 1D array is used, filters or tap-delay networks are necessary to process a wideband signal in these two domains.

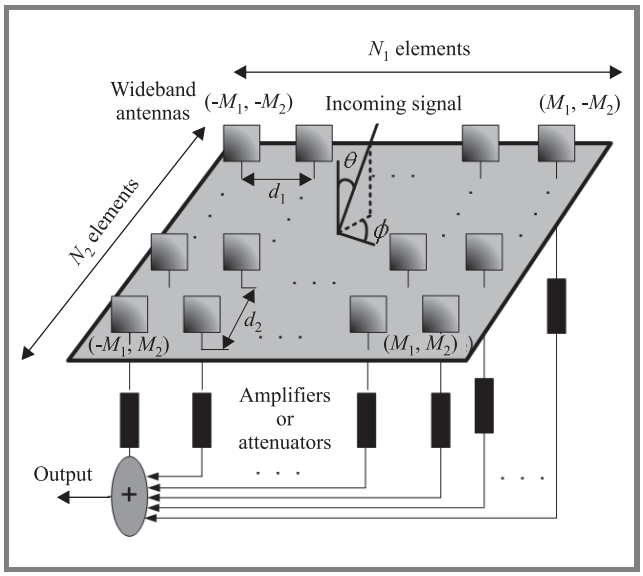

Fig. 1. Configuration of wideband beamformer constituted by wideband antenna elements arranged in a rectangular lattice followed by amplifiers/attenuators and a summing network.

2.2. Beamforming algorithm

Assuming that the signal arrives from azimuth ($\theta \sim 90^\circ$), which is the usual case in mobile communication, the radiation pattern of the array being the function of angle and frequency is given by

$$H(f,\phi) = G_a(f,\phi) \sum_{m_1=-M_1}^{M_1} \sum_{m_2=-M_2}^{M_2} W_{m_1 m_2} \mathrm{e}^{-\mathrm{j}(\frac{2\pi f}{c})(d_1 m_1 \sin\phi + d_2 m_2 \cos\phi)}, \quad (1)$$

where f is the frequency variable, c is the speed of signal and $G_a(f,\phi)$ stands for the frequency-angle dependent gain of each antenna element.

This formula neglects mutual coupling effects in the array and assumes that individual elements feature identical radiation pattern. In order to determine the weighting coefficients $W_{m_1 m_2}$ in Eq. (1) a modified IDFT is applied to H as shown in formula (2):

$$W_{m_1 m_2} = \left(\frac{1}{N_{u_1} N_{u_2}}\right) \left\{ \frac{\sum_{u_1=-0.5}^{0.5} \sum_{u_2=-0.5}^{0.5} H(u_1,u_2)}{G(u_1,u_2)\mathrm{e}^{-\mathrm{j}2\pi u_1 m_1} \mathrm{e}^{-\mathrm{j}2\pi u_2 m_2}} \right\}, \quad (2)$$

where u_1 and u_2 are defined by $(f d_1/c)\sin\phi$ and $(f d_2/c)\cos\phi$, respectively. The modification concerns the numbers of sampling points N_{u_1} and N_{u_2} in $u_1 - u_2$ plane. In [4], $N_{u_1} = N_1$ and $N_{u_2} = N_2$ were used. The d_1 and d_2 are element spacing in two directions of the array.

According to our investigations, this assumption leads to insufficient constraints on the weights when a small number of elements form the array. As a result, a radiation pattern significantly deviating from the assumed one is produced. The use of $N_{u_1} = 2N_1$ and $Nu_2 = 2N_2$ eliminates this problem. This number of sampling points is used in our modified beamforming algorithm. Note that in calculating the weighting coefficients in formula (2), the given frequency bandwidth is slightly larger than the one over which the smart antenna has to operate [4]. The reason is to avoid the edge effect when implementing IDFT technique.

2.3. Null steering

The null steering task is similar to the beam forming task and is related to devising a radiation pattern featuring a main beam accompanied by nulls. For small size arrays, only the task of producing a single null is usually considered. In the proposed approach a simple step linear function, which assumes a main beam being directed to a desired signal direction and a null in interference direction, is used to generate the desired radiation pattern H in $u_1 - u_2$ plane. Having assumed H, the signal weighting coefficients are obtained using formula (2).

2.4. Direction of arrival estimation

Forming the beam towards the desired user and nulls towards interfering signals relies on the assumption that DOA of desired signal, as well as of interfering signals, is known to the system. This task is accomplished using a DOA estimation method. Unfortunately, many of them [7] are not suitable for the wideband array antenna, which is investigated here. This is because the DOA estimation method of wideband signals has to be accomplished using only spatial signal processing. Here, we adapt the solution in [5] and [6] that concerns one-dimensional (1D) wideband arrays. In this method, a wide frequency band is divided into multiple narrow bands with center frequencies $\{f_i\}$. In each band the signal is assumed to be received by a virtual array, which is "stretched" or "compressed" version of nominal array. The stretch/compress factor is such that all of the virtual arrays have the same radiation pattern (response). Because the virtual arrays have the same response (at their operating frequencies) it is possible to combine the covariance matrices for the different frequencies by simple addition. The outputs from virtual arrays are obtained via interpolation technique from the real one-dimensional array. The interpolation coefficients are selected so as to minimize the interpolation error for a signal arriving from a given sector (a range of bearing angles), at a particular frequency. The size of the sector has to be chosen to give good estimates of the virtual array outputs. The design of interpolator is done once and off-line. For the 2D array investigated here, the steering vector is defined in Eq. (3):

$$\mathbf{A}(\omega_i) = \left[\mathbf{a}(\omega_i,\phi_1)\ \mathbf{a}(\omega_i,\phi_2)\ \ldots\ \mathbf{a}(\omega_i,\phi_K)\right], \quad (3)$$

where

$$\mathbf{a}(\omega_i,\phi_k) = \left[\mathbf{a}_{-M_2}(\omega_i,\phi_k)\ \ldots\ \mathbf{a}_{M_2}(\omega_i,\phi_k)\right]^T \quad (4)$$

and

$$\mathbf{a}_{m_2}(\omega_i,\phi_k) = \left[\mathrm{e}^{\mathrm{j}\phi_k(-M_1,m_2)}\ \ldots\ \mathrm{e}^{\mathrm{j}\phi k(M_1,m_2)}\right]^T, \quad (5)$$

and k is the number of a radiating source in azimuth.

Having obtained (via the virtue of an interpolated array technique), the transformation of the problem of DOA estimation of a wideband signal into DOA estimation of narrowband signal, the application of narrowband MUSIC algorithm is straightforward. The detailed steps of this algorithm are shown in [7] and thus are not repeated here.

3. Results

3.1. Prototype development

In order to demonstrate the validity of the described concept of wideband array antenna, a 4×4-element prototype for operation in the band from 1.9 to 2.5 GHz is developed. The photograph of the full prototype is shown in Fig. 2. In order to meet wideband performance and tight array spacing, the array uses a square planar monopole as its element.

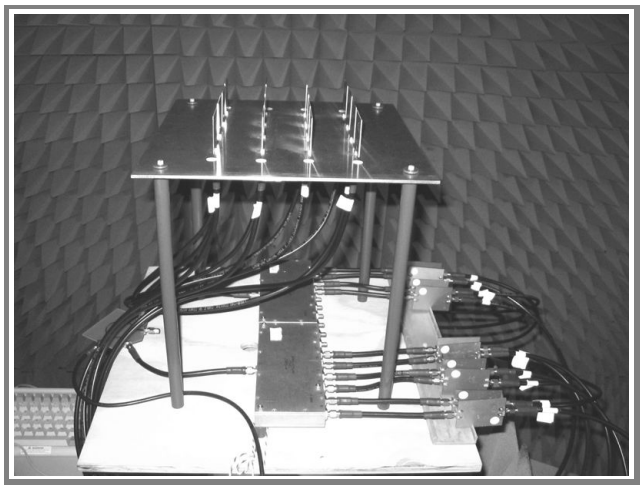

Fig. 2. Photograph of a 4×4 wideband array antenna with planar monopoles, two 1:8 dividers, attenuators and a rat-race hybrid.

This antenna element is designed using full EM analysis software based on the method of moments, FEKO® [8]. The 40-millimeter side size square planar monopole located 3 mm above the ground plane offers the 10 dB return loss bandwidth from 1.4 to 3.2 GHz, as proved by full EM simulations and measurements. The size of this antenna element meets half-wavelength spacing of $d_1 = d_2 = 5$ cm at 3 GHz. The feeding network uses two 1:8 power dividers, a rate race hybrid (to obtain signals of positive and negative amplitudes) and microstrip attenuators. The attenuators and the rat race hybrid are designed with the use of Agilent ADS® [9]. As the array is square in shape DOA and beam forming capabilities need to be checked only over the range of -45° to $+45^\circ$ angular sector. This is because the remaining ranges within the full sector of -180° and $+180^\circ$ are covered with respect to the other sides of the array.

3.2. Direction of arrival estimation performance

Figure 3 shows the results for DOA estimation using 2D (4×4) array compared with 1D (4×1) array [6] when the desired signal comes from the angles of 30° and -20° off boresight direction. To obtain the presented results,

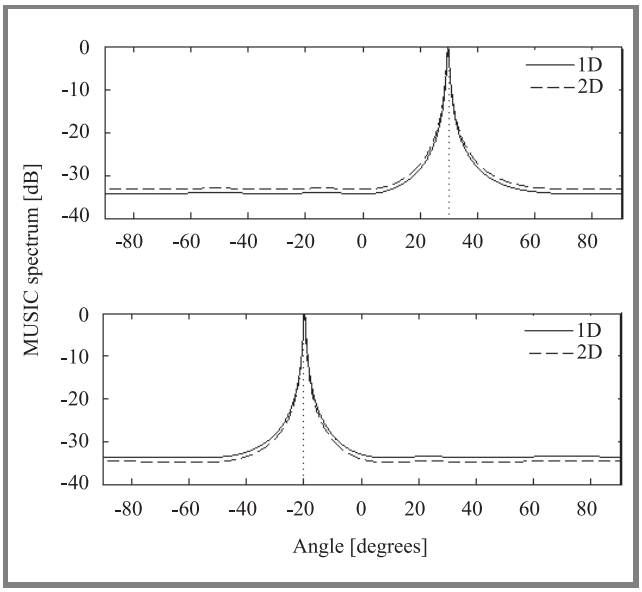

Fig. 3. MUSIC spectrum, $SNR = 10$ dB, fractional bandwidth = 27.3%, interpolated sector $[-45^\circ / +45^\circ]$, 7 frequency bins, 400 snapshots and 50 experiments.

400 snapshots (samples) in time domain, 7 frequency bins and 50 experiments over the angular sector of $-45^\circ / +45^\circ$ with the step size of 1° were used. The obtained results using the proposed DOA method for the 2D array are similar to those obtained with the DOA estimation algorithm devised for a 1D array [6].

3.3. Beamforming capabilities

Figure 4 shows the simulated (without and with mutual coupling) and measured results for the radiation pattern when the array points its main beam in the 45° off boresight direction. The assumed radiation characteristic H was chosen in the form of Chebyshev polynomial of 4th order to minimize side lobes, according to the strategy described in the paper. In order to achieve this radiation pattern, attenuators of 10, 5, 3 and 0.4 dB were used in the beamforming network.

It can be observed that the presence of mutual coupling increases sidelobe levels. However, as the assumed characteristic H (without mutual coupling) exhibits low side lobes, the actual radiation pattern (with mutual coupling taken into account) features an acceptable side lobes level. In all of the three cases presented in Fig. 4 the radiation patterns stay almost the same across the investigated frequency band between 1.9 and 2.5 GHz. In addition a good agreement between the measured and simulated (including mutual coupling) results is observed.

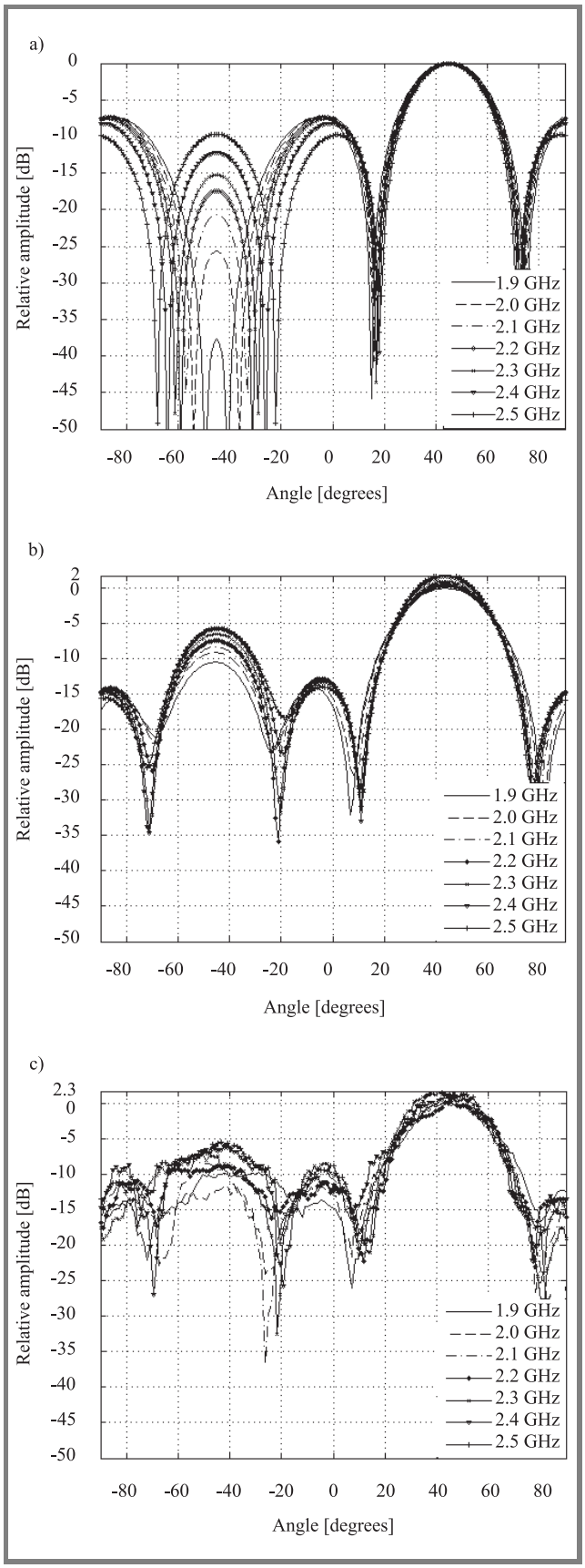

Fig. 4. Radiation pattern for the 4×4 array plotted for frequencies from 1.9 to 2.5 GHz when the desired direction is 45°: (a) simulated without mutual coupling; (b) simulated with mutual coupling; (c) measured.

Figure 5 presents the radiation pattern of the 5×5 array plotted from 1.9 to 2.5 GHz when the desired and undesired signal directions are 45° and 0°, respectively. The obtained

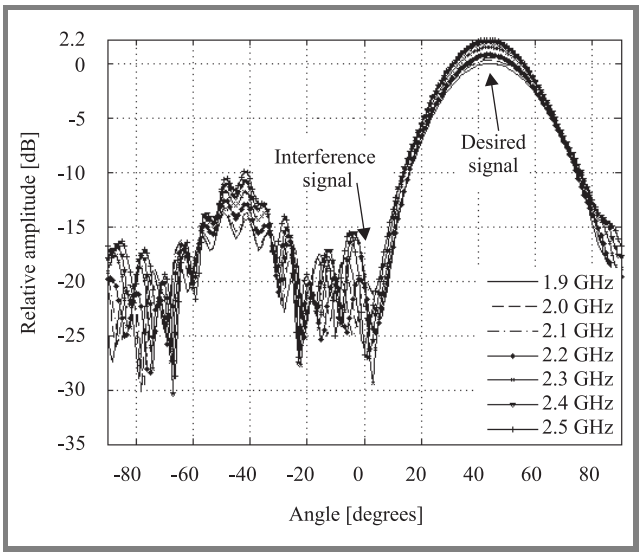

Fig. 5. Radiation pattern of a 5×5 element array plotted from 1.9 to 2.5 GHz when the desired beam direction is 45° and the desired null direction is 0°.

result indicates that the array is perfectly able to direct its main beam to 45° while the null located at 0° varies from −29 to −21 dB throughout the designated band. The sidelobes are at a lower level than of the 4×4 array.

4. Conclusion

The design of a compact smart array antenna capable of beam formation in azimuth over a wide frequency band using only spatial beam forming technique has been described. The antenna requires only real weighting coefficients to form a radiation pattern which is approximately constant with frequency. This weighting scheme is of practical value, as it can be realized using only amplifiers and attenuators without resorting to filters, phase shifters or delay circuits that are employed in conventional wideband beamformers. In this array, DOA estimation of a wideband signal is based on the interpolated array technique and the MUSIC algorithm. It has been shown that the 2D spatial beamformer offers a similar quality DOA estimation of a wideband signal as its 1D counter part. The presented antenna system is of low cost and thus should be of interest to designers of wideband smart antennas for wireless communications supporting high data rate transmission.

Acknowledgment

The authors acknowledge the financial support of the Australian Research Council via grant DP0450118.

References

[1] A. J. Goldsmith, "Smart antennas", *IEEE Pers. Commun.*, vol. 5, p. 9, 1998.

[2] M. Hefnawi and G. Y. Delisle, "Performance analysis of wideband smart antenna systems using different frequency compensation techniques", *IEEE Trans. Comput. Commun.*, pp. 237–242, July, 2001.

[3] M. Ghavami and R. Kohno, "Broadband partially adaptive antenna using a new IIR fan filter", in *Proc. IEEE/IEEJ/JSAI Int. Conf. Intell. Transp. Syst.*, Tokyo, Japan, 1999, pp. 495–500.

[4] M. Ghavami, "Wideband smart antenna theory using rectangular array structures", *IEEE Trans. Sig. Proc.*, vol. 50, no. 9, pp. 2143–2151, 2002.

[5] B. Friedlander and A. J. Weiss, "Direction finding for wide-band signals using an interpolated array", *IEEE Trans. Sig. Proc.*, vol. 41, no. 4, pp. 1618–1634, 1993.

[6] B. Friedlander and A. J. Weiss, "Direction finding using spatial smoothing with interpolated arrays", *IEEE Trans. Aerosp. Electron. Syst.*, vol. 28, no. 2, pp. 574–587, 1992.

[7] J. C. Liberti and T. S. Rappaport, S*mart Antennas for Wireless Communications: IS-95 and Third Generation CDMA Applications*. Upper Saddle River: Prentice Hall, 1999.

[8] FEKO – comprehensive EM solutions, http://www.feko.co.za

[9] ADS – Advanced Designed System 2003A, Agilent Technologies, http://eesof.tm.agilent.com/products/ads_main.html

Monthippa Uthansakul received the B.Eng. degree in telecommunication engineering from Suranaree University of Technology, Thailand, in 1997 and the M.Eng. degree in electrical engineering from Chulalongkorn University, Thailand, in 1999. From 1999 to 2003, she worked as a Lecturer at Suranaree University of Technology. At present, she persues her Ph.D. degree at the University of Queensland. Her research interests concern the design, simulation and testing of narrow and wideband adaptive antennas. Mrs. Uthansakul was a recipient of the 2nd Student Paper prize awarded by the Ansoft Corporation at the 16th MIKON Conference, Poland (2006).
e-mail: mtp@itee.uq.edu.au
School of Information Technology
and Electrical Engineering
University of Queensland
St Lucia, Brisbane, QLD 4072, Australia

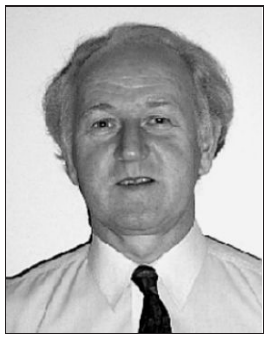

Marek E. Bialkowski received the M.Eng.Sc. degree (1974) in applied mathematics and the Ph.D. degree (1979) in electrical engineering from the Warsaw University of Technology, Poland, and the D.Sc. degree (2000) in computer science and electrical engineering from the University of Queensland, Australia. He held teaching and research appointments at universities in Poland, Ireland, Australia, UK, Canada, Singapore, Hong Kong and Switzerland. At present he is a Chair Professor in the School of Information Technology and Electrical Engineering at the University of Queensland. His research interests concern the modelling, design, and testing of microwave guiding and radiating structures for wireless communications and industrial and medical applications. He has published over 400 technical papers in these areas. His contributions earned him an IEEE Fellow award in 2002.
e-mail: meb@itee.uq.edu.au
School of Information Technology
and Electrical Engineering
University of Queensland
St Lucia, Brisbane, QLD 4072, Australia

Paper

Optimizing circular polarization within a beam of patch antenna elements

Monika Hornik, Paweł Hornik, Dominik Guzda, and Paweł Kabacik

Abstract— The paper presents the results of an investigation into patch antenna elements that would be capable of providing good circular polarization not only in the broadside direction, but also over a wide range of elevation angles.

Keywords— lightweight antennas, circularly polarized antennas, microstrip antennas.

1. Introduction

While many researchers have concentrated their studies on bandwidth widening techniques for microstrip antennas, there has been less concern paid to optimizing their polarization quality off the broadside direction. The increasing popularity of wireless services has brought about the designing of antennas capable of generating a high quality circular polarization not only in the broadside direction, but also over a broad angular range of beam, and is becoming a crucial issue. It is strongly advisable to provide such good circular polarization properties without sacrificing the antenna low profile – a property that is a primary advantage and is of paramount importance when undertaking application decisions.

In order to achieve the satisfaction of these requirements, we considered a number of antenna concepts, with a focus on shaping the antenna feed slots. Primary attention was also given to the patch shape, with parasitic elements in its proximity. Our research is being driven by the needs of two minisatellite missions. The first of them was completed successfully in October 2005 when SSETI-Express was launched and put into orbit, the second, ESEO, is scheduled for launch in 2008.

2. Methods of improving circular polarization in patch antennas

Figure 1 shows the general structure of the investigated antennas. It consists of a 31-mil thick microwave laminate bearing the ground and metal patch printed on the thin dielectric foil, which are separated by 10 mm thick dielectric foam. These values of substrate heights were selected in the course of lengthy simulations aiming at bandwidth broadening. The foam material features highly stable electrical parameters over a wide temperature range. In order to ensure broad impedance bandwidths, we designed our antennas using through-slot coupled transmission lines. Circular polarization for these kinds of antennas can be achieved using either a single slot or a dual slot feed (due to space limitations, we abandoned the interest in feeds made with two pairs of coupling slots). We focused on a dual slot feed

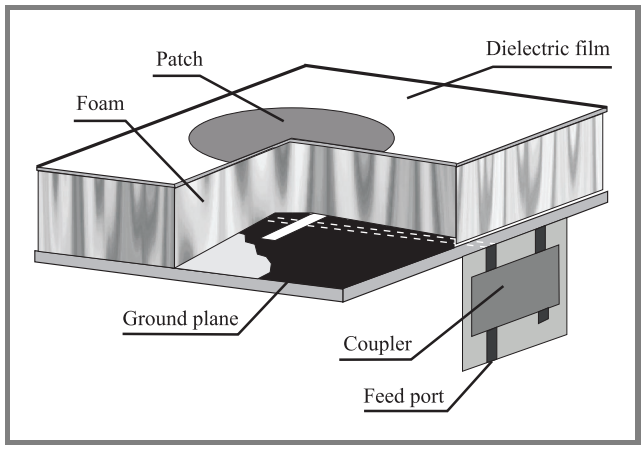

Fig. 1. General structure of the investigated antennas.

because we believe it offers much better axial ratio (*AR*) values and a larger axial ratio bandwidth than the single feed method as far as we are capable of providing a high quality external polarizer. Both output signals of the polarizer must have an equal magnitude and differ by a 90° phase shift in the whole operating bandwidth. A three-strip coupler proved to be of the highest utility for such requirements. Typically, for a 2.4 GHz center frequency, it features phase variations within 3° in roughly a band of 1 GHz. Manufac-

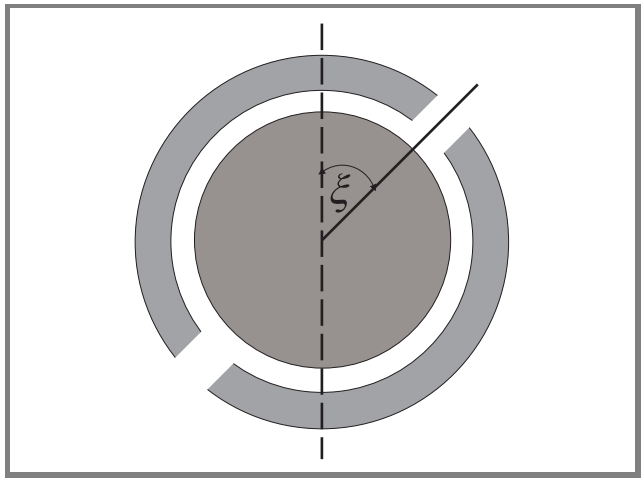

Fig. 2. One of the patches in the investigated antennas.

tured on a thin dielectric membrane, it does not contribute much to the weight and volume of the antenna and can be perfectly integrated with its structure. The methods of development for such couplers are described by Sachse and Sawicki [3].

Our investigation focused on determining the most advantageous shape of the slots and the geometry of their arrangement to be used. We compared a wide range of possible dimensions and shapes for the coupled slots [1]; the shape of the slots in a pair may be different, or the slots may be of identical shape and dimensions.

In order to improve the axial ratio over the broad angle of a main beam, we decided to use parasitic elements in the proximity of the patch, usually produced as a copper strip divided into two or four sectors (Fig. 2).

3. Discussion of results

In our analysis of printed, dielectric antennas, we used Ensemble of Ansoft. Several antenna models were manufactured and measured. Figure 3 presents the calculated return loss characteristics for three shapes of slots. When the slots are in a T arrangement, there are some difficulties in reaching equal impedance matches on two feed ports. In most cases, the impedance bandwidth of one port is wider than the other. These differences can be minimized if designed carefully. When the slots are in an L arrangement, these problems do not occur. The return loss characteristics, shown in Fig. 4, were measured for assembled CP antenna models (Fig. 1). The measured 20 dB bandwidth was about 600 MHz for the dual C-slot feed (2C), and 300 MHz for both 2H slot and C+R feeds.

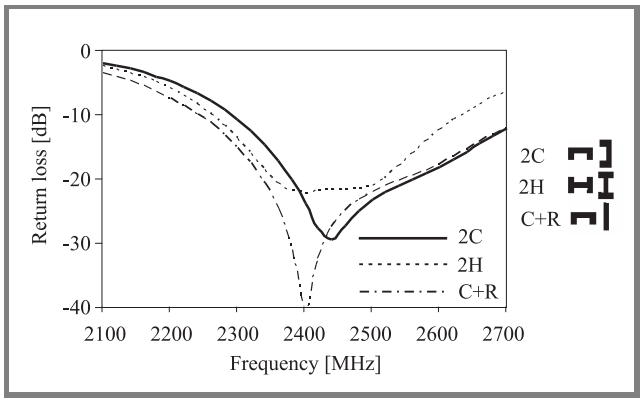

Fig. 3. Simulated return loss characteristics for antennas fed with a various pairs of slots (2C, 2H, C+R).

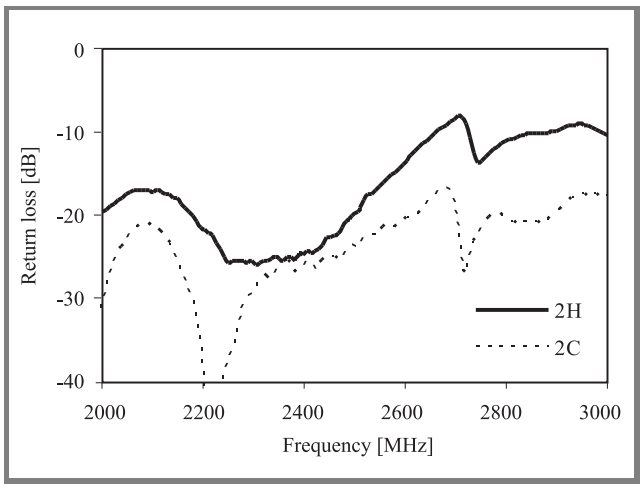

Fig. 4. Measured return loss characteristics for CP antennas fed with 2H and 2C slot pairs.

One of the conditions for generating an excellent circular polarization is the high isolation between the orthogonal ports. A remarkable increase in the degree of isolation can be obtained when the slots are in a T arrangement [2], especially when one of the slots is pushed a little to the side of the symmetry axis of the patch. Owing to the T arrangement, the isolation between the ports was increased by 12 dB in all cases. Thus, we had no problems achieving isolation better than 30 dB. However, it is difficult to obtain a compact feed line arrangement. The calculated isolation between the ports in the 2C case slightly exceeds 30 dB in the band. The calculated isolation values for 2H and C+R feed ranged between 22 and 30 dB. Measured characteristics were consistent with the calculated ones. The isolation was only frequency dependent to a small degree.

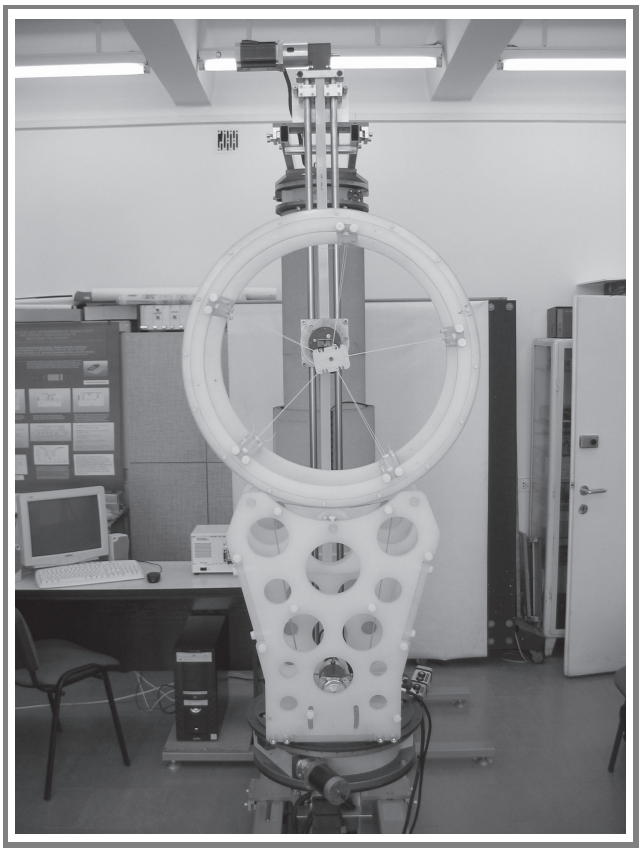

Fig. 5. The in-house developed measurement system in the microwave laboratory at the Institute of Telecommunications, Teleinformatics, and Acoustics, Wrocław University of Technology.

Most of electromagnetic computer tools and measurement systems are capable of determining axial ratio characteristics only in some cut-planes (usually in two orthogonal planes $\varphi = 0^\circ$ and $\varphi = 90^\circ$). In our research, we had to examine the axial ratio within the whole forward hemisphere. This has become possible with the measurement system shown in Fig. 5, developed in-house in our microwave laboratory.

Figure 6 presents the measured values of the axial ratio (in dB) within the forward hemisphere at 2400 MHz for a dual C-slot CP antenna. In the broadside direction ($\Theta = 0^\circ$), the measured axial ratio was 0.6 dB. The parameters of these antennas were additionally measured in Saab Ericsson Space antenna laboratories, where their excellent polarization quality was confirmed. Identical antennas were

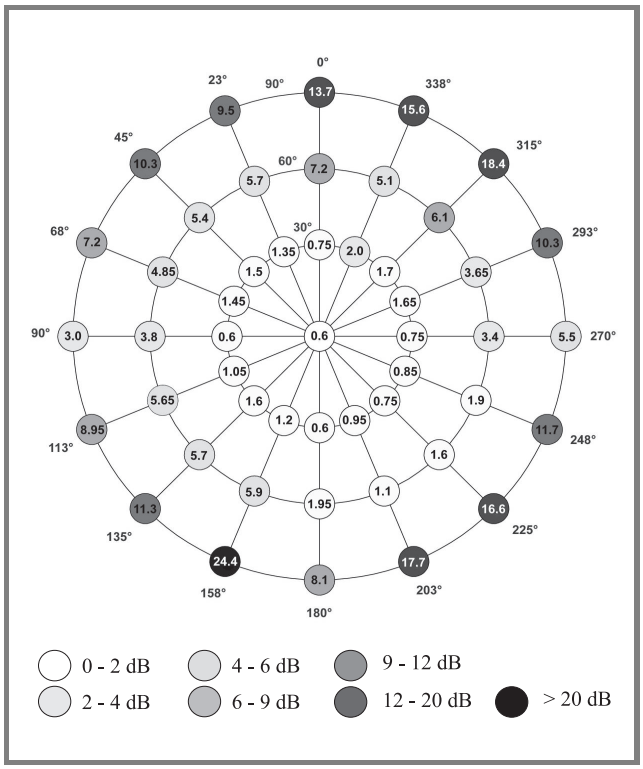

Fig. 6. The measured values of the axial ratio (in dB) of the 2C antenna at 2400 MHz in the forward hemisphere.

used onboard the SSETI-Express minisatellite. For the other two introduced antenna models, we obtained the axial ratio values 1.34 dB and 2.36 dB at the broadside for 2H-slot and C+R slots (Fig. 7), respectively.

However, the greatest interest was in providing a good degree of circular polarization in a possible wide angular range in the forward hemisphere of the radiation pattern. A great impact on this parameter was the shape and arrangement of the feed slots. The T arrangement, which significantly improves the isolation between the feed line ports, raises concerns in regard to symmetry. One of the slots must be pushed a little to the side of the symmetry axis of the patch. This leads to some asymmetry in the radiation pattern and in the CP quality of the antennas, which considerably differentiates the values of the axial ratio between the cut-planes. While there are excellent values at one cut-plane across the hemisphere, we should expect poorer axial ratio values at high elevation

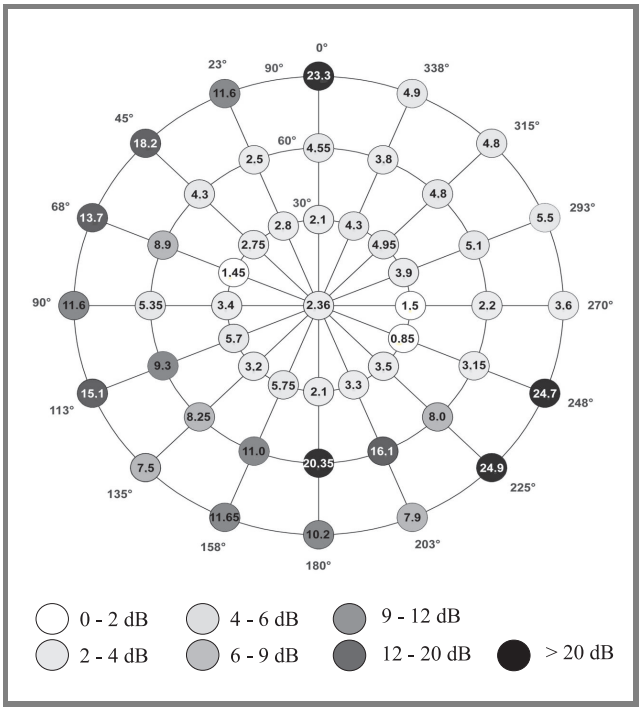

Fig. 7. The measured values of the axial ratio (in dB) of the C+R antenna at 2400 MHz in the forward hemisphere.

angles in the other principal cut-plane. Only with 2C and 2H antenna types, *AR* has taken the values below 2 dB in the broad angular range of the main beam. We observed that the 2C antenna features favorable *AR* values within at least 60° of the elevation angle (θ). In some cut-planes at elevation angles close to endfire, the circular polarization quality can deteriorate abruptly and actually become linear polarization within the narrow angular step (*AR* drop by more than 10 dB). Even with the best 2C type antennas, this drawback occurs at two diagonal cut-planes.

Our investigations have shown that in some cases, the polarization quality of the antenna can be significantly improved when a conductive parasitic strip partitioned into two or four sectors surrounds its patch. We have found that the axial ratio values may considerably depend on the angular orientation of the gaps between the sectors of the strip in respect to the feed slots (ξ angle shown in Fig. 2).

This claim is substantiated by plots (Figs. 8 and 9) showing the results of the simulations carried out for the antenna feed with two rectangular slots. In all considered directions ($\theta = 0^\circ$), ($\theta = 40^\circ$, $\varphi = 0^\circ$), ($\theta = 40^\circ$, $\varphi = 90^\circ$), etc., the *AR* value was the lowest for $\xi \in \langle 30^\circ, 40^\circ \rangle$.

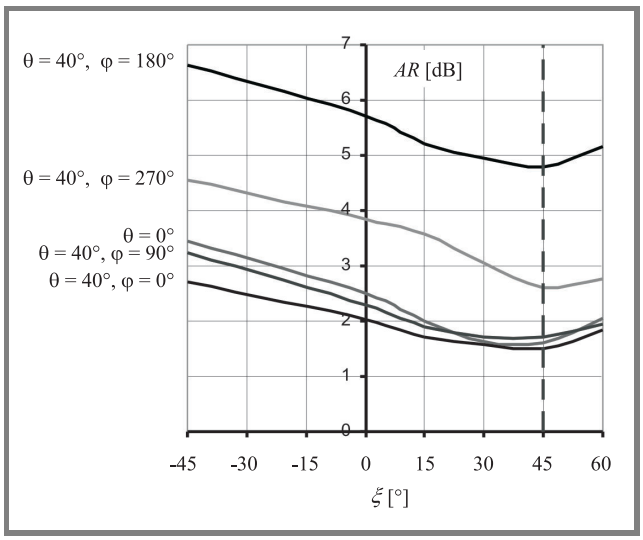

Fig. 8. Simulated values of the axial ratio in specified directions of the antenna as a function of angular orientation of the gaps between the strip sectors.

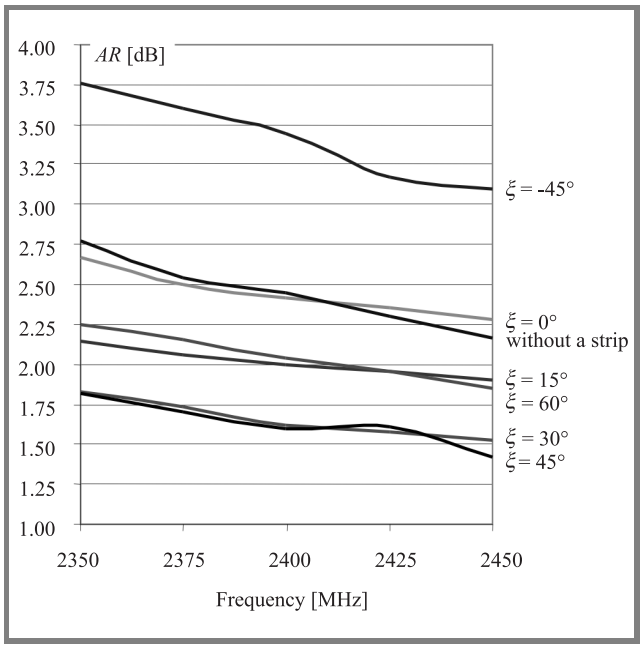

Fig. 9. Simulated values of the axial ratio for the different angular orientation of gaps between the strip sectors and for the patch without the strip in the operating band of the antenna.

In Fig. 9, the axial ratio of the antennas with patches surrounded by a strip (for varying ξ) are compared with patches without a strip in the 2350 MHz to 2450 MHz frequency band.

4. Conclusions

High quality of circular polarization over a broad angle of an antenna beam has been achieved with low profile microstrip patches. One of the antennas we had developed is characterized with favorable values (< 6 dB) of the axial ratio in some cut-planes even from $\theta = -90°$ to $\theta = +90°$. Good polarization properties have been shown in the large range of the forward hemisphere with a few other microstrip patch designs. The prerequisites of good polarization properties are compact forms of coupling slots used in the element feed (i.e., C), their careful arrangement under the patch (i.e., T geometry) and the use of parasitic, small conductive shapes in the proximity of an antenna patch. The axial ratio values are then likely to match those known from bulkier shapes and volumes, and until now, widely used antenna elements (e.g., helix).

The patches optimized and presented in this paper are to be used mostly in space communication, polarimetric radar and in radio interfaces of wireless services.

References

[1] P. Kabacik, K. Wincza, M. Kamaszuk, and P. Hornik, "Optimizing circular polarization in broadband lightweight patch antennas", in *IEEE AP Soc. Int. Symp.*, Washington, USA, 2005.

[2] S. K. Padhi, N. C. Karmakar, C. L. Law, and S. Aditya, Sr., "A dual polarized aperture coupled circular patch antenna using a C-shaped coupling slot", *IEEE Trans. AP*, vol. 51, no. 12, pp. 3295–3298, 2003.

[3] K. Sachse and A. Sawicki, "Quasi-ideal multilayer two- and three-strip directional couplers for monolithic and hybrid MIC", *IEEE Trans. MTT*, vol. 47, no. 9, pp. 1873–1882, 1999.

Monika Hornik was born in Bielsko-Biała, Poland, in 1982. From 2001 to 2006 she studied electrical and computer engineering at Wrocław University of Technology, Poland. In July 2006 she graduated with M.Sc. degree, with specialization in telecommunication, following presentation of her thesis on "Gain enhancement methods for lightweight microwave antennas". She was admitted on Ph.D. course in electrical engineering at Wrocław University of Technology. For three years she has taken part in the project Student Space Exploration and Technology Initiative (SSETI). She has carried on research on lightweight, low-profile, microstrip antennas for the use onboard International Space Station.

e-mail: Monika.Hornik@pwr.wroc.pl
Institute of Telecommunications, Teleinformatics, and Acoustics
Wrocław University of Technology
Wybrzeże Wyspiańskiego st 27
50-370 Wrocław, Poland

Paweł Hornik was born in Opole, Poland, in 1982. From 2001 to 2006 he studied electrical and computer engineering at Wrocław University of Technology, Poland. In July 2006 he graduated with M.Sc. degree, with specialization in telecommunication, following presentation of his thesis on "Cylindrical lightweight microstrip antenna array for space borne application". For three years he has taken part in the project Student Space Exploration and Technology Initiative (SSETI). He has carried on research on lightweight, low-profile, microstrip antennas for the use onboard International Space Station.

e-mail: hpol@poczta.fm
Institute of Telecommunications, Teleinformatics,
and Acoustics
Wrocław University of Technology
Wybrzeże Wyspiańskiego st 27
50-370 Wrocław, Poland

Dominik Guzda was born in Krapkowice, Poland, in 1981. He studied telecommunications on Faculty of Electrical and Computer Engineering at Wrocław University of Technology, Poland. He has taken part in the project Student Space Exploration and Technology Initiative (SSETI) for three years. Currently he is working in Siemens Networks company and is engaged in development of intelligent networks.

e-mail: dominik.guzda@gmail.com
Institute of Telecommunications, Teleinformatics,
and Acoustics
Wrocław University of Technology
Wybrzeże Wyspiańskiego st 27
50-370 Wrocław, Poland

Paweł Kabacik was born in Wrocław, Poland, in 1963. He received the M.Sc. degree in telecommunications (highest honors) from Wrocław University of Technology, Poland, in 1986. In 1996 he received the Ph.D. in electrical engineering (award). In January 1987, he joined the Institute of Telecommunications and Acoustics, Wrocław University of Technology. He was a visiting scholar to the Technical University of Denmark (1991/1992) and to the University of Queensland (1997, 2001, and 2006). He chaired the Mulitband Antennas and Conformal Array Mini-Team acting within the COST 260 Project and he chairs one of four research tasks in the current COST 284 Project. He is an expert of European Commission. His research interests include highly integrated antenna arrays, conformal antennas, terminal antennas, phased arrays, advanced antenna measurements and communication subsystems of small spacecraft. He was a Principal Investigator to several contracts funded by the National Research Council, Poland, and by industry. He is a member of Technical Committees at several international conferences. He received several recognitions for his research work, of which the most valuable is the "2000 Harold A. Wheeler Applications Prize Paper Award Honorable Mention" of the IEEE. In 1993 he received the Award for Young Scientists at the 7th National URSI Symposium, Poland. He was listed in six editions of "Marquis's Who's Who in Science and Engineering".

e-mail: Pawel.Kabacik@pwr.wroc.pl
Institute of Telecommunications, Teleinformatics,
and Acoustics
Wrocław University of Technology
Wybrzeże Wyspiańskiego st 27
50-370 Wrocław, Poland

Paper

Modified monopole ring antennas as a solution for HiperLAN1/2 and IEEE 802.11b/g standard devices

Anna Miskiewicz and Marek Kitliński

Abstract— A compact planar antenna for multisystem applications has been designed and manufactured. A modified feeding method has been used to meet the requirements of modern telecommunications devices. It has been shown, that by adjusting the size of the rings, required allocation of bands is possible. The proposed antenna is suitable for ISM band devices and gives perspectives for multi-standard operation. The antenna has been simulated using MoM 2.5D software Zeland IE3D, next fabricated and measured.

Keywords—fractal antennas, multiband antennas, HiperLAN, wireless LAN, modified monopole.

1. Introduction

In the past few years there has been a growing need for multiband and wideband antennas, as wireless networks have become much more popular and affordable for an end-user. Especially, wireless local area networks (WLAN) have increased the demand for compact, possibly omnidirectional antennas mounted over a small ground plane, working in two dedicated bands: 2.4 GHz (2.4–2.4835 GHz) and 5 GHz (5.15–5.35 GHz, 5.725–5.875 GHz for IEEE 802.11 standard and 5.18–5.32 GHz, 5.5–5.7 GHz for HiperLAN standard). In this paper a new configuration of ground plane and feeding is investigated to satisfy the requirements for WLAN applications using multiple ring antennas. Multiple ring antennas are usually compared with fractal antennas, such as Sierpinski or Parany gasket. However, they are not fractal antennas, but the way they are created can be as well described using an iterative procedure.

Basic configuration of a multiple ring antenna includes a number of rings (Fig. 1) with a common point, where the feeding line is connected to the radiating element. Usually, the radius of the following rings is in the ratio of 2:1 and there is no cut in the smallest circle. Therefore it can be said, the whole antenna is a set of single radiating elements, which should operate in different bands, hence the similarity to fractal antennas. It has been shown [1–3], that by changing the scale ratio of fractal antennas, operating frequencies of the antenna can be allocated, which has been the initial step for the design of the proposed multiple ring antenna.

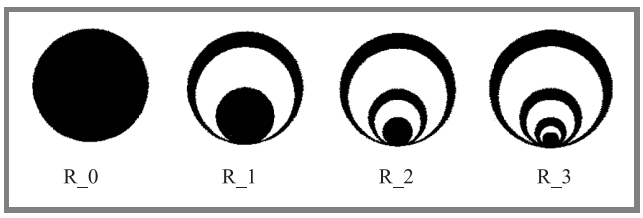

Fig. 1. Construction of multiple ring radiating element.

2. Antenna design

The antenna was fabricated using common substrate, TACONIC RF-35 of thickness $h = 0.762$ mm, relative permittivity $\varepsilon_r = 3.5$ @1.9 GHz and dielectric losses $tg\delta = 0.0018$. Parameters of the substrate used in the project were taken directly from the data sheet supplied with the material. Moreover, it has been assumed, that the permittivity does not change with the frequency, which made the calculations straightforward. So far, multiple ring antennas have been investigated using a configuration of a monopole perpendicular to finite ground plane [4], fed by a coaxial line. Since the need for miniaturization and compatibility, a modified solution had to be proposed.

A structure of a modified monopole has been used (Fig. 2). At the top of the substrate a microstrip line has been placed, which feeds the radiating rings. The characteristic impedance of the line has been calculated to be 50 Ω at the lower resonant frequency. At the bottom, the ground plane covers the surface underneath the microstrip line and does not exceed beyond it, which means, that there is no

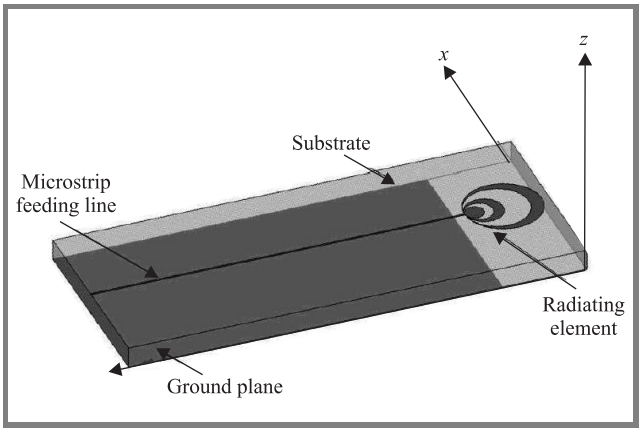

Fig. 2. Modified monopole structure using a multiple ring configuration.

ground plane below the radiating rings. Such configuration is known as modified monopole [5], and it has been shown, that it gives a good resemblance of characteristics with classical monopole configuration. This configuration is useful in wireless devices, such as mobile phones, wireless PC cards or multimedia applications, because it can be mounted at the back of the unit and receive and transmit signals in all directions. Moreover, there is no need to use additional air gap, which has been extensively used to broaden the operating bands [6, 7], as the chosen configuration of radiating elements fully satisfies the requirements, and even exceeds them. As it has been explained, multiple ring antennas are much the same as fractal antennas, because of the scale factor and iterative model of geometry.

For the project a number of configurations has been designed and numerically tested. To achieve two-band operation, two rings has been used, but a scale factor has been changed from 2 to 2.14 to get resonant modes near middle frequencies of both ISM-bands (Fig. 3). The size

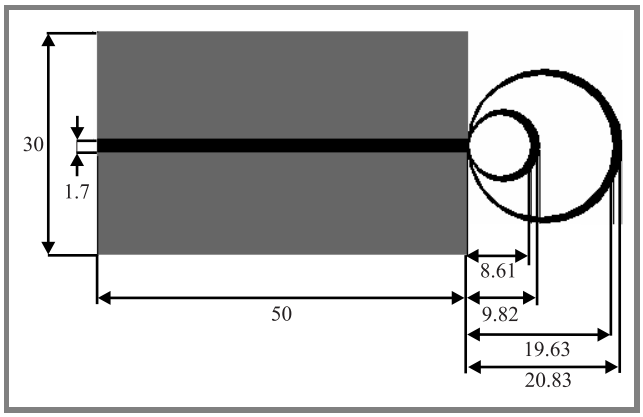

Fig. 3. Proposed multiple ring modified monopole antenna (all measurements in mm).

of the ground plane was chosen to fit the dimensions of a standard modern mobile phone. There is no ground plane below the radiating rings. To get the appropriate resonant modes, the perimeter P_o of the outer ring was calculated using the following equation:

$$P_o = \lambda_{2.45\,\mathrm{GHz}} = \frac{\mathrm{c}}{f\sqrt{\varepsilon_r}},$$

where: c is speed of light in the vacuum, $f = 2.45$ GHz and ε_r is the relative permittivity of the substrate.

The perimeter of the inner ring P_i was calculated as $\frac{P_o}{2.14}$. As there is no equation, which would describe the effective permittivity of the dielectric material in a configuration of a modified monopole, an assumption has been made, that the effective permittivity equals the relative permittivity of the substrate. However, if the permittivity of the material was high, additional tuning of the perimeters of the rings would have to be made.

3. Measured and experimental results

The proposed antenna presenting the most satisfying results for return losses and radiation characteristics has been fabricated and measured using a vector network analyzer Wiltron 37269A. The obtained results have been compared with the simulated ones from Zeland IE3D (Fig. 4). The highest frequency was set at 10 GHz with 15 cells per wavelength with additional meshing on edges to get sufficiently accurate results in reasonable time.

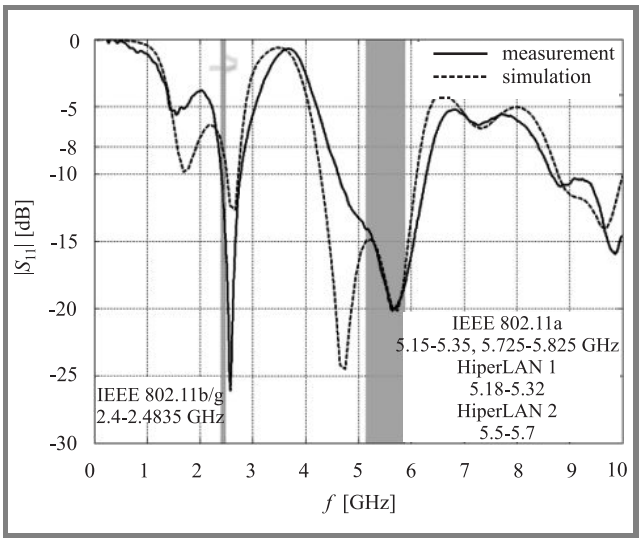

Fig. 4. Measured and simulated return losses $|S_{11}|$ of the proposed antenna.

For the maximum return losses of -8 dB a table was made presenting a comprehensive comparison of the predicted and measured parameters of the antenna (Tables 1 and 2), where $f_{\min}$ is a frequency of minimal return losses, f_0 is a middle frequency of the band calculated as an arithmetic mean of the band-defying frequencies.

Table 1
Simulated parameters of the proposed antenna

$f_{\min}$ [GHz]	f_0 [GHz]	B [%]
1.684	1.751	12.25
2.66	2.597	13.32
4.731/5.741	5.194	37.93

Table 2
Measured parameters of the proposed antenna

$f_{\min}$ [GHz]	f_0 [GHz]	B [%]
2.57	2.6	19.23
5.67	5.42	36

As predicted, the antenna exhibits multiband behaviour. Presented results show good agreement of simulation and measurements. The proposed antenna is matched

in the bands of IEEE 802.11b/g and HiperLAN2 standards, as it was intended to. Due to equipment limitations far-field radiation patterns were measured at the frequency

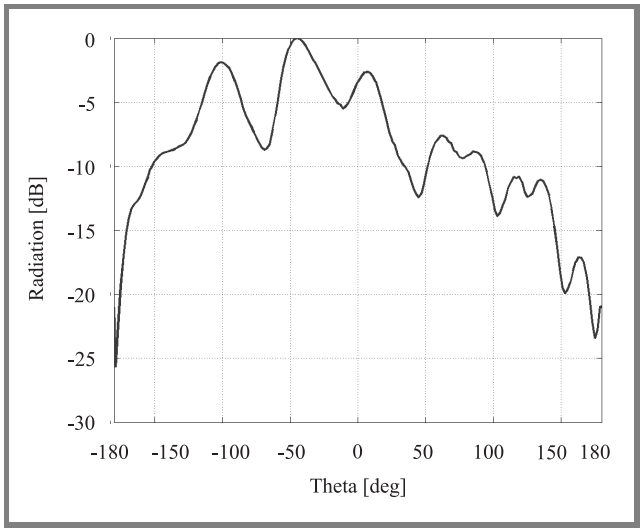

Fig. 5. Measured radiation pattern of total E-field in the elevation plane at 9.14 GHz.

of 9.14 GHz (Fig. 5). It can be seen, that the antenna radiates both front and backwards and has moderate small directivity.

4. Conclusions

A novel approach to monopole multiple ring antennas has been presented. It has been shown, that it is possible to allocate the required bands by adequate modifying the geometry to obtain compact planar antenna for mobile devices. The presented antenna is matched in the bands of IEEE 802.11b/g and HiperLAN1/2 standards. Finally, we should underline, that multiple ring antennas are a good example of construction, which can be used to design multiband or wideband antennas. Applying the new feeding technique it is possible to design and implement antennas which could operate in multi-standard terminals.

References

[1] J. Anguera, E. Martinez, C. Puente, C. Borja, and J. Soler, "Broadband dual-frequency microstrip patch antenna with modified Sierpinski fractal geometry", *IEEE Trans. Anten. Propagat.*, vol. 52, no. 1, pp. 66–73, 2004.

[2] G. F. Tsachtsiris, C. F. Soras, M. P. Karaboikis, and V. T. Makios, "Analysis of a modified Sierpinski gasket monopole antenna printed on dual band wireless devices", *IEEE Trans. Anten. Propagat.*, vol. 52, no. 10, pp. 2571–2579, 2004.

[3] S. R. Best, "Operating band comparison of the perturbed Sierpinski and modified Parany gasket", *IEEE Anten. Wirel. Propagat. Lett.*, vol. 1, pp. 35–38, 2002.

[4] C. T. P. Song, P. S. Hall, and G. Ghafouri-Shiraz, "Multiband multiple ring monopole antennas", *IEEE Trans. Anten. Propagat.*, vol. 51, no. 4, pp. 722–729, 2004.

[5] M. Kitlinski and R. Kieda, "Compact CPW-fed Sierpinski fractal monopole antenna", *IEE Electron. Lett.*, vol. 40, no. 22, pp. 1387–1388, 2004.

[6] J. Guterman and A. Moreira, "Microstrip fractal antennas for multistandard terminals", *IEEE Anten. Wirel. Propagat. Lett.*, vol. 3, pp. 351–354, 2004.

[7] P. Ciais, R. Staraj, G. Kossiavas, and C. Luxey, "Compact internal multiband antenna for mobile phone and WLAN standards", *IEE Electron. Lett.*, vol. 40, no. 15, pp. 920–921, 2004.

Anna Miskiewicz received her M.Sc. degree in electronic engineering from Gdańsk University of Technology, Poland, in 2005. After graduation she worked for IT industry in Poland. She joined Infineon Technologies AG, Germany, in 2006. She is currently working toward a Ph.D. degree in the field of RF system engineering. Her major interests are satellite systems and RFIC design with a focus on GPS and Galileo receivers.
e-mail: Anna.Miskiewicz@infineon.com
Infineon Technologies AG
Am Campeon 1-12
D-85579 Neubiberg, Germany

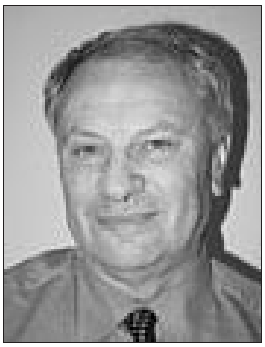

Marek Kitliński was born in Sopot, Poland, in 1947. He received the M.Sc.E.E., Ph.D., and habilitation degrees from the Gdańsk University of Technology, Poland, in 1969, 1975 and 1987, respectively. From 1984 to 1987 he was a Researche Associate with the Kernforschungszentrum Karlsruhe, Germany. Since 1987 he is an Associate Professor with Gdańsk University of Technology, Poland. His research interests include ferrite devices, integrated circuits for microwave and millimeter wave applications, integrated antennas for wireless communication.
e-mail: maki@eti.pg.gda.pl
Microwave and Antenna Engineering Department
Gdańsk University of Technology
Narutowicza st 11/12
80-952 Gdańsk, Poland

Paper

Phased array antennas in MIMO receiver

Sebastian Kozłowski, Yevhen Yashchyshyn, and Józef Modelski

Abstract— In this paper, a computer simulation of a MIMO system comprising phased array antennas (PAA) in all receiving branches is presented. In order to examine the system performance under relatively realistic conditions, a ray-tracing simulator was applied to generate a baseband channel impulse response matrix *H*. A bit error rate (BER) of two systems utilizing different detection methods: V-BLAST and simple matrix inversion was examined in order to determine phased array antennas applicability. Results of an attempt to determine relationship between BER and properties of particular matrix *H* realization are also provided.

Keywords— MIMO systems, phased array antennas.

1. Introduction

Telecommunications require increasing amount of data to be transferred as well as increasing bit rates. That, in turn, causes the need for developing the data transfer methods and systems utilizing frequency band in a highly effective way. Consequently, researches on radiocommunication systems with transmitters and receivers provided with more than one antenna, so called MIMO (multiple input multiple output) systems, have been intensified in recent years. The base for this approach is to utilize a space as an additional dimension, what enables establishing several orthogonal subchannels simultaneously in the same frequency band. Such subchannels may carry either independent data streams, what means increase of system capacity [1, 2], or the same data reducing the bit error rate (BER) in the radiolink [3].

Phased array antennas (PAA) have been extensively investigated and have already been widely used, for instance in radars and satellite communications. In personal communications they may be applied in order to mitigate interference caused by other users or systems, mitigate intersymbol interference, or to direct the beam toward terminal. Application of phased array antennas in MIMO receivers and transmitters was also considered. In papers [5–7] such antennas were used in order to improve the performance of MIMO system exposed to the interferences. Phased array antennas can also bring benefit to the system utilizing Alamouti scheme [3] by causing significant signal to noise ratio (SNR) increase [4]. Current paper presents possibility of BER reduction by means of PAAs application in every branch of a MIMO receiver, in the system utilizing orthogonal subchannels for transferring independent data streams.

2. MIMO system model

General block diagram of a MIMO system is shown in Fig. 1. Presented model of the system is valid under following assumptions. Transmitted signals have narrow frequency band, and consequently the radio channel is characterized by flat fading, so there is no intersymbol interference. Vector $x_{[Nt,1]}(t_n)$ of complex symbols selected from the predefined constellation is transmitted and vector $y_{[Nr,1]}(t_n)$ of complex signals is received in every time moment t_n (the dimension of the matrix or vector is enclosed within square brackets). The baseband channel impulse response matrix $H_{[Nr,Nt]}$ is precisely determined and does not change during the transmission of the burst comprising large number of symbols. Every element h_{ij} of the matrix H represents the transmission from the jth transmitter to the ith receiver. Operation of the system can be described by means of formula (1):

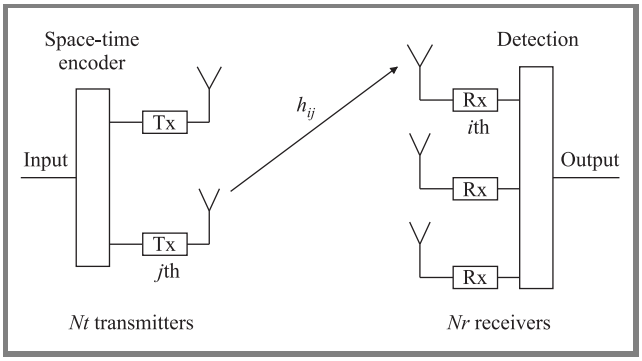

Fig. 1. Block diagram of MIMO system.

$$y(t_n) = H \cdot x(t_n) + n(t_n), \tag{1}$$

where $n_{[Nr,1]}(t_n)$ is the vector of noise samples.

It should be stressed that the useful signal detection (determination of x from the Eq. (1)) is possible only if the matrix H is well conditioned. This is usually satisfied if there is no line of sight (LOS) between the transmitter and receiver and the propagation takes place in the rich scattering environment. Resulting Rayleigh fading, which is harmful to the classical radio systems, is in case of MIMO systems highly desirable since it assures low correlation between different subchannels.

3. Simulation of MIMO system incorporating phased array antennas

A MIMO system comprising two transmitting and two receiving antennas was simulated as an example. Every receiving antenna was realized as 2-element phased array controlled by the tunable (0–360 degrees) lossless phase shifter (Fig. 2). Radiation pattern of a single radiating element is assumed to be omnidirectional and no coupling between any elements is concerned. Radiolink is supposed to be characterized by following parameters: central frequency: 2 GHz, bandwidth: 0.2 MHz, single transmitter output power: 0 dBm, modulation: quadrature phase shift keying (QPSK). Additionally, every element of phased array antenna receives useful signal as well as the noise of given mean power. Each noise sample is a realization of variate described by Eq. (2):

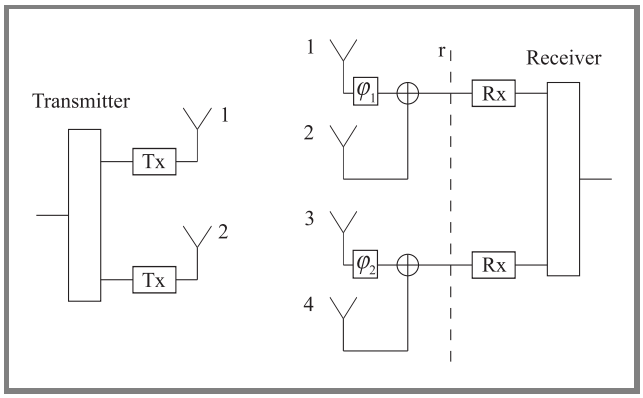

Fig. 2. MIMO system incorporating phased array antennas in each receiver branch (φ – phase shifter, antenna spacing: λ in transmitter, $\lambda/2$ in receiver).

$$n = N(0,\rho^2) + j \cdot N(0,\rho^2), \tag{2}$$

where $N(x,y)$ means normal distribution with mean value x and variance y.

System presented in Fig. 2 can be described by formula analogous to (1):

$$y_{[4,1]}(t_n) = H_{[4,2]} \cdot x_{[2,1]}(t_n) + n_{[4,1]}(t_n). \tag{3}$$

System description can be moved to the "r" plane by means of appropriate processing, involving multiplication by weights and summing:

$$y_{r[2,1]}(t_n) = H_{r[2,2]} \cdot x_{[2,1]}(t_n) \tag{4}$$

while H_r and y_r depend on the phase shifters settings. Please notice that in real system only values of the H_r and y_r are known, as opposed to the values of y and H.

Matrix $H_{[4,2]}$ was generated by means of electromagnetic waves propagation simulator employing ray-tracing 2.5D method. The environment was simulated as the interior and the neighbourhood of the building made of various components and materials (walls, doors, windows) characterized by different permittivity and losses. Figure 3 shows field distribution in small fragment of propagation environment. Two curves are presented, each one corresponds to power level of a signal from one transmitter. Two facts can be deduced from the figure. Firstly, the power level of signals from different transmitters are very different when reaching the receiving antenna located at fixed position. Secondly, because of interference of a number of reflected waves, power level of aforementioned signals changes rapidly when receiving antenna is being moved. The conclusion is that assumed propagation environment satisfies the conditions under which MIMO transmission is possible.

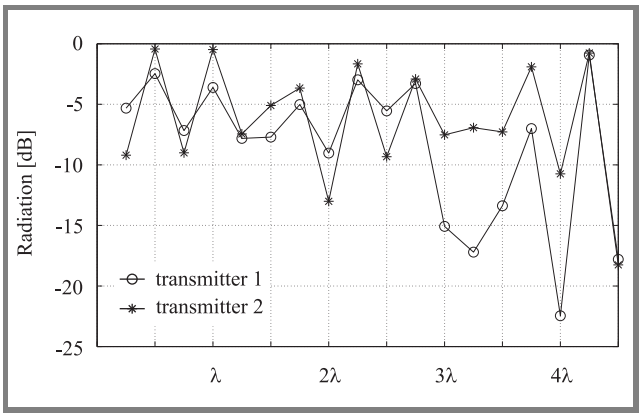

Fig. 3. Field distribution in assumed propagation environment.

Receivers were subsequently positioned in 25 random locations. A transmission of 10 000 symbols (two simultaneous independent streams, 5 000 symbols each) was simulated for every receiver location and for various phase shifters settings. Two detection methods were applied. First was the V-BLAST algorithm [2] and the second, denoted in this paper as INV, consisted in solving the Eq. (4) by simple matrix H_r inversion operation. Results of the experiment are shown in Fig. 4. Particular columns represent BER obtained for the V-BLAST and INV detection for two cases of receiver configuration, first, a receiver provided with two omnidirectional radiators (marked as "2×2" and a dark bar in Fig. 4), and second, a receiver provided with PAAs (marked as "2×4" and a white bar). For the latter case only the lowest BER level has been presented, obtained for the best set of weights. Phase shifters were switched at 2 degrees intervals, noise power level was chosen for every receiver so as to obtain average SNR equal to 10 dB. Results show that application of PAA in every MIMO receiver's branch can provide significant BER reduction – up to ten times.

Testing BER for every set of weights is time-consuming during the simulation and impossible to realize in practice. Consequently determination of the relationship between BER and matrix H_r is more than desirable. Concerning the fact that $|h_{ij}|$ represent the attenuation of the transmitted signal, it seems obvious that they should be as high as possible. For the given noise power level, the higher they are, the greater SNR in receiver's branches is.

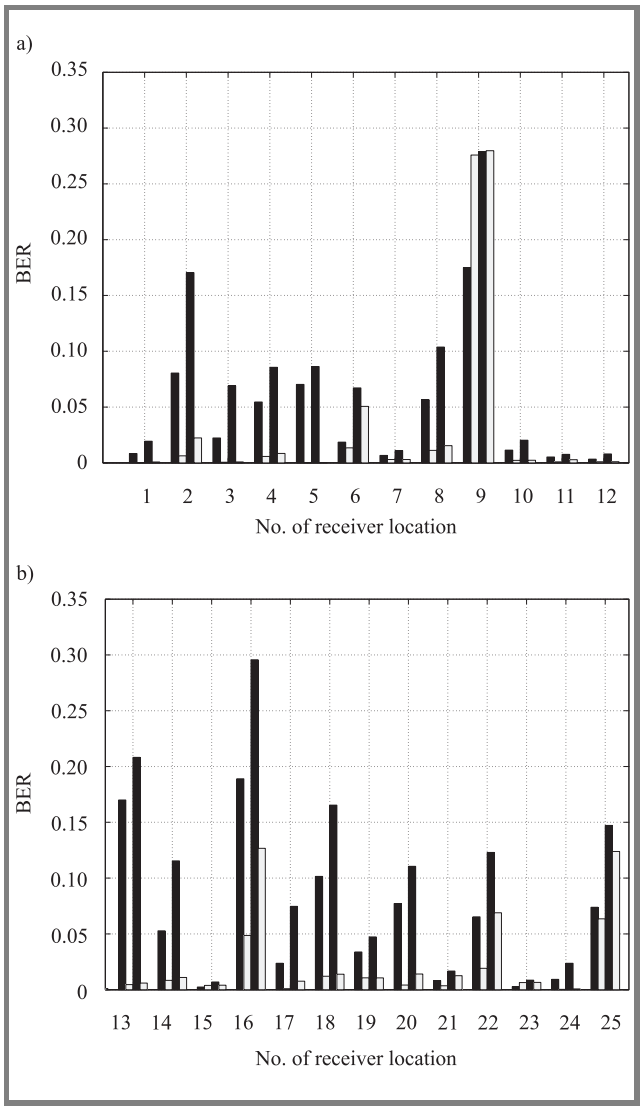

Fig. 4. BER for different receiver locations and: (a) V-BLAST 2×2 (dark bar), V-BLAST 2×4 (white bar); (b) INV 2×2 (dark bar), INV 2×4 (white bar).

However, it should be noticed that during the detection process matrix H_r is subjected to inversion or pseudoinversion operation, so its condition number (ratio of the largest and smallest singular value) $cond(H_r)$ is of great importance. An attempt to find the qualitative relationship enabling to determine which of the given matrix H_r realisation is better concerning the BER has been undertaken. It has been assumed that this relationship can be described as formula with two arguments: $||H_r||^2$ and $cond(H_r)^{-1}$, where $||X||$ means Frobenius norm of the matrix X. It can be easily shown that when the noise with constant power level described by formula (2) is present, then $||H_r||^2$ is proportional to the average SNR measured at the "r" plane. Consequently, if other conditions are unchanged, then increase of $||H_r||^2$ causes better system performance. The better is matrix conditioned, the higher is $cond(H_r)^{-1}$, which reaches its maximum equal to 1 for the identity matrix. Lines of constant BER on the plane $[cond(H_r)^{-1}, ||H_r||^q]$ are shown in Fig. 5. Parameter $q > 0$ is a number empirically determined to be equal to 1.1.

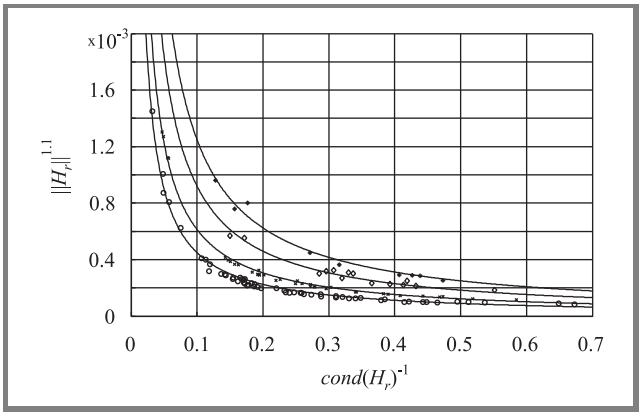

Fig. 5. Constant BER lines for V-BLAST detection.

Lines presented in Fig. 5 correspond to the approximation of simulation results by means of hyperbolas described by equation:

$$F[BER] = ||H_r||^q \cdot cond(H_r)^{-1}, \tag{5}$$

where $F[BER]$ is a certain unknown, but decreasing function of BER. It means that the most advantageous for the system performance should be such matrix H_r for which the right side of Eq. (5) reaches maximum. The problem of choosing appropriate exponent q remains unsolved and will be investigated in future research.

4. Conclusion

Phased array antenna in each branch of receiver has been proposed to decrease BER of MIMO system utilising two subchannels in order to transmit two independent data streams. It has been shown that application of phase shifters only (neither amplifiers nor attenuators) can improve significantly the system performance. Preliminary results of an approach to evaluate BER on a base of current realization of baseband channel impulse response matrix have been also provided. Performance of narrowband MIMO system depends on many factors. In particular, if matrix H is badly conditioned, then system will not operate properly, no matter how high SNR is.

Acknowledgements

The first author Sebastian Kozłowski was supported by Fundation for Polish Science.

References

[1] G. J. Foschini, "Layered space-time architecture for wireless communication in a fading environment when using multiple antennas", *Bell Lab. Tech. J.*, vol. 1, no. 2, pp. 41–59, Autumn 1996.

[2] P. W. Wolniansky, G. J. Foschini, G. D. Golden, and R. A. Valenzuela, "V-BLAST: an architecture for realizing very high data rates over the rich-scattering wireless channel", in *URSI ISSSE'98*, Pisa, Italy, 1998, pp. 295–300.

[3] S. M. Alamouti, "A simple transmit diversity technique for wireless communications", *IEEE J. Selec. Areas Commun.*, vol. 16, no. 8, 1998.

[4] Y. Nakaya, T. Toda, S. Hara, J. Takada, and Y. Oishi, "Array and diversity gains of an RF-AAA used on MIMO receiver", in *6th Int. Symp. Wirel. Pers. Multimed. Commun.,* Yokosuka, Kanagawa, Japan, 2003.

[5] Y. Hara, A. Taira, and T. Sekiguchi, "Weight control scheme for MIMO system with multiple transmit and receive beamforming", in *IEEE VTC 2003 Spring*, Jeju, South Korea, 2003, vol. 2, pp. 823–827.

[6] Y. Nakaya, T. Toda, S. Hara, and Y. Oishi, "An RF-adaptive array antenna incorporated in a MIMO receiver under interference", in *IEEE VTC 2004 Spring*, Milan, Italy, 2004, vol. 1, pp. 44–48.

[7] Y. Nakaya, T. Toda, S. Hara, and Y. Oishi, "MIMO receiver using an RF-adaptive array antenna with a novel control method", in *Proc. ICC 2004*, Paris, France, 2004.

[8] D. S. Shiu, G. J. Foschini, M. J. Gans, and J. M. Khan, "Fading correlation and its effect on the capacity of multielement antenna systems", *IEEE Trans. Commun.*, vol. 48, no. 3, 2000.

Sebastian Kozłowski was born in Warsaw, Poland, in 1980. He received M.Sc. degree in radioelectronics engineering from the Warsaw University of Technology (WUT), Poland, in 2004. His thesis concerned wideband phase shifters and multiport systems for measurements of scattering parameters. Since 2004 he is Ph.D. student at Institute of Radioelectronics, WUT. His current research interests include antenna techniques and MIMO systems.
e-mail: S.Kozlowski@ire.pw.edu.pl
Institute of Radioelectronics
Warsaw University of Technology
Nowowiejska st 15/19
00-665 Warsaw, Poland

Yevhen Yashchyshyn was born in Lviv, Ukraine, in 1957. He received his M.Sc., Ph.D. and D.Sc. degrees in radioelectronics and telecommunications from Lviv University of Technology in 1979 (Ukraine), Moscow Institute of the Electronic Machine Building (MIEM) in 1986 (Russia) and Warsaw University of Technology (WUT) in 2006 (Poland), respectively. In 1991 he obtained the Senior Scientist title. Until 1999 he worked at Lviv Polytechnic National University. Since 1999 he has been with the Institute of Radioelectronics, WUT, as an Associated Professor. His research interests are in the areas of antenna theory and technique, smart beamforming and design of communications antennas. He has published 2 monographs, over 150 technical papers and has obtained 6 patents.
e-mail: E.Jaszczyszyn@ire.pw.edu.pl
Institute of Radioelectronics
Warsaw University of Technology
Nowowiejska st 15/19
00-665 Warsaw, Poland

Józef W. Modelski was born in 1949 in Poland. He received M.Sc. in 1973, Ph.D. in 1978 and D.Sc. in 1987, respectively, all in electronics, at the Warsaw University of Technology (WUT), Poland. He received State Professor's title in technical sciences in 1994. Since 1973 Professor Modelski has been with the Institute of Radioelectronics, Warsaw University of Technology, holding in sequence all academic positions from teaching/research assistant to tenured professor. Since 1996 he has been Director of the Institute. In 1976/77 he spent one year in the USA as a Fulbright grantee. In 1986 for two years he joined the Braunschweig Technical University as a senior scientist. His research interests include the area of: microwave modulators and shifters with semiconductor and ferrite elements, dielectric resonators and their applications, ferroelectric and smart antennas for communication systems. He is the author of 4 monographs, over 250 technical papers. He acts as a consultant to industry and Polish government agencies. J. Modelski has been Senior Member of IEEE since 1990 and Fellow Member since 2001, a Member of MTT-S, AP-S and AES-S. Member of AdCom MTT since 2000, a member of Technical Committees MTT-17 and MTT-20. He was elected 2007 MTT-S President-Elect. He has been a member of the TPCs of MTT-S International Microwave Symposium and the European Microwave Conference since 1996; since 1995 he has been Chair of the International Conference on Microwaves, Radar and Wireless Communications MIKON. He is a member of numerous local conferences in Europe. He received many distinctions in Poland, including Awards of the Minister of National Education and the Minister of Science; he was also the recipient of IEEE Third Millennium Medal and the Walter Cox Award.
e-mail: J.Modelski@ire.pw.edu.pl
Institute of Radioelectronics
Warsaw University of Technology
Nowowiejska st 15/19
00-665 Warsaw, Poland

Paper

X-band coaxial monopole antenna with an additional metal screen

Maksym Khruslov and Vadym Pazynin

Abstract— The novel coaxial monopole antenna design with an additional metal screen is presented. The radiation characteristics of this antenna are investigated depending on a distance between the ground plane and additional metal screens, as well as on a size of the latter. Measured and calculated radiation patterns are compared within limits of the operative frequency band and their revealed distinctions are discussed. The antennas characteristics allow pronounce that it can be considered as a promising candidate for various practical applications both a single radiator and a composite element of antenna arrays.

Keywords— monopole antenna, near field, radiation pattern, FDTD technique.

1. Introduction

Monopole antennas have found the wide applications in wireless local area network (WLAN) systems [1], subsurface communication, geophysical exploration, biomedical telemetry, for mobile terrestrial and aerospace communication systems, etc. With respect to the class of coaxial monopole antennas there is a possibility to form the different conical radiation patterns by changing the architecture of the separate antenna elements, for example, a geometrical shape [2, 3] and size [4] of the proper monopole. It stimulates a search of new modifications of these antennas to improve their performance, as well as to design both the individual radiator and arrays with new qualities.

The main objective of this research is the establishment of basic regularities of the radiation pattern formation with reference to the proposed novel design of X-band coaxial monopole antenna with an additional metal screen.

2. Theoretical and experimental methods

Numerical modeling has been carried out by the finite-difference in time domain (FDTD) technique, in which the exact "absorbing" conditions are used to solve a problem of the effective restriction of the computation space [5, 6]. The special software package developed allows one to compute all basic space-time and space-frequency characteristics of the axially-symmetrical radiators of both pulse and monochromatic waves.

Experimental investigations have been performed in the anechoic chamber by means of the method and software developed by us earlier [7] which provides a possibility to make signal processing and analyze the radiation pattern characteristics in real time over the entire operative frequency band (7.8–11.1 GHz) with a discrete of 10 MHz in every point of the receiving antenna position (the angular step is 0.5°).

3. Monopole antenna designs under testing

In this paper we present the results of theoretical and experimental investigations of radiation performances of the original monopole antenna consisting of the vertical monopole ($d_{r1} = \lambda/4$) with two screens, namely: ground plane with the radius R and additional metal screen with the radius C. The distance d_r between both screens has been as a variable parameter (Fig. 1). Some antenna prototypes with the parameters depicted in the Table 1 have been investigated to determine the effect of additional screen on the radiation characteristics of monopole antennas under testing.

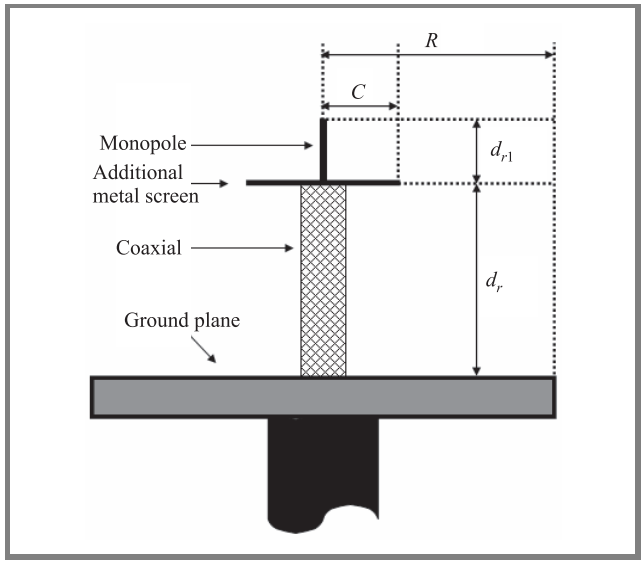

Fig. 1. Side view of the coaxial monopole antenna.

Table 1

Geometric parameters of antenna prototypes

Antenna N	1	2	3	4	5	6	7	8	9	10	11	12
d_r [mm]	19	30	7.5	15	19	22.5	30	7.5	15	19	22.5	30
C [mm]	10	10	10	10	10	10	10	15	15	15	15	15
R [mm]	∞	∞	230	230	230	230	230	230	230	230	230	230

4. Results and discussions

The analysis of calculated radiation patterns of antennas N1 and N2 with different distance between screens (Fig. 2) in the operative frequency band shows the availability of characteristic regions with sharp changing in the elevation angle of peak directivity due to the modes interaction of the open resonator formed by two plane metal screens. For both antenna prototypes we can mainly observe the monobeam radiation patterns with slow changing of the elevation angle of peak directivity with the frequency increase. So, for antenna N1 the elevation angle is changed from $\theta = 38^\circ$ to $\theta = 56^\circ$ in the frequency band $f = 7.80$–8.58 GHz. With the further frequency increase the elevation angle of peak directivity is not virtually changed and remains equal $\theta = 25^\circ$. Under these conditions the radiation pattern shape is not qualitatively changed too, although its beamwidth increases. In contrast to the antenna N1 for the antenna N2 the cut-off frequency between two frequency regions is shifted to the higher frequency ($f = 10.5$ GHz, see Fig. 2b). In this case we can also observe a change in the elevation angle ($\Delta\theta = 30^\circ$), whereas a beamwidth is not virtually changed in the limits of the frequency band under testing.

Thus, as it follows from the analysis of radiation pattern shape of the monopole antenna with an additional metal screen, the power radiation is concentrated in the main beam close to zenith unlike the conventional monopole antenna, and two frequency regions with different elevation angles of peak directivity are observed (Fig. 2). We emphasize that with the additional screen diameter increase the main beam of radiation pattern tends to zenith. The process of radiation pattern formation one may retrace on the near field pictures (Fig. 3). As can be seen from those, the main contribution in the radiation field of antenna gives the EM

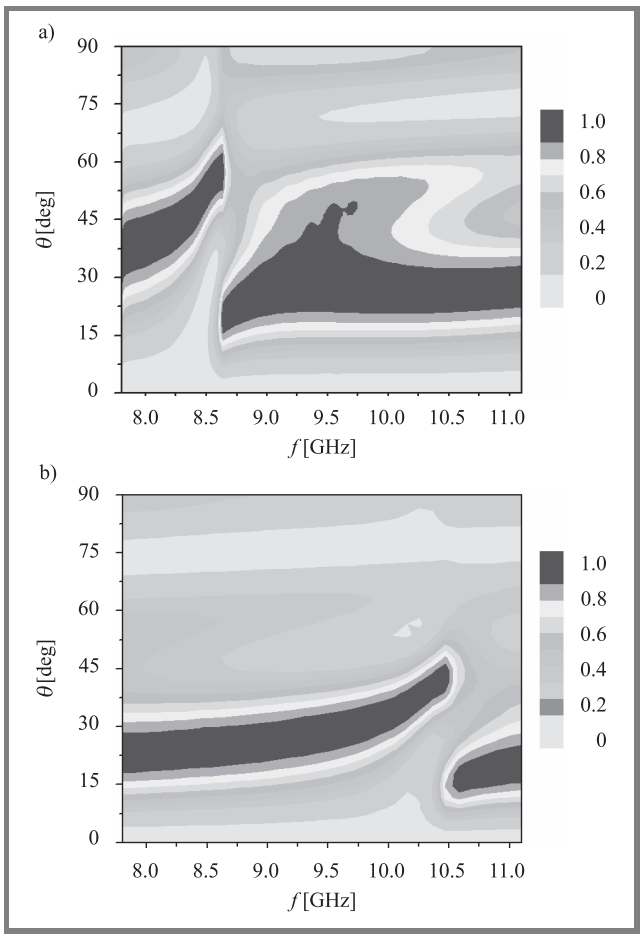

Fig. 2. Calculated radiation patterns normalized at the every fixed frequency: (a) antenna N1; (b) antenna N2.

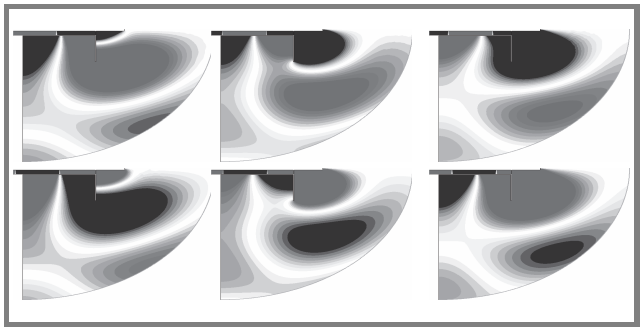

Fig. 3. Calculated near field distributions ($H\varphi$-component) highlighted in the successive time points of the antenna N1 at the frequency $f = 7.9$ GHz.

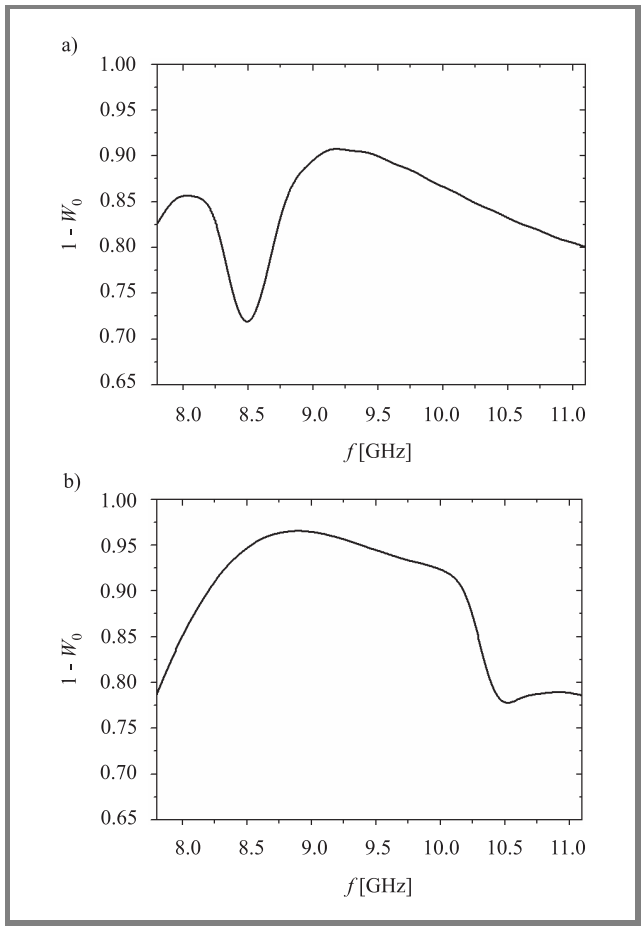

Fig. 4. Calculated antenna efficiency (W_0 is the power reflection coefficient from the antenna aperture): (a) antenna N1; b) antenna N2.

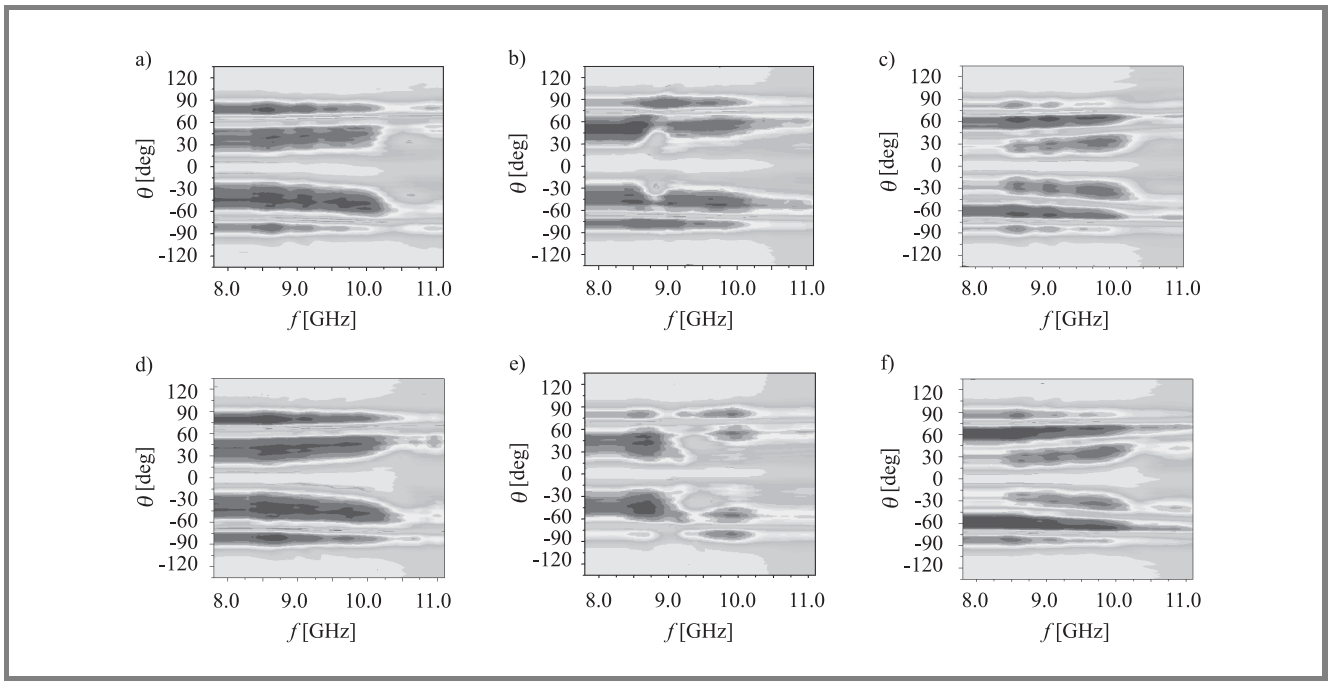

Fig. 5. Experimental radiation patterns of the following antenna prototypes: N4 (a); N5 (b); N7 (c); N9 (d); N10 (e); N12 (f).

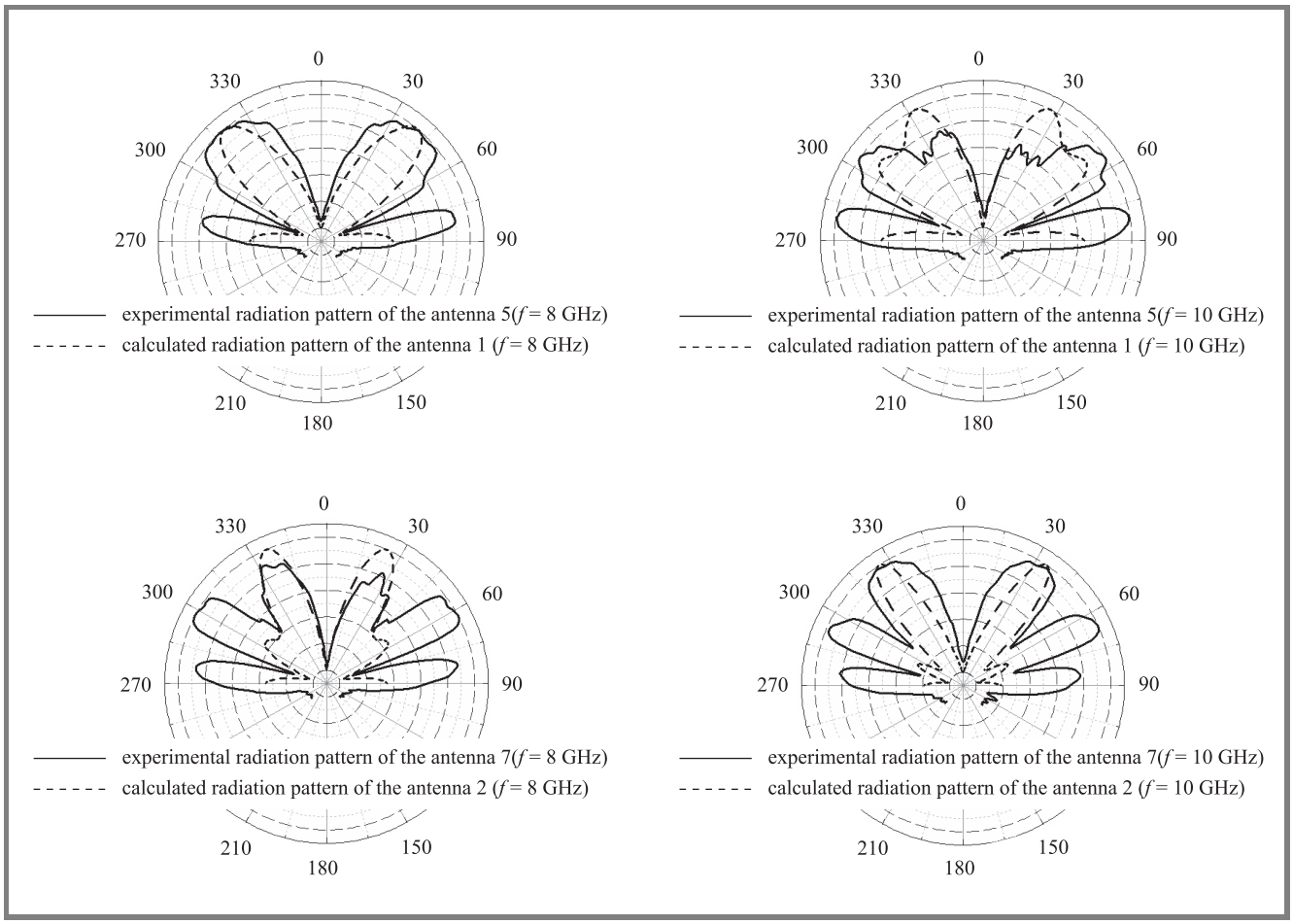

Fig. 6. Radiation patterns of some antenna designs.

field scattered from the additional metal screen and, correspondingly, the change in its diameter leads to the shift of the elevation angle of peak directivity from azimuth.

According to the calculations the antenna efficiency decreases with the additional screen radius reduce (Fig. 4) and maximal efficiency of antenna N2 reaches 97% (Fig. 4b). It is worth noting that the calculated efficiency of these monopole antennas indicates a visible degradation of antenna performance just in the aforementioned cut-off frequencies (Fig. 4).

Unlike the theory, the experimental radiation patterns of antenna prototypes under testing are found to be multibeam ones and the pronounced cut-off frequency regions also appear but they are weaker (Fig. 5). The most probable reason of the revealed discrepancy is the use of infinite ground plane in theory that does not permit to take into account the effect of its finite dimensions in experiment on the radiation pattern formation. It is quite reasonable to suppose that the finite ground plane availability will give rise to the appreciable contribution of EM field scattered from that in the radiation pattern formation. The comparison of measured and calculated radiation patterns at the fixed frequencies shows that they really differ by the radiation power in beams closer to the azimuth (Fig. 6). By choosing both a radius of the additional metal screen and a distance between this screen and ground plane (for example, antennas N5 and N7) one may obtain two-or three-beam radiation patterns. In this case both antennas demonstrate a good bandwidth (22–24%).

We note also one more feature of the presented antenna, namely the elevation angle change with an additional screen radius increase (Fig. 7). In other words, we can change the elevation angle of peak directivity in the wide limits with increasing a distance between the ground plane and the additional metal screen.

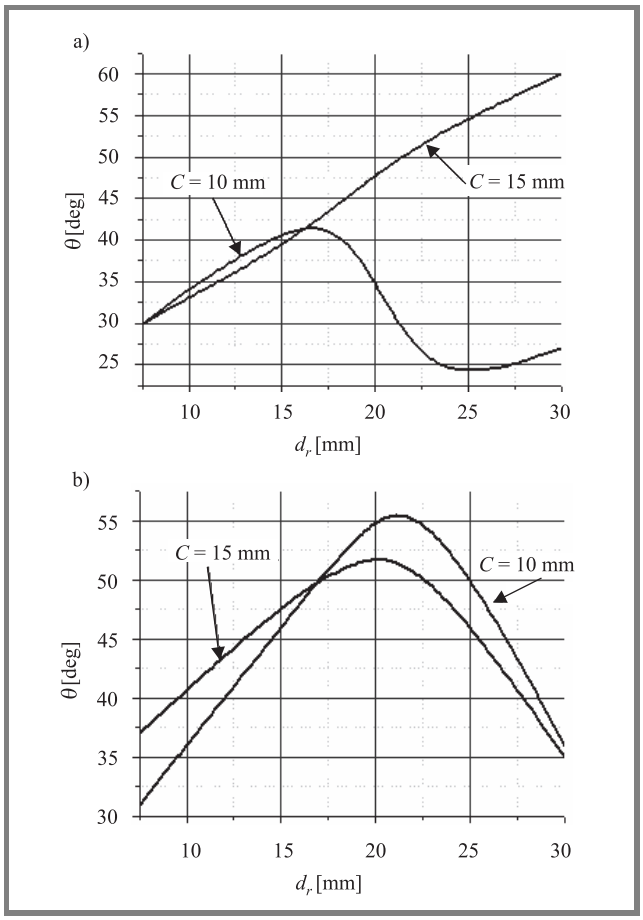

Fig. 7. The elevation angle of peak directivity versus the parameter d_r for antennas with different radius of additional screen C: (a) $f = 8$ GHz; (b) $f = 10$ GHz.

5. Conclusions

The novel broadband monopole antenna design with high efficiency is presented. It was found that the different conical radiation patterns can be formed by variations the distance between this screen and ground plane, as well as the additional screen radius. We note that the multibeam radiation patterns in experiment are formed due to the interference between the waves scattered from the finite ground plane and additional metal screen. A possibility of antenna operation in the dual-band mode has been shown. This original coaxial monopole antenna design can be used as a basic one in manufacturing the compact and effective antenna arrays due to its.

Acknowledgements

This particular research was performed in the frame of the STCU Project P#217 titled “Theory and design of antenna arrays”, and supported by the International Research Center for Telecommunications and Radar, Delft University of Technology, Netherlands.

References

[1] Y.-L. Kuo and K.-L. Wong, “Printed double-T monopole antenna for 2.4/5.2 GHz dual-band WLAN operations”, *IEEE Trans AP*, vol. 51, no. 9, pp. 2187–2192, 2003.

[2] M. J. Ammann and Z. N. Chen, “A wide-band shorted planar monopole with bevel”, *IEEE Trans AP*, vol. 51, no. 4, pp. 901–905, 2003.

[3] G. Kumar and K. P. Ray, “Wide-band planar monopole antennas”, *IEEE Trans. AP*, vol. 46, no. 2, pp. 294–295, 1998.

[4] D. N. Tam and R. H. MacPhie, “The admittance of a monopole antenna fed through a ground plane by a coaxial line”, *IEEE Trans. AP*, vol. 39, no. 8, pp. 1243–1247, 1991.

[5] Yu. K. Sirenko, “Modeling and analysis of transition processes in open periodical, waveguide and compact resonators”, *EDENA*, vol. 1, p. 363, 2003 (in Russian).

[6] Yu. K. Sirenko, V. L. Pazinin, A. I. Vyaz’mitinova, and K. Yu. Sirenko, “Compact inhomogeneities of free space: virtual boundaries in scalar and vector “open” initial boundary-value scattering problems of unsinusoidal electromagnetic waves”, *Electromagnet. Wav. Electron. Syst.*, vol. 8, no. 11-12, pp. 33–54, 2003 (in Russian).

[7] I. V. Ivanchenko, A. M. Korolev, N. Y. Lukyanova, and N. A. Popenko, “Broadband omnidirectional circular patch antenna”, in *17th Int. Conf. Appl. Electromagnet. Commun.*, Dubrovnik, Croatia, 2003, pp. 164–167.

Maksym Khruslov was born in Kharkov, Ukraine, in 1982. He received the M.Sc. degree in radiophysics and electronics from Karazin Kharkov National University, Ukraine, in 2004. Since 2004, he works in the Institute for Radiophysics and Electronics of the National Academy of Sciences of Ukraine, Kharkov, Ukraine, where he is currently an engineering with the Radiospectroscopy Department. His research interest includes the near-field technology, computational modeling of microwave antennas.

e-mail: ireburan@yahoo.com
Usikov Institute for Radiophysics and Electronics
National Academy of Sciences of Ukraine
Ac. Proskura st 12
Kharkov 61085, Ukraine

Vadym Pazynin was born in Kharkov, Ukraine, in 1977. He received the M.Sc. degree in radiophysics from Karazin Kharkov National University, Ukraine, in 1999. Since 1999, he was with the Institute for Radiophysics and Electronics of the National Academy of Sciences of Ukraine, Kharkov, Ukraine, where he is currently working toward the Ph.D. degree in physics and mathematics, in 2003. From 2003, he is researcher with the Department of Mathematic Physics. His current research interests are processes of radiation, propagation and scattering of the pulse electromagnetic waves.

e-mail: ireburan@yahoo.com
Usikov Institute for Radiophysics and Electronics
National Academy of Sciences of Ukraine
Ac. Proskura st 12
Kharkov 61085, Ukraine

Paper

Analysis and optimization of outputs of high power microwave tubes

Paweł Węgrzyniak, Wojciech Gwarek, and Dariusz Baczewski

Abstract— The subject of this work is optimization of outputs of L-band high power microwave tubes. These outputs are constructed as coaxial-to-waveguide transitions with a vacuum barrier in a form of glass or ceramic cup. The goal of optimization is to obtain sufficiently low reflection loss in the predefined frequency band and to avoid so called hot spots caused by excessive dissipation of microwave power in parts of the cup. Electromagnetic simulator has been applied to model the behavior of the optimized transition and to propose its optimum shape. The proposed solutions were verified by Z.E. Lamina SA in prototypes of high power (pulsed 600 kW) amplitrons and are to be used in manufacturing practice.

Keywords—high power microwave tubes, optimization of outputs.

1. Introduction

Design of reflectionless transitions between different waveguiding structures is one of typical problems of microwave engineering. The task becomes difficult when the input is supposed to be placed in vacuum and the output under the regular air pressure. In such a case the transition must incorporate a barrier which for technological reasons usually needs to be made of a high-permittivity dielectric. The difficulties are much amplified when high power is supposed to be transmitted through the transition. The chosen solution must assure suffiently low power dissipation in materials and sufficiently low electric field to avoid berakdown through ionized channels in air. Power dissipation and E-field intensity may rise sharply for resonant frequencies of the transition and thus avoiding of spurious resonances in the band of exitation of the structure is of major interest here.

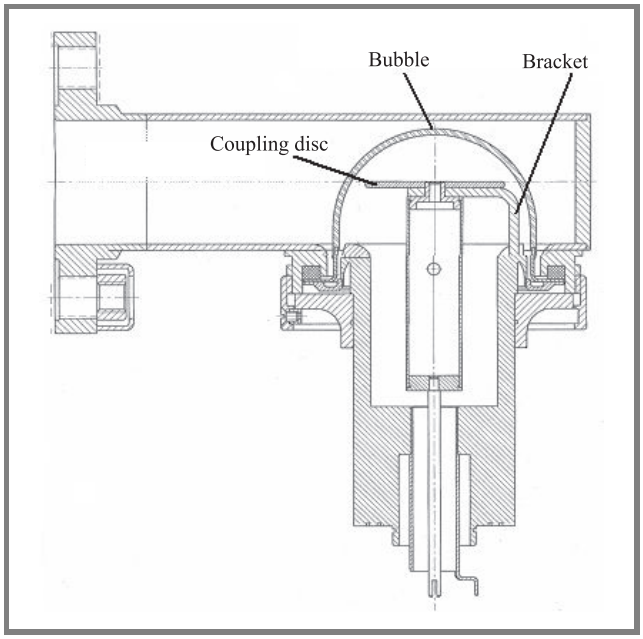

Fig. 1. Long section of the LM113 tube output.

The subject of this presentation is the investigation of the output of chosen high-power tubes of amplitron type [1, 2] manufactured by Z.E. Lamina SA. The tubes are supposed to work in L-band with the central frequency of 1340 MHz and used with a pulsed signal up to 600 kW. The long section of a typical transition considered is shown in Fig. 1. In the original Z.E. Lamina SA production the vacuum barrier was made of glass in a form of a glass bubble.

The manuafacturer found that in some cases hot spots are developed in the glass leading sometimes to the melting of the glas and thus to the damage of the tube.

The aim of this work was:

- to investigate the design options leading to elimination or reduction of the hot spots in glass;
- to investigate the possibility of replacing the glass barrier by a more heat-resistant alumina barrier (such replacing is difficult because alumina has higher permittivity and the cup must be thicker than one made of glass);
- to optimize the structure for lower reflections in the entire band of interest.

The investigation was based on full-wave electromagnetic simulations performed with QuickWave-3D [3] package. The modified structures were manufactured and tested.

2. Optimization of the structure with a glass barrier

The first of the considered structures was the output of LM113 tube manufactured by Z.E. Lamina SA presented in Fig. 1. It can be seen that in that coax-to waveguide transition a mixed magnetic-electric coupling is used. The magnetic coupling is assured by a copper bracelet connecting the inner conductor of the coaxial line with the waveguide wall. The electric coupling is controlled by the size of a copper disc placed at the top of the inner connector inserted into the waveguide. The vacuum barrier has a form of a glass bubble.

Extensive simulations of the structure were conducted. First they concerned the *S*-parameter characteritics versus frequency using the method of [4] (see Fig. 2). Then we

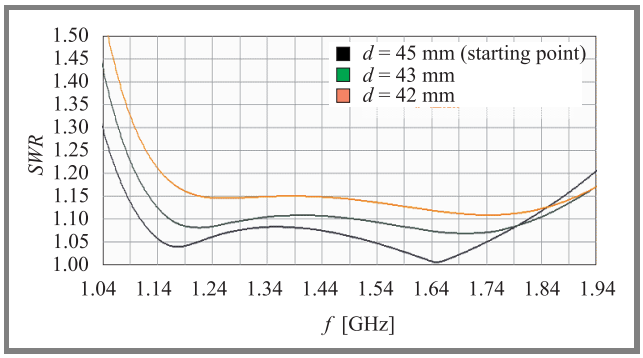

Fig. 2. Standing-wave ratio (*SWR*) versus frequency of the tube output with different ring size.

conducted a detailed study of the power distribution inside the glass. Examples of that study concerning the frequencies 1340 MHz and 1000 MHz are presented in Fig. 3. It should be noted that frequency 1000 MHz is placed outside the band of operation of the tube, but it is still below the cutoff frequency of the waveguide. We cannot

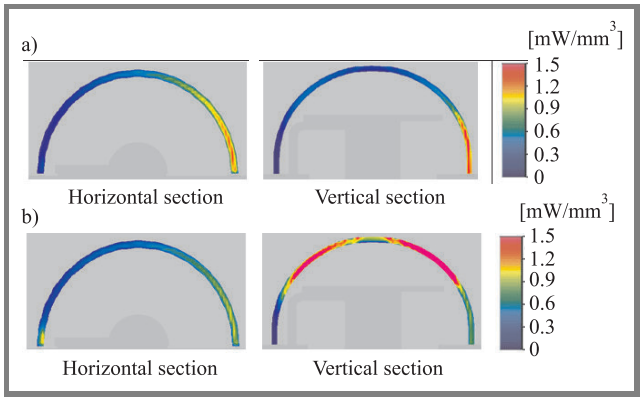

Fig. 3. Average dissipated power density at: (a) 1340 MHz and (b) 1000 MHz.

exclude some parasitic generation of the power by the tube in that band. From Fig. 3b it can be seen that such a generation (even at relatively low level) may cause damage to the tube.

The results of simulations were confronted with the experience of the manufacturer and the following conclusions were drawn.

- Overheating takes place at glass impurities when they appear in the area of high power dissipation.
- Damages in the upper part of the glass bulb are most probably caused by spurious generations of the tube outside the band of interest.
- Damages below the disc plane are due to the power dissipation during the normal, stable work.

The first two causes of possible problems are beyond the scope of this work. We have concentrated on the third cause concerning normal operation of the tube.

We first approached the tube optimization by assuming that three parameters can be modified: the radius of the disc, its position above the waveguide wall and the radius of the glass tube. We have found that the disc diameter of 43 mm produces is relatively good choice giving the hot spot power density reduced by about 15% and *SWR* still below 1.1 in the entire band. However the drop of 15% was judged insufficient for full safety of future tubes. That is why we have also conducted investigation of structures with non-circular discs. Very interesting results were obtained with a disc of the cardioidal shape as presented in Fig. 4.

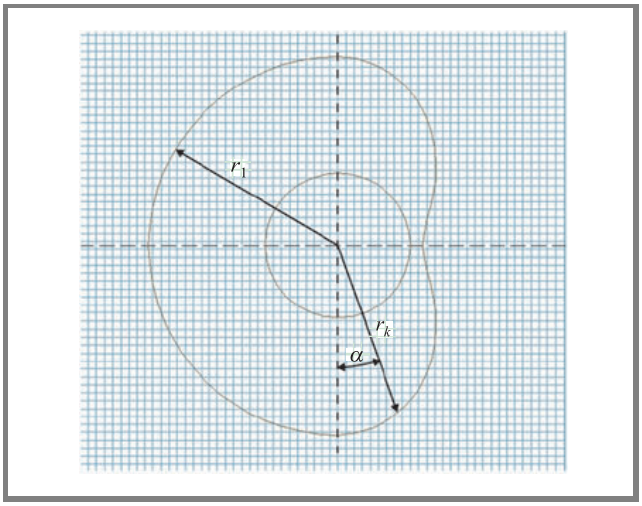

Fig. 4. Coupling disc of cardioidal shape.

Although *SWR* slightly increased (to 1.15 as shown in Fig. 5), the power dissipated in the hot spot dropped by 36%, as shown in Fig. 6.

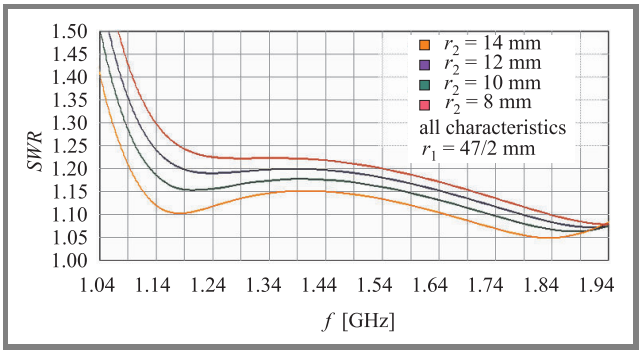

Fig. 5. *SWR* for LM113 output with cardioidal coupling part.

Above investigation was a basis for improvement of the glass barrier in the new types of tubes. Hardware prototypes of the new types have been tested and improvement of their properties has been experimentally confirmed. However it should be also mentioned that damages of the older

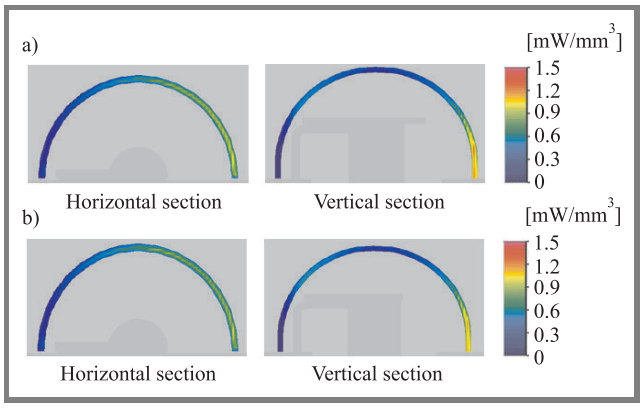

Fig. 6. Average dissipated power density, cardioidal: (a) $r_2 = 8$ mm and (b) $r_2 = 14$ mm.

types of tubes had incidental character and thus only a long-time observation of several copies of new tubes may be a proof that the problem has been completely solved.

3. Design of a structure with a ceramic barrier

Mechanical and thermal properties of alumina (Al_2O_3) ceramic are clearly superior to those of glass. Moreover alumina barrier shape can be made more repeatable in manufacturing. The main disadvantage of alumina is its high relative permittivity ($\varepsilon_r = 9.8$). The problems are amplified by the fact that it is difficult to make the ceramic cup very thin. Relatively thick material of high permittivity restricts the possibility of wideband matching and enhances the danger of spurious resonances of the structure. These problems caused that Z.E. Lamina SA had not been using the ceramic barriers for such purpose before this study.

We have run investigation of the possibility of application of a ceramic barrier under the same assumptions as in the case of the glass barrier. Examples of simulated $|S_{11}|$ versus frequency for different configurations of the structure are presented in Fig. 7. It was not possible to obtain sufficiently good matching in the entire band of interest (1240–1440 MHz) as it had been the case of the glass barrier. However in fact the entire band is divided into two sub-bands1240–1340 MHz and 1340–1440 MHz served by different types of tubes. Thus the manufacturer has judged that preparation of two types of the output for two different sub-bands is not a major practical problem.

Prototype of a tube with ceramic barrier has been manufactured by Z.E. Lamina SA and measured. Good results have been obtained as presented in Fig. 8. The heat dissipation properties were tested by measurements of the cooling air temperature versus average output power for both constructions of the tube. It was found that increase of the cooling air temperature above the room temperature was about 30% lower when alumina barrier was applied. Taking into account that alumina can work without damage in much higher temperature than glass this is a very promising result for manufacturing practice.

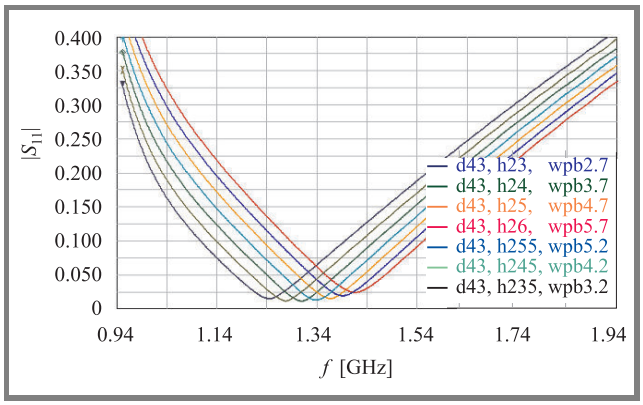

Fig. 7. $|S_{11}|$ for several different dimension configurations.

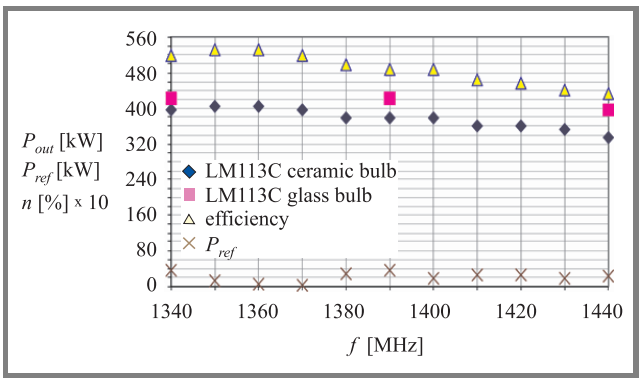

Fig. 8. Output power and efficiency obtained for the tubes with glass and ceramic barriers.

4. Modeling of the entire tube structure

So far we have treated the coax-to-waveguide transition as a stand-alone structure. This does not provide full picture of the physical setup. The transition is placed at the output of a complicated slow wave structure of the tube as shown in Fig. 9. We have used the 3D drawing provided by Z.E. Lamina SA to prepare a QW-3D model of

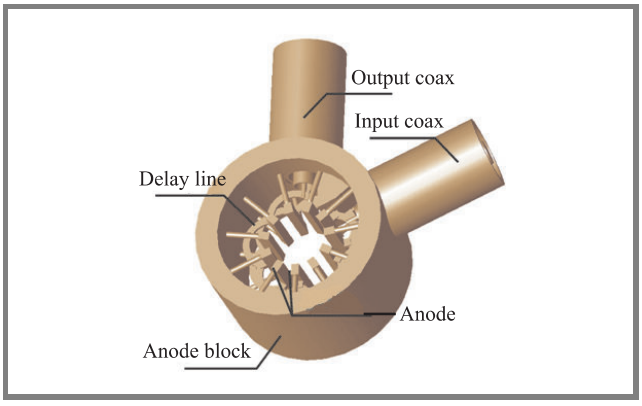

Fig. 9. 3D model of LM113 tube without outputs.

the entire tube. To increase the efficiency of calculations we have segmented the structure into three parts: input transition, slow wave structure and output transition. Each of the parts was calculated separately and the resulting S-matrices were combined using S-Converter [5] of QW-3D package.

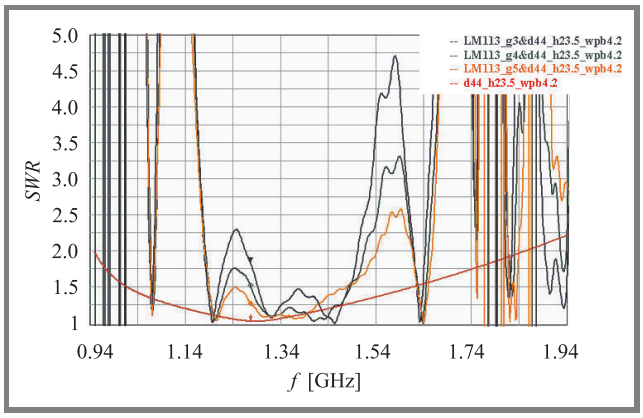

Fig. 10. *SWR* of the structure of whole tube calculated in QW-3D software.

Figure 10 shows calculated *SWR* of the entire structure. The results confirm good properties of the entire structure in the band of interest and indicate possibilities of further optimization. It should be noted however that these results concern so called "cold test" when the tube is not active and electron beam does not interacts with the electromagnetic wave. Relations between the "cold test" properties and actual properties of the tube during its normal operation are beyond the scope of this work.

5. Conclusions

The task of optimization of the output structures of L-band power amplitrons has been conducted. Electromagnetic modeling permitted better understanding of the physical phenomena concerning power dissipation in the coax-to-waveguide transitions used in the tubes. It helped to understand the cause of occasional damage by overheating of the glass bubbles used in the tubes. New design was proposed, manufactured and tested showing its superior properties with respect to earlier designs. Alternative output of the tube using an alumina barrier was designed and tested. It was the first time that such barrier was successfully applied to that kind of tubes. It was also shown that it is practically possible to model the entire structure of the tube comprising the input, output nd the slow-wave structure. This opens new possibilities of optimization of the design of the amplitron tubes.

References

[1] J. Hennel, *Lampy mikrofalowe*. Warsaw: WNT, 1976 (in Polish).

[2] R. Litwin and M. Suski, *Technika mikrofalowa*. Warsaw: WNT, 1972 (in Polish).

[3] *QuickWave-3D, Manual for the Software, Ver. 2.2*, Warsaw: QWED, 2003.

[4] W. Gwarek and M. Celuch-Marcysiak, "A differential method of reflection coefficient extraction from FD-TD simulations", *IEEE Microw. Guid. Wave Lett.*, vol. 6, no. 5, pp. 215–217, 1996.

[5] T. Ciamulski and W. Gwarek, "FD-TD analysis of microwave circuits using segmentation method with multimode transmission between segments", in *Int. Conf. Sig. Electron. Syst.*, Ustroń, Poland, 2000, pp. 375–380.

[6] P. Węgrzyniak, "Analysis and optimization of outputs of high power microwave tubes", B.Sc. thesis, Warsaw, Warsaw University of Technology, 2004.

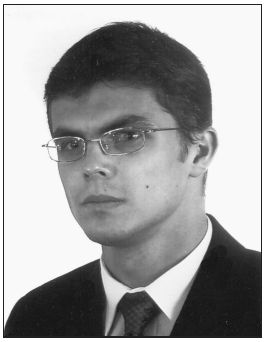

Paweł Węgrzyniak was born in 1980 in Poland. He received the B.Sc. in electronic engineering from Warsaw University of Technology, Warsaw, Poland, in 2004 and studying towards M.Sc. at Faculty of Electronics, Warsaw University of Technology. His research inerests are in the areas of electromagnetic modeling, microwave measurements, and design of microwave circuits.
e-mail: pwegrzyn@qwed.com.pl
Institute of Radioelectronics
Warsaw University of Technology
Nowowiejska st 15/19
00-665 Warsaw, Poland

Wojciech Gwarek graduated in 1970 from the Faculty of Electronics, Warsaw University of Technology, Poland, where he has been employed since. In 1973–74 he did postgraduate course at the Massachusetts Institute of Technology, USA (Center for Advanced Engineering Study) and received M.Sc. in electrical engineering. In 1977 he received his Ph.D. (honours) at the Warsaw University of Technology, and in 1988 became Associate Professor. He is a Full Professor since 1994. His academic activities included co-operation with several foreign institutions in USA, France, and Germany. In 1992–93 he was a co-organizer of the Franco-Polish School of New Information and Telecommunication Technologies in Poznań, directing the Electronics and Physics Department there. He is co-author of "The Theory of Electromagnetic Field" (WNT, 1978, 1985, 1990) – a textbook used by most Polish universities. He has also acted as an industrial consultant for several companies. Professor Gwarek's specialised field is microwave technology and electromagnetic theory. Since 1984 he has been concentrating on the time domain computational electromagnetics, becoming the world's recog-

nised expert. The achievements in this domain brought him the rank of Fellow of the IEEE. He is author of over 100 publications, mainly on electromagnetic modeling, including frequently quoted dozen of publications for the "IEEE Transactions on Microwave Theory and Techniques". He serves as reviewer for several IEEE Journals and as a member of the Technical Programme Committee of the IEEE International Microwave Symposia. Professor Wojciech Gwarek is co-author of QuickWave software, co-founder and President of QWED.

e-mail: W.Gwarek@ire.pw.edu.pl
Institute of Radioelectronics
Warsaw University of Technology
Nowowiejska st 15/19
00-665 Warsaw, Poland

Dariusz Baczewski was born in 1973 in Poland. He received M.Sc. in physics from Division of Solid State Theory in Institute of Physics, University of Łódź, Poland. He works in Z.E. Lamina SA since 2000, as a designer microwaves tubes.

e-mail: dbacz@lamina.com.pl
Z.E. Lamina SA
Puławska st 34
05-500 Piaseczno, Poland

Paper

On the ambiguity function for accelerating target in FMCW radar

Rafał Rytel-Andrianik

Abstract— In the paper, we are concerned with FMCW radar detection of an accelerating target, echo of which is buried in an additive white Gaussian noise. We derive and analyze three-dimensional generalized ambiguity function for target range, velocity and acceleration. We interpret known properties of this function and obtain new ones, which allows us to specify resolutions and regions of unambiguity for range, velocity and acceleration. The obtained resolutions we express in terms of corresponding Cramer-Rao bounds.

Keywords— FMCW radar, detection, ambiguity function.

1. Introduction

In the paper, we are concerned with a linearly frequency modulated continuous wave radar (L-FMCW radar) that transmits T-periodic constant amplitude signal with frequency linearly rising in each period. If we denote the carrier frequency by f_c and frequency modulation slope as α, the instantaneous frequency of a transmitted signal is $f_c+\alpha t$ for one period $-T/2<t<T/2$, and frequency deviation is αT. An illuminated target at range $r(t)$ backscatters the transmitted signal to the radar, where it is received and mixed with a copy of the transmitted signal.

The obtained beat signal is block processed, each block corresponds to $2K+1$ modulation periods. We assume in the paper, that within the time $(2K+1)T$ of a signal block (the measurement time or coherent integration time), the illuminated target is moving with constant acceleration with respect to the radar, thus the range is:

$$r(t)=r_0+v_0t+0.5at^2 \tag{1}$$

during the measurement time

$$-(2K+1)T/2<t<(2K+1)T/2. \tag{2}$$

In the range Eq. (1), the parameter $r_0=r(0)$ is target range in the middle of the measurement time Eq. (2), v_0 is target radial velocity for $t=0$, and a is target radial acceleration.

The beat signal is sampled with sampling frequency f_s omitting transients at the beginning of each modulation period. We denote the obtained discrete beat signal as $y(m,k)$ for discrete time within each modulation period $m=-M,...,M$ and modulation periods $k=-K,...,K$. This signal is sum of the useful component $Ae^{j\phi_0}x(m,k)$ (that is "template" $x(m,k)$ and complex amplitude $Ae^{j\phi_0}$) and an additive complex circular white Gaussian noise $n(m,k)$ of variance σ^2:

$$y(m,k)=Ae^{j\phi_0}x(m,k)+n(m,k) \tag{3a}$$

for

$$k=-K,...,K \quad \text{and} \quad m=-M,...,M \tag{3b}$$

Neglecting range walk, the template $x(m,k)$ of the useful signal can be approximated (see [3, 5]) as:

$$x(m,k)=\exp\{j(\theta_r m+b_v k+b_a k^2)\}, \tag{4}$$

where the parameters θ_r, b_v, b_a are normalized range, normalized velocity, and normalized acceleration, respectively:

$$\begin{aligned}\theta_r&=2\pi\tfrac{2\alpha}{cf_s}r_0,\\ b_v&=2\pi\tfrac{2f_cT}{c}v_0,\\ b_a&=2\pi\tfrac{f_cT^2}{c}a,\end{aligned} \tag{5}$$

where c is speed of light. From Eqs. (4) and (5) we see that the beat signal is (a) linear-phase with respect to the "fast time" m, and (b) quadratic-phase with respect to modulation period index, or "slow time", k.

In order to use a vector notation, we define the vector $\mathbf{y}$ containing all samples of the measured beat signal:

$$\begin{aligned}\mathbf{y}=[&y(-M,-K),\cdots,y(M,-K),\cdots,\\ &,\cdots,y(-M,K),\cdots,y(M,K)].\end{aligned} \tag{6}$$

Analogously, we define vector $\mathbf{x}$ of the useful signal template Eq. (4), and vector $\mathbf{n}$ of a noise component. The norm of vector $\mathbf{x}$ is $||\mathbf{x}||^2=(2M+1)(2K+1)$.

2. Detection and ambiguity function

In the detection problem we need to decide if the target echo is present in the received signal (hypothesis H_1: $\mathbf{y}=Ae^{j\phi_0}\mathbf{x}+\mathbf{n}$ as in Eq. (3)) or target echo is not present (hypothesis H_0: $\mathbf{y}=\mathbf{n}$). For the Neyman-Pearson criterion [4], we do the optimal test by calculating the test statistic D defined as:

$$D=\frac{1}{||\mathbf{x}||^2\sigma^2}\left|\mathbf{x}^H\mathbf{y}\right|^2 \tag{7}$$

and compare it with a threshold γ. If the threshold is exceeded we decide "target present" (H_1), if not we decide otherwise (H_0), that is:

$$D\underset{H_0}{\overset{H_1}{\gtrless}}\gamma. \tag{8}$$

The threshold is a function of designed probability of false alarm: $\gamma = -\ln P_{fa}$.

Calculation of the test statistic D (Eq. (7)) requires knowledge of $\mathbf{x}$ and, according to Eq. (4), knowledge of target parameters r_0, v_0, a. If these parameters are unknown, then we do multiple tests for a discrete set of hypothetical target motion parameters, specified on a certain grid. The question that here appears is how dense and how wide should this grid be. In order to answer this question, we use the ambiguity function concept.

We denote unknown true normalized target parameters as $[\theta_r^+, b_v^+, b_a^+]$, and useful signal template corresponding to these parameters as $\mathbf{x}(\theta_r^+, b_v^+, b_a^+)$. Using this notation and assuming that the target is present, we have $\mathbf{y} = Ae^{j\phi_0}\mathbf{x}(\theta_r^+, b_v^+, b_a^+) + \mathbf{n}$, and the detection statistic Eq. (7), calculated for hypothetical target parameters $[\theta_r, b_v, b_a]$, is

$$D(\theta_r, b_v, b_a) = \frac{1}{||\mathbf{x}||^2\sigma^2}\left|\mathbf{x}^H(\theta_r, b_v, b_a)(Ae^{j\phi_0}\mathbf{x}(\theta_r^+, b_v^+, b_a^+) + \mathbf{n})\right|^2. \quad (9)$$

Defining the ambiguity function as:

$$H(\theta_r - \theta_r^+, b_v - b_v^+, b_a - b_a^+) = \left|\frac{\mathbf{x}^H(\theta_r^+, b_v^+, b_a^+)\mathbf{x}(\theta_r, b_v, b_a)}{||\mathbf{x}||^2}\right|^2 \quad (10)$$

and signal to noise ratio as $\mathrm{SNR} = A^2||\mathbf{x}||^2/\sigma^2$, we may rewrite the test statistic Eq. (9) as:

$$D(\theta_r, b_v, b_a) = \left|\sqrt{\mathrm{SNR}\cdot H(\theta_r - \theta_r^+, b_v - b_v^+, b_a - b_a^+)} + n_1\right|^2, \quad (11)$$

where n_1 represents complex random value with Gaussian pdf $CN(0,1)$. The last equation means that probability of detection depends only on SNR, shape of the ambiguity function, and how close the hypothetical parameters $[\theta_r, b_v, b_a]$ are to the unknown true parameters $[\theta_r^+, b_v^+, b_a^+]$. The width of the main lobe of the ambiguity function tells us how dense should the hypothetical parameter grid be (radar resolution) and period of this function specifies size of the grid (region of unambiguous parameters). In next section we analyze the ambiguity function Eq. (10).

3. Analysis of the ambiguity function

Since in Eq. (11) we have only differences $\theta_r - \theta_r^+$, $b_v - b_v^+$ and $b_a - b_a^+$, we may assume for simplicity that true target parameters are all zeros, that is $[\theta_r^+, b_v^+, b_a^+] = [0,0,0]$. According to Eq. (4), we can rewrite the ambiguity function as:

$$\begin{aligned} H(\theta_r, b_v, b_a) &= \left|\frac{1}{(2M+1)(2K+1)}\sum_{m=-M}^{M}\sum_{k=-K}^{K}\exp\{j\theta_r m\}\right. \\ &\quad \left.\times\exp\{j(b_v k + b_a k^2)\}\right|^2 \\ &= H_r(\theta_r)\cdot H_b(b_v, b_a), \end{aligned}$$

where

$$H_r(\theta_r) = \left|\frac{1}{2M+1}\sum_{m=-M}^{M}\exp\{j\theta_r m\}\right|^2 \quad (12)$$

and

$$H_b(b_v, b_a) = \left|\frac{1}{2K+1}\sum_{k=-K}^{K}\exp\{j(b_v k + b_a k^2)\}\right|^2. \quad (13)$$

We see, that the ambiguity function is a product of function $H_r(\theta_r)$ dependant only on range, and function $H_b(b_v, b_a)$, dependent only on the movement parameters b_v, b_a. Thus, radar movement characteristics are, in this sense, independent of range characteristics. We will call functions $H_r(\theta_r)$ and $H_b(b_v, b_a)$ *range ambiguity function* and *movement ambiguity function*, respectively.

3.1. Ambiguity function with respect to range

The range ambiguity function $H_r(\theta_r)$ from Eq. (12) is a squared modulus of a rectangular window spectrum normalized in such a way that its maximum is equal to one:

$$H_r(\theta_r) = \left|\frac{\sin[(2M+1)\theta_r/2]}{(2M+1)\sin[\theta_r/2]}\right|^2. \quad (14)$$

The zero-to-zero width of the main lobe of this function is equal to $4\pi/(2M+1)$. Defining the range resolution $\triangle\theta_r$ as half of this value, we obtain:

$$\triangle\theta_r = 2\pi/(2M+1). \quad (15)$$

The density of the range grid on which the detection tests are done should not be smaller than $\triangle\theta_r$. Furthermore, the function $H_r(\theta_r)$ is 2π-periodic, thus the maximal unambiguous range is $0 \le \theta_r < 2\pi$.

3.2. Ambiguity function with respect to velocity and acceleration

The movement ambiguity function $H_b(b_v, b_a)$ defined in Eq. (13) is depicted in Fig. 2. It is more complicated than previously analyzed range ambiguity function $H_r(\theta_r)$. We cannot express this function in a simple form, but a few interesting properties can be derived directly from its definition Eq. (13).

Property 1 (maximum): The function $H_b(b_v, b_a)$ acquires maximum for $b_v = b_a = 0$, and this maximum is equal to 1. To prove it, we can easily check that $H_b(b_v, b_a) = 1$, and using the Schwartz inequality we have:

$$\begin{aligned} H_b(b_v, b_a) &= \left|\sum_{k=-K}^{K}\frac{1}{2K+1}\exp\{-j(b_v k + b_a k^2)\}\right|^2 \\ &\le \sum_{k=-K}^{K}\left|\frac{1}{2K+1}\right|^2 \\ &\quad \times \sum_{k=-K}^{K}\left|\exp\{-j(b_v k + b_a k^2)\}\right|^2 = 1. \end{aligned}$$

This property together with Eq. (11) means that for high SNR, the statistic $D(\theta_r, b_v, b_a)$ acquires maximum in the vicinity of true parameters $[\theta_r, b_v, b_a] = [\theta_r^+, b_v^+, b_a^+]$ and this maximum is approximately (because of noise) equal to SNR.

Property 2 (symmetry): It was shown in [1], that:

$$H_b(b_v, b_a) = H_b(-b_v, -b_a) = H_b(b_v, -b_a). \tag{16}$$

The property is illustrated in Fig. 1. Its intuitive interpretation is that positive and negative values of motion parameters (velocity and acceleration) are not much distinct from each other.

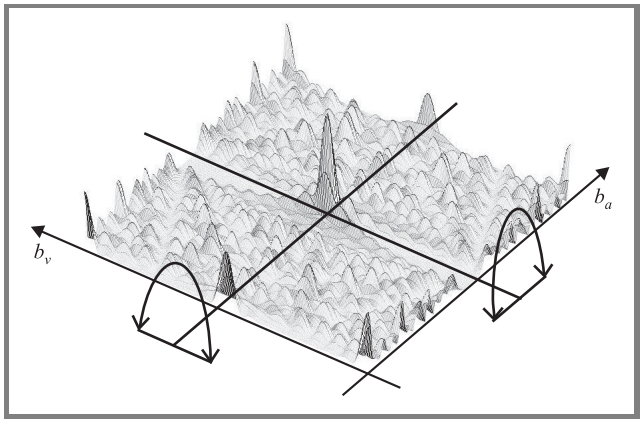

Fig. 1. Symmetry of the motion ambiguity function $H_b(b_v, b_a)$.

Property 3 (periodicity): It was also shown in [1], that

$$H_b(b_v, b_a) = H_b(b_v + \pi n_1, b_a + \pi n_2) \tag{17}$$

for integers n_1 and n_2 such that $n_1 + n_2$ is even.

This property means that periods of the ambiguity function are $(2\pi, 0)$, $(0, 2\pi)$, (π, π), $(\pi, -\pi)$, $(-\pi, \pi)$, $(-\pi, -\pi)$, $(0, -2\pi)$, $(-2\pi, 0)$. This periodicity is visible in Fig. 2a.

Property 3 allows us to find a region of unambiguous velocity and acceleration b_v, b_a. We do it by observing that if $[b_v, b_a]$ is in this region, then $[b_v + \pi n_1, b_a + \pi n_2]$ is not. We may notice that shape of this region is not unique. A few possible regions of unambiguous velocity and acceleration are depicted in Figs. 2b-e. For example in the Fig. 2b we have unambiguous velocity-acceleration region such that:

$$-\pi \leq b_v < \pi,$$

$$-\pi/2 \leq b_a < \pi/2. \tag{18}$$

We may notice that in Eq. (18), the maximal unambiguous velocity $\pm\pi$ is the same as in the constant velocity case when $b_a \equiv 0$. In other words, extending target range model to include acceleration, does not affect ambiguity of velocity measurement.

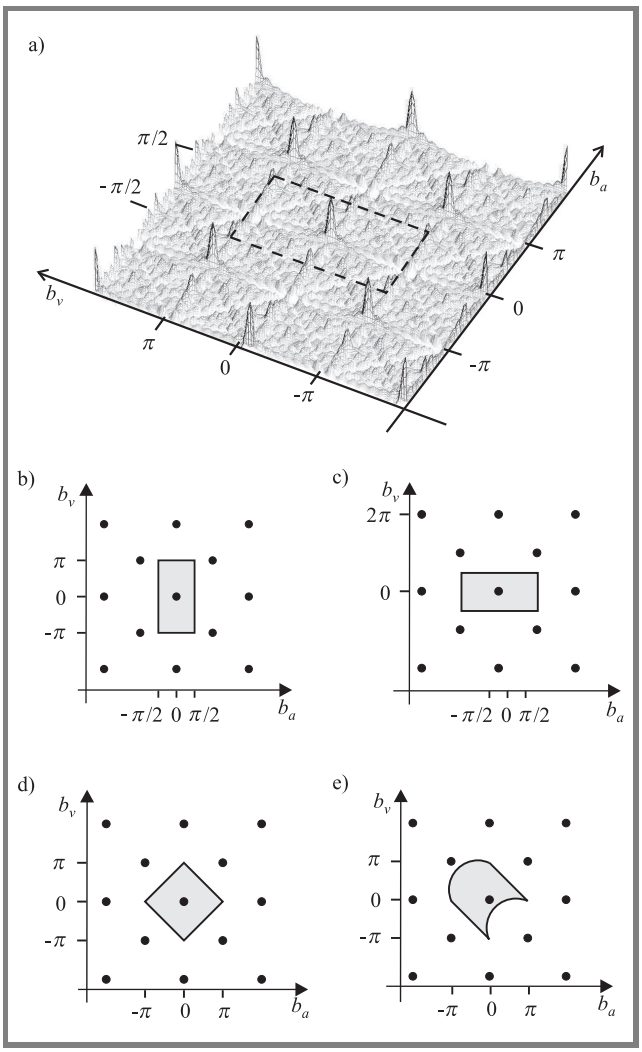

Fig. 2. (a) Plot of the ambiguity function $H_b(b_v, b_a)$ with marked unambiguity region corresponding to (b). Figures (b)-(e): a few examples of unambiguity regions for parameters b_v, b_a (dots symbolize periodically repeated maxima of $H_b(b_v, b_a)$).

It is worth noting that sidelobes for $b_a \approx \pi/2$ are very high and it would be difficult to use the whole range of unambiguous acceleration $-\pi/2 \leq b_a < \pi/2$ in a multi-target detection. Hence, the radar parameters should be chosen to assure that acceleration of a typical target is much smaller than $\pi/2$.

Property 4 (intersection for $b_a = 0$): Intersection of $H_b(b_v, b_a)$ for $b_a = 0$, that is $H_b(b_v, 0)$, is the squared modulus of the rectangular window spectrum.

This property can be derived directly from definition of function $H_b(\cdot)$. Thanks to this property we know that radar velocity resolution is

$$\triangle b_v = 2\pi/(2K+1) \tag{19}$$

and is the same as in the case of constant velocity target. Radar velocity resolution is illustrated in Fig. 3.

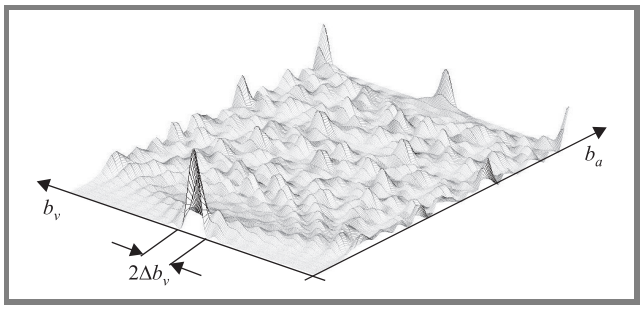

Fig. 3. Cross-section of $H_b(b_v, b_a)$ for $b_a = 0$ and radar velocity resolution $\triangle b_v$.

Property 5 (intersection for $b_v = 0$): If b_a is small, and K is big enough, then $H_b(0, b_a)$ is a function of $b_a(2K+1)^2$ only (not independently of b_a and K).
This property can be proved by approximating the function $H_b(0, b_a)$ with the corresponding integral:

$$\begin{aligned} H_b(0,b_a) &= \left| \frac{1}{2K+1} \sum_{k=-K}^{K} e^{jb_a k^2} \right|^2 \\ &\approx \left| \frac{1}{2K+1} \int_{-K-1/2}^{K+1/2} e^{jb_a t_1^2} \mathrm{d}t_1 \right|^2 \\ &= \left| \frac{1}{(2K+1)\sqrt{b_a}} \int_{-(2K+1)\sqrt{b_a}/2}^{(2K+1)\sqrt{b_a}/2} e^{jt^2} \mathrm{d}t \right|^2 . \end{aligned} \quad (20)$$

The last equality was obtained by setting $b_a t_1^2 = t^2$.
The main result of this property is that half of the main lobe width, that is radar acceleration resolution (see Fig. 4) is

$$\triangle b_a = 2\pi \frac{c_a}{(2K+1)^2} \quad (21)$$

for a constant c_a. Using computer simulations we showed that for half of a *minimum-to-minimum* main lobe width (we can call it radar acceleration resolution) $c_a \approx 3.676$. Hence, the non-normalized acceleration resolution is (from Eq. (5)): $\triangle a = 3.68\lambda/[(2K+1)T]^2$, where $\lambda = c/f_c$ is a wavelength. We may use this equation to decide if target acceleration should be taken into account in the detection test design. If expected maximal acceleration of a typical useful target is smaller than $\triangle a$ then we may neglect acceleration and assume constant velocity what corresponds to having only one acceleration cell centered at $a = 0$. If the acceleration is greater, then more acceleration cells should be created, otherwise, velocity spectrum would be smeared (see [6]) considerably reducing probability of detection.

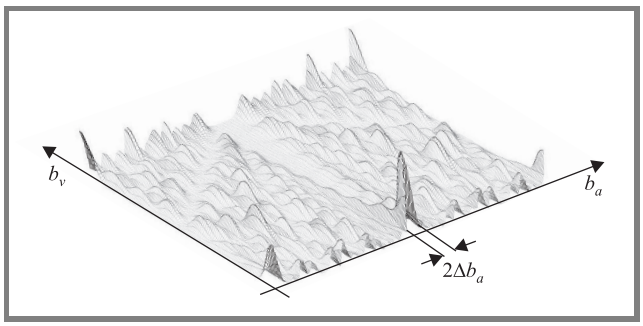

Fig. 4. Cross-section of $H_b(b_v, b_a)$ for $b_v = 0$ and radar acceleration resolution $\triangle b_a$.

Property 6 (relation to the Cramer-Rao bounds): Velocity and acceleration resolutions $\triangle b_v$ and $\triangle b_a$ are related to respective Cramer-Rao bounds $\mathrm{CRB}\{b_v\}$ and $\mathrm{CRB}\{b_a\}$ according to the equations:

$$\sqrt{\mathrm{CRB}\{b_v\}} = \frac{0.39}{\sqrt{\mathrm{SNR}}} \triangle b_v, \quad (22)$$

$$\sqrt{\mathrm{CRB}\{b_a\}} = \frac{0.41}{\sqrt{\mathrm{SNR}}} \triangle b_a. \quad (23)$$

According to [3] and [2], the Cramer-Rao bounds for normalized velocity and acceleration are:

$$\mathrm{CRB}\{b_v\} = \frac{6}{\mathrm{SNR} \cdot (2K+1)^2}, \quad (24)$$

$$\mathrm{CRB}\{b_a\} = \frac{90}{\mathrm{SNR} \cdot (2K+1)^4}. \quad (25)$$

The Cramer-Rao bounds $\mathrm{CRB}\{b_v\}$ and $\mathrm{CRB}\{b_a\}$ are lower bounds on variance of any unbiased estimator of parameters b_v and b_a, respectively. Hence, Eqs. (22) and (23) reveal proportionality of bounds on standard deviations to radar resolutions obtained from the analysis of the ambiguity function. It is interesting, that although cross sections of $H_b(b_v, b_a)$ across velocity and acceleration dimensions are quite different, the two proportionality coefficients $0.39/\sqrt{\mathrm{SNR}}$ and $0.41/\sqrt{\mathrm{SNR}}$ are almost the same.

4. Conclusions

We analyzed the ambiguity function for accelerating target. This allowed us to calculate radar resolutions and specify regions of unambiguous range, velocity and acceleration. We showed that due to choosing measurement time Eq. (2) symmetrical around $t = 0$, maximal unambiguous velocity and velocity resolution are the same for an accelerating target as would be in a constant velocity case. We also related radar resolutions to corresponding Cramer-Rao bounds.

References

[1] T. J. Abatzoglou, "Fast maximum likelihood joint estimation of frequency and frequency rate," *IEEE Trans. Aerosp. Electron. Syst.*, vol. AES-22, no. 6, pp. 708–715, 1986.

[2] B. Ristic and B. Boashash, "Comments on "The Cramer-Rao lower bound for signals with constant amplitude and polynomial phase", *IEEE Trans. Sig. Proces.*, vol. 46, pp. 1708–1709, 1998.

[3] R. Rytel, "Estymacja parametrów ruchu obiektów wykrywanych przez radar FMCW", Ph.D. thesis, Warsaw, Warsaw University of Technology, 2005 (in Polish).

[4] H. L. Van Trees, *Detection, Estimation and Modulation Theory*. Part I. New York: Wiley, 1968.

[5] A. Wojtkiewicz and R. Rytel-Andrianik, "Optimal detection and estimation in FMCW radar", in *Proc. Conf. MIKON 2002*, Gdańsk, Poland, 2002.

[6] A. Yasotharan and T. Thayaparan, "Strengths and limitations of the Fourier method for detecting accelerating targets by pulse Doppler radar", *IEE Proc. Radar Son. Navig.*, vol. 149, no. 2, 2002.

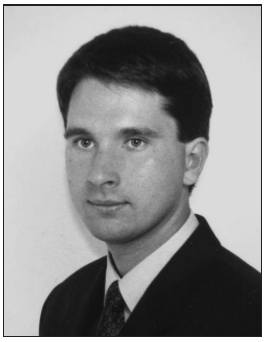

Rafał Rytel-Andrianik was born in 1975 in Otwock, Poland. He received M.Sc. degree in speech recognition, and Ph.D. degree in radar signal processing, both from the Warsaw University of Technology, Poland, in 1999 and 2005, respectively. His current interest concentrate around digital statistical signal processing.

e-mail: rrytel@elka.pw.edu.pl
Institute of Electronic Systems
Warsaw University of Technology
Nowowiejska st 15/19
00-665 Warsaw, Poland

Paper

Technologies for low cost small satellites

Krzysztof Kurek

Abstract— Paper presents short description of satellite structure and characterization of its subsystems. Review of technologies used in small satellite missions is presented, considering possible solutions in low cost projects. Three common solutions: the use of commercial off the shelf (COTS) components, miniaturization, remote testing and integration of subsystems can be used to significantly reduce cost of the satellite.

Keywords—small satellites, satellite systems, space technology.

1. Introduction

Satellite industry is one of the most dynamically developing discipline of world economy, beside of satellite communications other applications, like navigation and positioning systems, observation of the Earth and space, stay more important [1]. Last years it is observed increase of interest of small satellites (mini- and microsatellites) placed in low Earth orbits (LEO), used specially in no communications applications. Small satellites although their small dimensions and mass do not differ from large ones, including practically the same systems and blocks and realizing the same functions. Classical satellites are large and expensive, and process of their building lasts for many years and requires vast financial expenditures that can be bear only by large organizations. Technology development leading to miniaturization of electronic elements has allowed to build small satellites that could be used in different applications [2, 3]. Short time of building and smaller costs of launch makes use of these satellites very attractive.
Small satellites can be used in many applications:

- **Earth observations**. Standard methods of observations using large satellites are expensive. Small satellite using proper instruments (cameras, sensors) can realize observations with large resolution.
- **Tests and verification of new technologies in space environment**. Because of cost and time of realization of a small satellite is considerably smaller, it is ideal to realize different tests of a behavior of units and materials in space.
- **Education and training**. It is a cheap method to educate engineers in area of space technology. Education process includes project, realization and tests of the satellite, launch, monitoring and control of the satellite in an orbit.
- **Military applications**.
- **Exploration of space**.
- **Special communications**.

Electronic elements working on the satellite have to meet specific requirements relating to miniaturization, energy savings, resistance to gravity load and radiation, reliability. Scientific research considering possibilities of use in small satellites of commercial off the shelf (COTS) components instead special space ones are done [4]. Use of these components requires proper system solutions, securing large reliability, but can significantly reduce cost of the satellite building, that is essential matter in short time and education missions, i.e., SSETI ESEO satellite [5].

2. Satellite structure

All systems of the satellite can be divided on two parts:

1. Payload – containing instruments, equipment, transponders necessary to realize mission of the satellite.
2. Satellite bus (space platform) – ensuring conditions to proper work of payload. Following subsystems can be identified:
   - mechanical structure – carriage, alignment of systems, shielding, heat dissipation, interface with launcher;
   - communication system (Comm) – realization of communication with ground stations and eventually with other satellites;
   - on-board data handling system (OBDH) – control and steering of all satellite systems;
   - attitude control system (ACS) – control of satellite orientation in the orbit;
   - electrical power system (EPS) – generation of voltages to supply all subsystems;
   - thermal system – control of temperature inside the satellite;
   - propulsion system – realization of orbit maintenance.

Satellite in the orbit is exposed on environment conditions that have influence on its subsystems:

- Gravity overload and vibrations during launch – all satellite subsystems have to work properly after such stress.
- Vacuum – problems with heat dissipation, degassing of some materials.

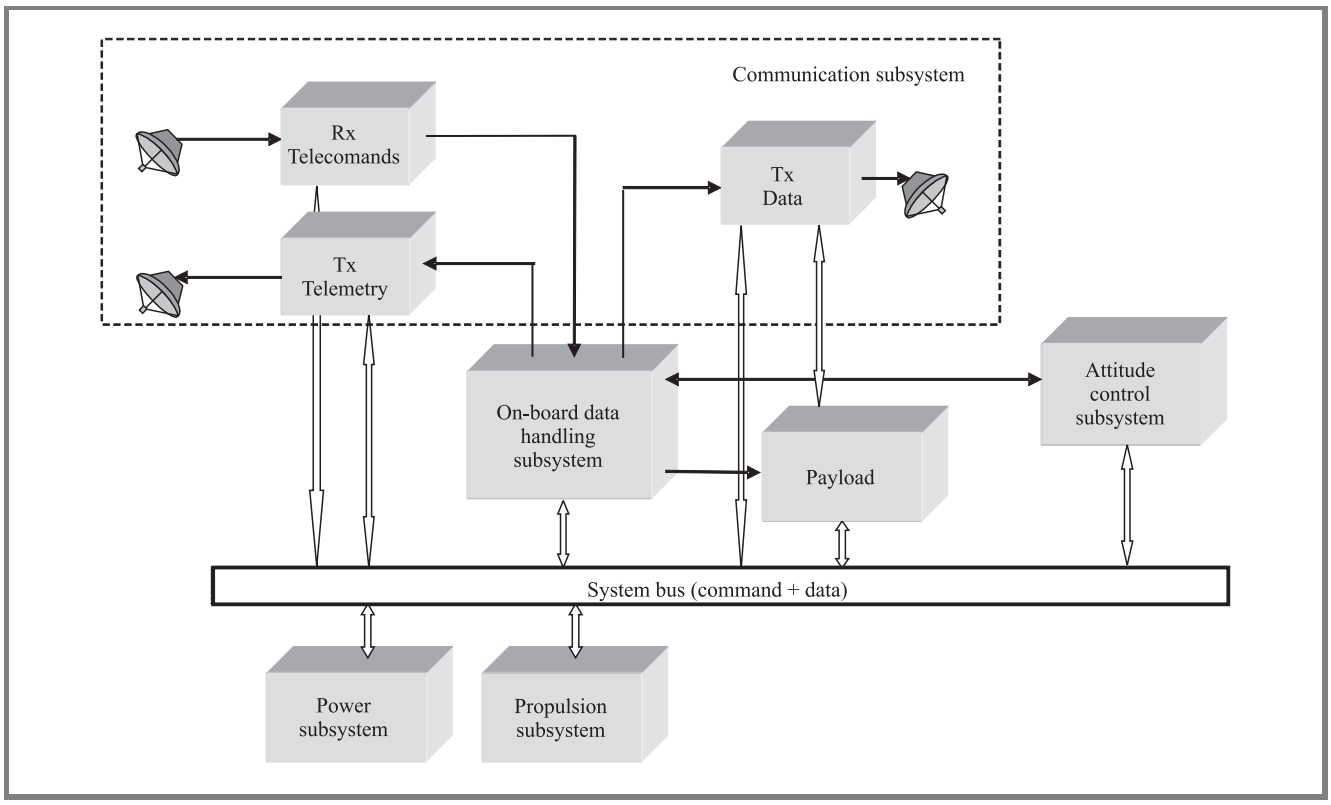

Fig. 1. Structure of the satellite.

- Radiation (large energy particles: electrons, protons, heave ions; electromagnetic wave) – causes errors in electronic circuits, specially in semiconductors (single event effects: SEL, SEU). Crucial parameter for semiconductors is total doze of accepted radiation, determining possibility of circuit failure. Level of radiation depends on orbit height, the higher orbit the larger radiation, but additionally around the Earth there are van Allen belts, where radiation is very high.
- High range of temperatures.

Connections between satellite subsystems are presented in Fig. 1. Communications between them is realized by system bus that allows OBDH to send commands to and receive telemetry data from all subsystems. Considering space environment conditions and impossibility of repair all satellite systems should be reliable and resistant to environmental stresses. Fulfilment of such requirements requires the use of elements able to work in space and proper system configurations. Systems important for satellite proper work are redundant (hot or cold redundancy).

On-board computer (OBC) of OBDH system controls and monitors proper operation of other subsystems, it realizes, by communications subsystem, communication with the ground control station receiving telecommands and sending telemetry data. Also ACS and payload can include computers supporting realization of main functions of these systems: respectively attitude control and correction and payload data processing. In low cost noncommercial missions, i.e., education, nanosatellites, there is often only one computer system on satellite, realizing functions of OBDH, ACS and recording of data from payload.

System bus allows to realize communications between satellite subsystems and have to guarantee high resistance to data distortions caused by space environment (radiation), therefore standards of serial transmission like CAN, RS-422, or I^2C in nano- and picosatellites, are commonly used.

In general payload can realize transmission and reception of data depending on mission principles (i.e., telecommunications satellites), but in earth observation and scientific missions data collected by payload are sent to the ground stations.

Depending on mission assumptions and aims configuration of satellite subsystems may be less or more complicated.

2.1. Mechanical structure

Satellite body must be light, simple and practical construction that can be adapted to requirements of different missions and launch rockets in easy way. It is build using aluminium or composite materials often as honeycomb structure. It should be modular construction easy to modification, with minimum number and variety of parts. All satellite systems are mounted to the structure and for different task realized by satellite different solutions are optimal (i.e., stacked panels, modules mounted to external frame).

2.2. Electrical power system

Solar arrays are main source of electrical power for satellite systems. In small satellites they are placed on its body, but in order to increase available power they can be also realized as deployable panels that are deployed after placing the satellite in the orbit. In such a case sun tracking system is not used, because of its necessary mechanical elements increase overall weight of the satellite. In order to maximize power obtained from the arrays for different illumination conditions and temperatures peak power track (PPT) systems are used.
Space qualified solar arrays are very expensive and terrestrial technology arrays are used in many low cost missions. Some modifications to improve arrays reliability and resistance to space environment must be considered. The solar cells are encapsulated between two layers of special polymer resistant to UV light and with good mechanical properties. Solar cells are built using two main single crystal materials:

- Si – wide use in space missions, efficiency: $\sim$10%;
- GaAs – higher efficiency: $\sim$20%, but larger weight and cost.

To increase of light conversion efficiency double and triple junctions cells can be used. Thin film photovoltaic (TFP) materials are other interesting solution [6]. Such materials have smaller efficiency, but they are chipper, flexible, more radiation resistant and have significantly smaller weight. Less mass of TFP solar arrays can significantly reduce weight and cost of satellite for certain missions. Additionally flexibility of these materials allows to build deployable panels in easy way – arrays can be rolled up during a launch and then deployed in an orbit.
When satellite is in the Earth shadow chemical battery must be used to allow proper continues work of satellite systems. Battery is charged during sunlight and special charge controller is used to protect the battery against overcharging and from other side against discharging. Regulation of power taken from the battery is realized by proper choose of modes of satellite systems (scheduling of tasks) in such a way that maximum power is taken when the battery is charged. When there is shortage of power, systems no critical for proper functioning of the satellite are switched off. Three main types of chemical batteries are mainly used in space applications:

- NiCd – high robustness and cycle life, but small energy density;
- NiH2 – larger energy density, high cycle life, pressure vessels;
- Li-ion – high energy density, more expensive, shorter cycle life.

In many missions in order to cost decrease terrestrial batteries, after tests of their proper operation in space environment, are used.

Voltage from the battery is used to generate all voltages necessary to supply all satellite systems, using switching mode DC/DC converters, and then distribute them to systems using separate lines protected by current tripping switches or by fuses.
Power system must be reliable and autonomous. Solar arrays are divided on independent modules and redundancy of electrical circuits is used to increase reliability. Simple logic unit, independent on OBDH, is used to control and monitor work of the system. Considering small weight and dimensions of small satellites (specially nanosatelites) the use of effective solar cells is critical factor. In addition other systems (antennas, payload) must be placed on the surface of satellite, that also limit size of solar array and results in significant power limitation for small satellites.

2.3. Communication system

Communication system realizes three communication channels with the Earth :

- telecommand channel (TC) – reception of commands steering work modes of satellite systems;
- telemetry channel (TM) – transmission of data about status of all satellite systems;
- payload/data channel – used to transmission of data obtained by payload.

Structure of transmitter/ receiver blocks responds standard solutions used in radiocommunication systems, but elements in satellite system must fulfil additional requirements coming from space environment conditions. For the sake of importance of communication with the ground control station for proper operation of satellite redundancy is used. Two receivers in TC channel operate simultaneously, and from two transmitters in TM channel only one operates (cold redundancy – in order to minimize power consumption by high power amplifiers). When the ground station does not receive telemetry data, it sends command to switch on second transmitter.
Transmission in TC and TM channels is realized using packet transmission with bitrate up to a few tens kilobits. In many cases (specially in nanosatellites) standard radioamateur UHF bands are used. This allows to receive signals from the satellite by radioamateurs in different locations, and increase amount of data received from the satellite. Antennas used in TC and TM channels must have wide radiation patterns assuring communication with the satellite independently on its orientation. It is possible using one omnidirectional antenna or a few sector ones properly placed on the satellite body. Transmission in data channel is realized when the satellite is in operation mode and it has proper orientation, so high gain narrow beam antenna can be used to improve properties of the link. If the same antenna is used to transmission and reception of signals the use of diplexer to separate frequency bands of the transmitter and receiver branches in antenna output is necessary.

2.4. On-board data handling system

The OBDH system consists of on-board computer, system bus to communicate with all satellite system, and direct connection to communications system to realize telecommand receiving and telemetry transmitting. Considering OBC special configurations and solutions are used assuring required high reliability and robustness, because of errors in program and data can cause wrong operation of the satellite systems. For digital circuits in space radiation is the most danger, it can cause damages or distortions in processed, stored and transmitted digital data. Separate RAM memories are used for data and program, and start up program is stored in EPROM, that is more resistant to radiation. Memories are protected against radiation errors. Performed research has shown that radiation level and caused by it errors depend on orbit height. For LEO errors occur rarely as single bit distortion in single words. When large amount of data (long block) is stored in memory two bit errors in single word can be observed, but probability of such situation is much smaller.

Three solutions are commonly used to protect memory data: triple voting memory, error detection and correction (EDAC) memory, and block code protection of blocs of data.

For the satellite placed into low orbit total doze of radiation is small, bellow 20 krad, and COTS elements can be used instead of special space radhard versions. Many different microprocessors are used in space applications depending on specific and requirements of the mission: Intel PC family, power PC, single chip microprocessors. Using of software processors implemented in programmable structure (field programmable gate array – FPGA) is other interesting solution. It allows to integrate all OBC systems (microprocessor, data and program RAM, I/O interfaces, system bus controller) in single structure – system on chip [7].

Some technology aspects are important when the choice of microprocessor is considered: small power consumption, resistance against radiation (proper technology and supply voltage), good software support.

2.5. Attitude control system

The aim of ACS is assure proper orientation and stabilization of the satellite position with required accuracy that depends on mission requirements. Stabilization can be realized using passive or active methods. In passive system spin of the satellite or gravity gradient are used to attitude control. These are simple solutions, but their accuracy is small (range of a few degrees). To increase accuracy active methods are used. Such a system consists of sensors, actuators that allow to change the satellite orientation, and control system (often realized as a Kalman filter) that generates steering signals for actuators using data from sensors.

Sun sensors, magnetometers, gyroscopes, earth surface sensors are used as sensors, and momentum wheels, magnetic torques, jet and compressed gas propulsions as actuators.

Actuators, specially momentum wheels are large and massive devices considering small satellite point of view. Conventional wheel can have 10–15 cm diameter and 5–10 cm height, mass above 1 kg and power consumption of 10 W. It can be used in satellites that have weight larger than 20–30 kg. For smaller satellites gravity booms and magnetic torques can be used, but achieved precision of attitude control is smaller. When life of a mission is very short microjets can be used. For longer missions micro-wheels, using MEMS (micro-electro-mechanical system) technology [8] or/and high temperature superconductors (HTS) [9], can be practical solution. Such micro-wheels can be used to attitude control and also to energy storage instead chemical batteries. Using pairs of counter-rotating wheels integrated in one package energy can be added and extracted from them without changes of the satellite orientation.

Nowadays also multiple antenna GPS (global positioning system) receiver can be used to determine of the satellite orientation. Using three or more antennas differently paced on the satellite body calculation of the satellite attitude can be realized with accuracy better than one degree. GPS is also a source of reference time for satellite systems.

3. Technology trends

Technical research in area of realization of low cost small satellites should consider following aspects:

1. Miniaturization and integration of satellite systems allowing to decrease dimensions, weight and cost of the satellite:
   - new types of batteries and solar cells (i.e., thin film technology);
   - the use of MEMS systems (micro-propulsion, micro-momentum wheels, micro-cooling);
   - electronic modules:
     - new types of microwave components to the transmitter and receiver modules (small light filters, high efficiency power amplifiers, patch antennas);
     - the use of programmable circuits (i.e., FPGA) to digital signal processing (DSP) realizing baseband and IF signal processing in communications subsystem (modulators, demodulators, filters, distortion precorrectors); this will allow to realize all signal operations in one unit in digital form, excluding only RF module and A/D, D/A converters; changes of parameters of the received or the transmitted signal can be realized by software changes;
     - integration of on-board computer OBC in single chip (system on the chip solution) in FPGA structures.

2. The use of COTS elements and methods of increasing of reliability of modules used such elements. In order to minimize cost of the satellite system in low orbit COTS solutions are preferable in both areas: hardware and software. Specially it is essential in education missions when minimization of cost is critical issue. For assumption of short mission life it is an optimal solution. But using proper elements and system configurations (redundancy, environment ground tests) it can also be adapted to commercial longer life missions, allowing required system reliability.

3. Remote testing and virtual integration of systems using Internet. Integration systems and complex tests of the satellite are ones of more essential stages of its design. Correction of any errors found in this stage is expensively and tools to earlier detection of such errors and problems should be considered. The use of Internet to virtual communications between satellite systems will be good solution, specially when the satellite is realized in international cooperation. After implementation of interfaces between systems and Internet virtual testing can be performed and if results will be positive real integration will be realized.

4. Conclusions

Short overview of satellite structure and technologies used in small satellites has been presented. The use of such satellites is attractive in many different applications, i.e., Earth observation, in-space technology validation and education missions. Limitations of weight, dimensions and available electrical power require the use of proper technical solutions of satellite subsystems. In case of LEO satellites COTS elements are commonly used, allowing to significantly reduce cost of satellite. But this requires proper system configuration and realization of ground tests to verify proper operation of such elements in space environment. Tendency to minimize size and weight of satellite subsystems, keeping their performances, is other important factor in small satellite missions. In this case MEMS systems that can realize different functions, are very promising solution. Also the use of thin film photovoltaic materials in solar panels and high temperature superconductors in momentum wheels can create new possibilities.

References

[1] *Satellite Observations of the Earth's Environment: Accelerating the Transition of Research to Operations*. Washington: National Academies Press, 2003.

[2] H. P. Roeser, "Cost effective Earth observation missions – fundamental limits and future potentials", *Acta Astron.*, vol. 56, no. 1-2, pp. 297–300, 2005.

[3] S. R. Cvetkovic and G. J. Robertson, "Spacecraft design considerations for small satellite remote sensing", *IEEE Trans. Aerosp. Electron. Syst.*, vol. 29, no. 2, pp. 391–403, 1993.

[4] F. Bernelli-Zazzera, A. Ercoli Finzi, M. Molina, and M. Cattaneo, "In-orbit technology validation for a university microsatellite", in *Proc. 4th IAA Symp. Small Satell. Earth Observ.*, Berlin, Germany, 2003.

[5] Student Space Exploration and Technology Initiative (SSETI), http://sseti.gte.tuwien.ac.at/WSW4/eseo1.htm

[6] J. W. Tringe, "Trends in thin film photovoltaic technology development [for space application]", in *Proc. IEEE Aerosp. Conf.*, Big Sky, USA, 2000, pp. 61–68.

[7] T. Vladimirova and M. Sweeting, "System-on-a-chip development for small satellite onboard data handling", *J. Aerosp. Comput., Inform. Commun.*, vol. 1, no. 1, pp. 36–43, 2004.

[8] A. Peczalski, M. Elgersma, D. Quenon, and J. Jacobs, "Micro-wheels for attitude control and energy storage in small satellites", in *Proc. IEEE Aerosp. Conf.*, Big Sky, USA, 2001, pp. 2483–2492.

[9] E. Lee, "Microsatellite combined attitude/energy systems", *IEEE Aerosp. Electron. Syst. Mag.*, vol. 19, no. 4, pp. 27–32, 2004.

Krzysztof Kurek was born in 1970 in Poland. He received his M.Sc. and Ph.D. degrees in electronics engineering from Warsaw University of Technology (WUT), Faculty of Electronics and Information Technology, in 1996 and 2002, respectively. Since 2002 he is Assistant Professor of Institute of Radioelectronics, WUT. His research interests are in the radiocommunications and microwave technology areas: propagation in wireless systems, satellite communications and space technologies, mobile communications. Since 2001 he is a member of IEEE.
e-mail: k.kurek@ire.pw.edu.pl
Institute of Radioelectronics
Warsaw University of Technology
Nowowiejska st 15/19
00-665 Warsaw, Poland

Paper

MUPUS insertion device for the Rosetta mission

Jerzy Grygorczuk, Marek Banaszkiewicz, Karol Seweryn, and Tilman Spohn

Abstract— An original mechanical device designed to insert a penetrator into a cometary nucleus in an almost gravity-free environment is described. The device comprises a hammer and a power supply system that stores electrical energy in a capacitor. The accumulated energy is discharged through a coil forming a part of electromagnetic circuit that accelerates the hammer. The efficiency of converting the electrical energy to kinetic energy of the hammer is not very high (amounts to about 25%), but the system is very reliable. Additionally, the hammer energy can be chosen from four power settings, hence adjustment of the stroke's strength to nucleus hardness is possible. The device passed many mechanical, functional, thermal and vibration tests and was improved from one model to another. The final, flight model was integrated with the lander Philae and started its space journey to comet Churyumov-Gerasimenko in March 2004.

Keywords— comets, penetrators, hammering device.

1. Introduction

The European Space Agency (ESA) cornerstone mission Rosetta to comet Churyumov-Gerasimienko comprises the main spacecraft that will become a comet companion for at least half a year and the Philae lander [1]. Philae weights about 100 km and includes eight instruments that will measure chemical composition and physical properties of the comet [2]. Space Research Centre participates in the experiment MUPUS (multi-purpose sensors for surface and sub-surface science) [3, 4] that is dedicated to obtain temperature profile of nucleus' subsurface layers to a depth of 40 cm and thermal conductivity of cometary material. The experiment MUPUS is developed by a multinational team led by Prof. T. Spohn from the Muenster University.
The main engineering problems that had to be solved in the design phase were:

– how to insert a 40 cm long penetrator equipped with thermal sensors into the nucleus composed of a porous ice-dust mixture;

– how to deploy the penetrator and its insertion device to a distance of about 1 m from Philae, in order to avoid thermal perturbations caused by the lander.

In this short paper we will address the first issue only.
The cometary environment is very unusual and poses severe requirements on the instrument. First of all, the nucleus is a small body (2–3 km in diameter), with almost negligible gravity (more than four orders of magnitude smaller that on the Earth) and with low pressure and temperature, 10^{-6} bar and 130 K, respectively. The gravity-free condition does not allow using the lander body as an inertial support; it will recoil easily after each stroke of the insertion device, in agreement with the conservation of momentum in an isolated system. In the vacuum and low temperature on the nucleus it is very important to avoid cold-welding effect between metal parts of the device and carefully design all moving and driving subsystems (e.g., motors). Additional constraints are due to sparse lander resources: an average power assigned to MUPUS is 1.5 W, and the instrument should not weight more than 2 kg.

2. Device concept and development

The first issue to be decided about was what type insertion device would be used:

– a single impulse engine (rocket), powered by gunpowder, chemical fuel or high-pressure gas, or

– a multi-stroke system that would slowly insert the penetrator into the nucleus.

For safety reasons and because of uncertainty in our knowledge about the material strength of the nucleus, the first option was abandoned and the hammering concept was chosen. The Philae power supply system delivers energy to its instruments in a form of low voltage electric current. In order to execute hammer strokes energetic enough to penetrate the surface this power must first be stored in the insertion device and then released with maximum efficiency possible. Three kinds of energy storage systems were considered:

– mechanical potential (spring);

– mechanical kinetic (reaction wheel);

– electric (capacitor).

The capacitor has an advantage that there is no need to convert the supplying current to any form of mechanical energy and was, therefore, accepted. Following this choice, an electromagnet was implemented as the hammer accelerating subsystem. The static hollow cylindrical carcass made of iron forms together with a hammer an electromagnetic circuit. The discharge of capacitor converts the current energy to magnetic field and forces the hammer to move inside the iron cylinder to close the circuit.
After having solved the hammer engine problem, one has to consider the basic issue of how to design the mechanical system that would be able to continuously insert the penetrator into the cometary ground without supporting gravity.

The concept applied in the MUPUS insertion device employs three masses: the penetrator, the hammer and the counter-mass. The counter-mass is connected to the other masses with weak springs. A single stroke can be described as a sequence of events:

a) acceleration of the hammer;

b) forward motion of the hammer and slower motion of the (heavy) counter-mass backwards (from momentum conservation);

c) the hammer hits the penetrator and recoils;

d) the penetrator moves forwards, into the ground, the hammer and the counter-mass together move backwards;

e) the penetrator stops or moves backwards for a short time;

f) the counter-mass and the hammer stop.

Since the counter-mass is much heavier than the hammer and the penetrator tube, therfore it moves slower and the average force acting from it through the spring on the penetrator in stages (d) and (e) is much smaller than the forward force pushing the penetrator into the ground just after the hammer hit. In Fig. 1 the insertion scenario during a single

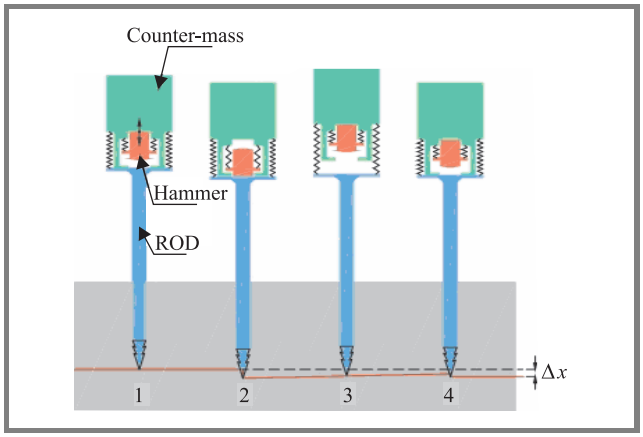

Fig. 1. Four phases of insertion during a single stroke: 1 – hammer acceleration; 2 – hammer hits the penetrator and recoils; 3 – the masses move backwards; 4 – the motion stops.

stroke is illustrated. The phase 1 in the figure corresponds to event (a) in the scenario. Events (b) and (c) are shown as phase 2, while events (d) and (e) are merged in the figure into phase 3. Finally, the last event (f) corresponds to phase 4.

In Fig. 2 time dependence of the force acting on the penetrator is shown. The energetic phase of penetration, in which the force exerted on the penetrator is large, is followed by a much slower (due to the counter-mass inertia) recoil that tries to pull out the penetrator with a much weaker force. If this latter force is below the level of friction/anchoring force between the medium and the penetrator, then the penetrator will not be pulled out of the ground during recoil. An elementary analysis of the efficiency of momentum exchange in hammer-penetrator collisions as well as of push in and pulling out forces acting on the penetrator from the counter-mass shows that the mass distribution between the penetrator, the hammer and the counter-mass should be close to the relation 1:1:10. In practice, the masses are limited by functional constraints, choice of material, geometry, etc., therefore it is difficult to reach the ideal proportions. In the final, flight model of MUPUS the penetrator weights 60 g, the hammer 30 g, and the counter-mass 350 g.

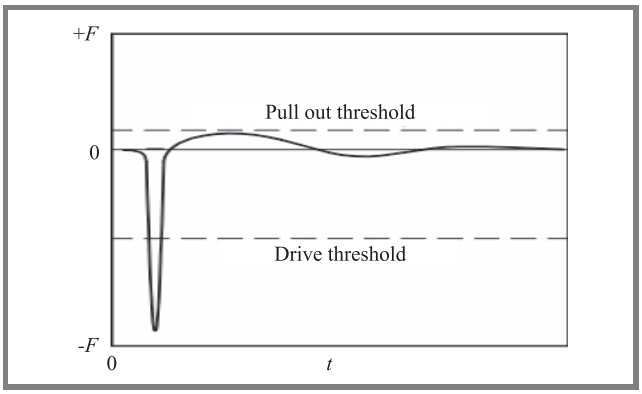

Fig. 2. Time dependence of the force exerted on the penetrator during a single stroke. The first part corresponds to the hitting of the penetrator by the hammer. The second part shows the pulling out force that acts during the recoil.

The last problem to consider is how to support the hammering device during the initial stage of insertion, when the penetrator is not yet stuck in the ground. Here, the deployment device composed of two expandable tubular booms comes to the rescue. It links the insertion device with the lander with a force of about 1 N that is strong enough to bring the penetrator tip back to the ground after the recoil following the stroke. The penetrator tip is equipped with a set of anchoring whiskers, which efficiently increase the resistance of the penetrator against the pulling out force.

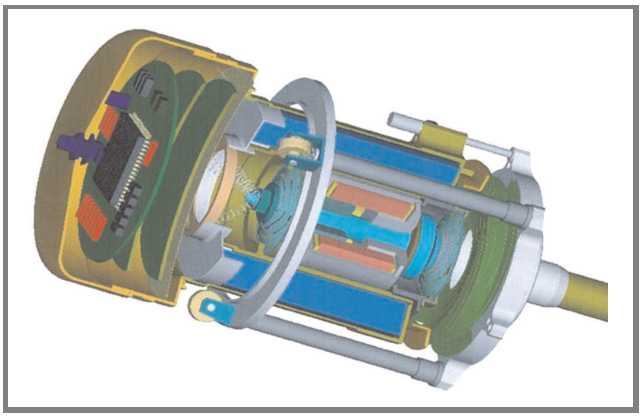

Fig. 3. Cross-section of the hammering device. Only the upper part of the penetrator rod is shown.

The cross-section of the hammering device is shown in Fig. 3. The housing contains the capacitor that surrounds the electromagnet with the hammer inside it. Above, there is an electronic compartment with the hammer controlling circuits and chips.

3. Performance and tests

The device was carefully tested, first at the level of subsystems (electromagnet, capacitor, mechanical part, etc.) then as a whole. The electromagnetic circuit was simulated by finite element method (FEM) and its parameters were optimized [5]. The most interesting were the functional tests of insertion into cometary like materials. Those were simulated by Ytong and solid foam blocks. To imitate the gravity free condition, the penetrator was suspended horizontally on a pair of strings (Fig. 4). The blocks were highly

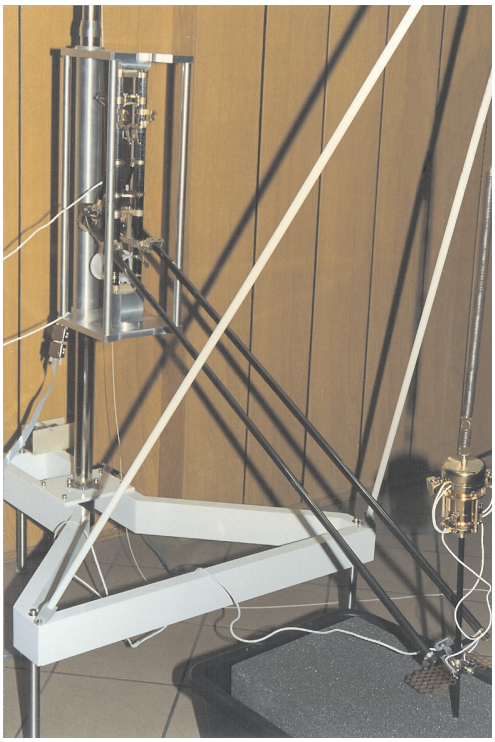

Fig. 4. The stand for functional test of the insertion device (left picture).

porous (up to 90%) that appropriately mimics cometary material but not at all weak; their compressive strength ranged from 0.79 MPa, through 1.75 MPa, to 5–7 MPa (for solid silica foam). The estimated strength of cometary nuclei vary from 25 kPa to 2.5 MPa. Since the test were passed successfully, one can assume that the hammering device would be able to insert the penetrator into the comet as well. The attempts to insert the penetrator into the ice were moderately successful. If its strength did not exceed 3 MPa, the penetrator worked fine. Above this limit, it could only be inserted to a certain depth and then got stuck in the ice.

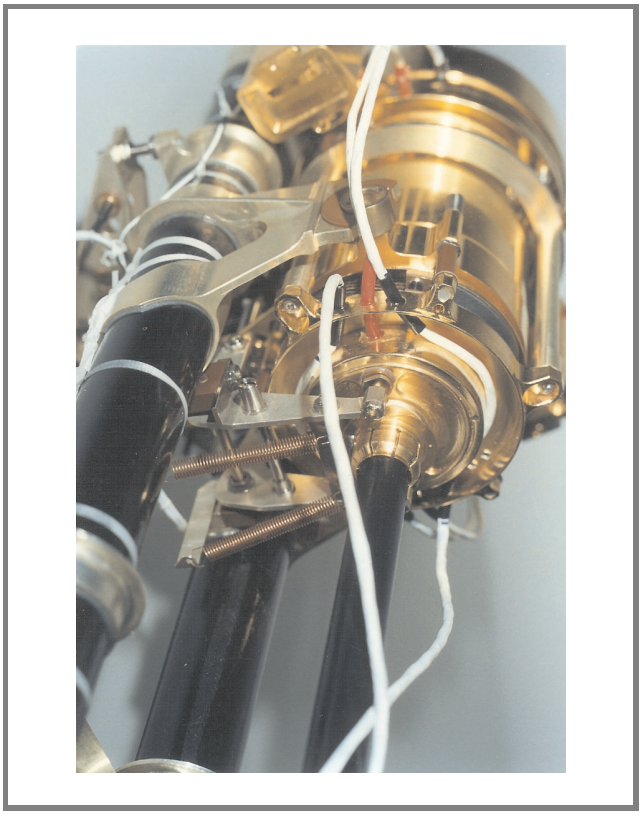

Fig. 5. The flight model of MUPUS insertion device in the stowed position on the lander balcony (right picture).

The functional tests of the insertion device were followed by several other tests of the whole MUPUS device: vacuum-thermal, electrical, vibrational, and electromagnetic compatibility (EMC). The most severe test were applied to the engineering model, so that the final flight model of MUPUS (Fig. 5) were subject to only moderately heavy loads and environmental tests.

4. Conclusions

The MUPUS is one of the most complicated space instruments developed in Space Research Centre. It is also the only so far designed and developed cometary penetrator. It took 6 years to develop the instrument, starting from the first conceptual study in 1996 till the delivery of the flight model to ESA in 2001. The insertion device described in this paper comprises only a pat of the whole experiment. It includes two other scientific elements: IR mapper that is placed on the lander balcony and accelerometer and temperature sensor located in the anchor that will be shot into the nucleus at the moment of landing. Those two units were developed by German and Austrian colleagues, respectively. What concerns Polish contribution, we developed the deployment device, thermal sensors for the pene-

trator, depth sensor to measure the insertion progress, part of the on-board and the whole hammer electronics, and flight software to control the experiment. The outcome of the tests are the data that are now used in computer simulations [6]. The involvement in MUPUS enabled the Polish team to gain the knowledge and expertise necessary to participate in most demanding space endeavors.

References

[1] ESA Rosetta mission, http://www.esa.int/esaMI/Rosetta/index.html

[2] DLR Resetta lander Philae, http://www.dlr.de/rs/forschung/roland/

[3] W. Marczewski *et al.*, "Prelounch performance evaluation of the cometary experiment MUPUS-TP", *J. Geophys. Res.*, vol. 109, pp. 1–17, 2004.

[4] T. Spohn *et al*., "MUPUS – a thermal and mechanical properties probe for the Rosetta lander Philae" (submitted to *Space Sci. Rev*.).

[5] A. Demenko, L. Nowak, W. Szeląg, and J. Grygorczuk, "Symulacja dynamicznych stanów pracy elektromagnetycznego urządzenia wbijającego do penetratora gruntu komety", in *Symp. PPEE*, Ustronie, Poland, 1997, pp. 104–109 (in Polish).

[6] K. Seweryn, M. Banaszkiewicz, M. Grunwald, J. Grygorczuk, and T. Spohn, "Thermal model of MUPUS penetrator", *Int. J. Heat Mass Trans.*, vol. 48, pp. 3713–3721, 2005.

Jerzy Grygorczuk has been employed at SRC-PAS since 1977. Has participated in the development of mechanical subsystems of satellite instruments for over twenty space missions, including Cassini, Rosetta and Mars Express. His field of interest include: aerospace mechanisms and mechanical properties of the soil of extraterrestrial bodies.
e-mail: jurekgry@cbk.waw.pl
Space Research Centre
Polish Academy of Science
Bartycka st 18a
00-716 Warsaw, Poland

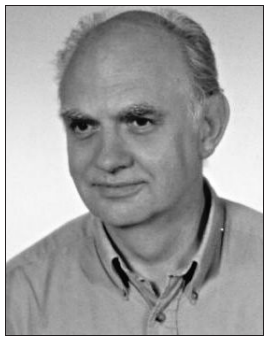

Marek Banaszkiewicz has graduated from Warsaw University, Poland, in solid state physics in 1968. He received a Ph.D. degree in theoretical physics (in 1982) and D.Sc. (habilitation in 2000) in astrophysics. He is a specialist in planetology and space physics and participated in several ESA missions: Cassini/Huygens, Ulysses, Rosetta, SMART1, Bepi Colombo.
e-mail: marekb@cbk.waw.pl
Space Research Centre
Polish Academy of Science
Bartycka st 18a
00-716 Warsaw, Poland

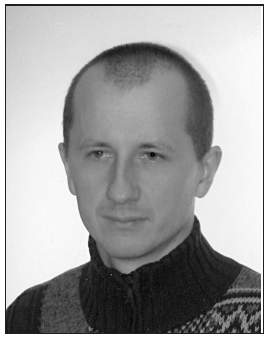

Karol Seweryn is currently a Ph.D. student in the Space Research Centre of the Polish Academy of Sciences, Poland. He received his bechelor's and master's of science degrees from Technical University of Kraków in 2003 in the automatics and robotics discipline. His main research interest are the dynamics and control of spacecraft and space robots. Other fields of activities are: spacecraft thermal control systems, finite elements analysis and mechanical engineering.
e-mail: kseweryn@cbk.waw.pl
Space Research Centre
Polish Academy of Science
Bartycka st 18a
00-716 Warsaw, Poland

Tilman Spohn
German Aerospace Center DLR
Rutherford st 2
12489 Berlin, Germany

Paper

Control and reconfiguration of satellite formations by electromagnetic forces

Roman Wawrzaszek and Marek Banaszkiewicz

Abstract— Current concept of interferometric missions assume that they employ formations of spacecraft. The cooperation between members of a multisatellite formation is a challenging problem. One of the main difficulties is to implement a reliable system for position control and actuation. A precise control of the position and orientation of each satellite in the array is a key factor in obtaining high quality images of distant objects. The controlling system should frequently collect data about geometry and kinematics of all array elements and use actuators to keep them as close as possible to their nominal positions. Forces that are required for actuation or array reconfiguration in space can be produced by engines of various types. In most cases chemical propulsion is used, with a drawback of limited fuel resources and a danger of polluting optical elements. In our work, we analyze dynamics of satellite formation flight, in which interaction forces result from electromagnetic fields generated by coils with current. We use simple controller equation proposed by members of MIT team to control a formation of two or three aligned satellites rotating around the array's mass center.

Keywords— electromagnetic formation flight (EMFF), satellite formations.

1. Introduction

Current concept of interferometric missions assumes that they employ formations of spacecraft. Optical (Darwin, Terrestial Planet Finder – TPF [1]) as well as microwave missions (TechSat21 [2]) are considered. The cooperation between members of a multisatellite formation is a challenging problem. One of the main difficulties is to implement a reliable system for position control and actualisation. In an interferometric mission, relative distances between array members have to be known with accuracy comparable with the length of detected waves. It means that for optical astrometry with micro-arcsecond resolution intramember distances have to be determined with an accuracy of at least 5 nm [3]. Measurements of relative positions with such accuracy are very difficult. Whatever sophisticated measurement (e.g., laser interferometry) and actuation systems are used, they have to operate permanently, to keep the required spacecraft configuration against perturbing forces (gravitation, solar radiation, etc.).

Apart from the problem of keeping the satellite formation in a stable but fixed state there is another one: how to reconfigure the formation by change the intersatellite distances or the plane of their motion. On the other hand, the stability of the formation should be continuously control against external perturbing forces, such as gravity of the Earth, magnetic field, etc. Both problems pose severe requirements on the control system that should be efficient, flexible and robust.

Following Miller and Sedwick [4], we consider the electromagnetic system of control and actualisation for a multisatellite interferometric mission. The system consists of a few (1–3) orthogonal magnetic dipoles located on each satellite and realized as coils (3 coils get possibility to obtain any resultant direction of magnetic field moment). In addition, flywheels acting as angular momentum storage are used. Kong *et al.* [1] describe such concept in detail.

2. Electromagnetic interactions and system controller

The elementary interaction of two coils is shown in Figs. 1 and 2. It results in producing both radial and transversal forces as well as twisting torques (equations on this figures).

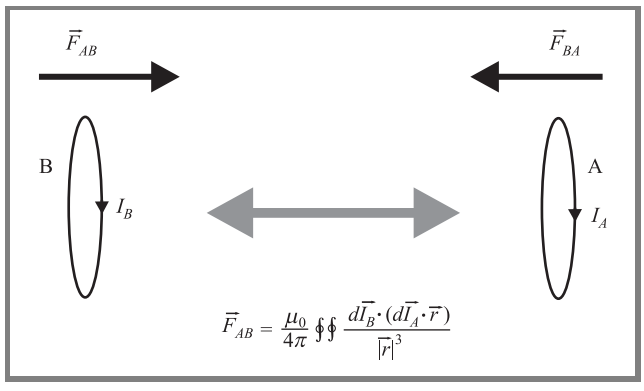

Fig. 1. Radial forces generated by electromagnetic coils.

It is not possible to get stable, static system based on electromagnetic forces only. The stabilising force has to be introduced. For a two-member formation, the stabilising factor can be centripetal force resulting from rotation of spacecraft around the common centre of mass [4, 5]. Such rotation, with an angular velocity Ω, corresponds to an

equilibrium but still unstable state of the system, therefore a specially constructed controller is needed.

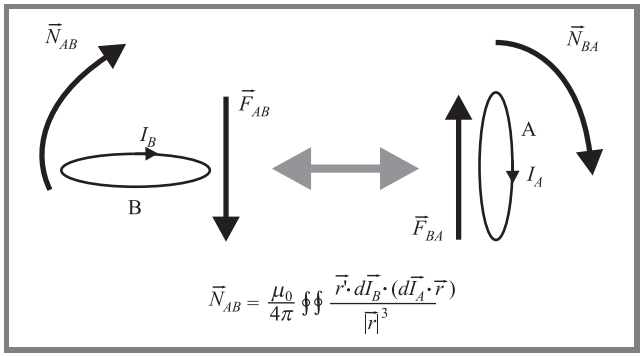

Fig. 2. Transversal forces and torques generated by electromagnetic coils.

After linearising the equations of motion about the equilibrium state and employing the minimum cost-function approach, the resulting equations for control parameter $\underline{u}$ read:

$$\dot{\underline{x}} = A\underline{x} + B\underline{u}, \tag{1}$$

$$\underline{u} = -K\underline{x}, \tag{2}$$

$$K = -\left[\frac{1}{2}\left(1+\sqrt{1+4\frac{\lambda}{\rho}}\right),\ \frac{1}{\sqrt{2\Omega}}\sqrt{1+\sqrt{1+4\frac{\lambda}{\rho}}}\right], \tag{3}$$

where the state vector $\underline{x}$ consists of differences from nominal values in radial distance and radial velocity components.

The only free parameter is λ/ρ. Stability analysis shows that one eigenvalue of linear system Eq. (1) has positive real part what means that nominal system is unstable.

3. Results

All simulations are made in MATLAB. The equations of motion are solved for a multi body system with objects interacting via electromagnetic forces. All calculations are performed in 3-dimensional space. Each object is represented by a 1 kg heavy coil of 1 m radius supplied with tuneable current.

3.1. Free space simulations

Figures 3 and 4 show simulation results for unstable system without controller. Each trajectory corresponds to a different initial separation error in the range from –20 to 20 nm. Actually, there is no possibility of obtaining a stable trajectory without using the controller. Even when the formation starts with the exact nominal values of parameters, the formation collapses or its members escape after about 2000 s. In the figures trajectories only one object are presented for clarity, the second one can be obtain by mirror transformation.

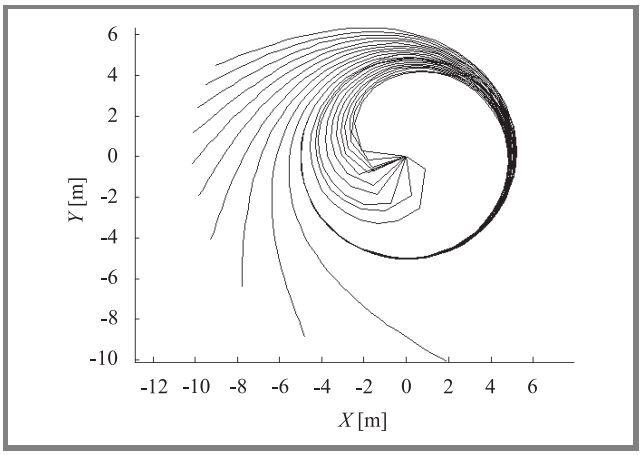

Fig. 3. Trajectories of two object formation member in the motion plane with different initial parameters.

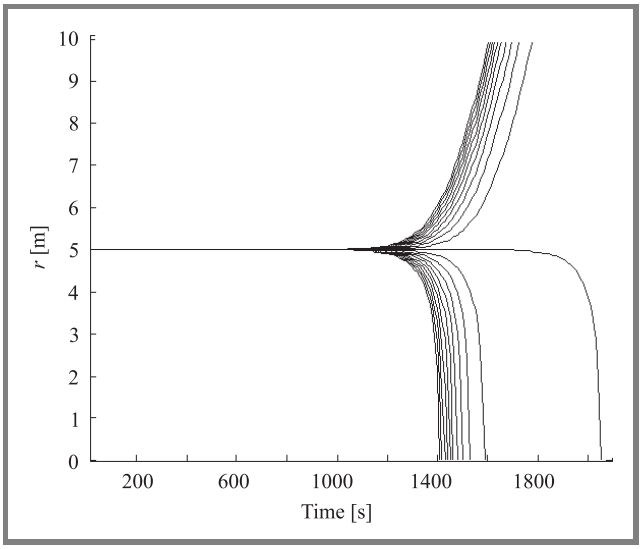

Fig. 4. Distance changes from common mass center for two object formation member with different initial parameters.

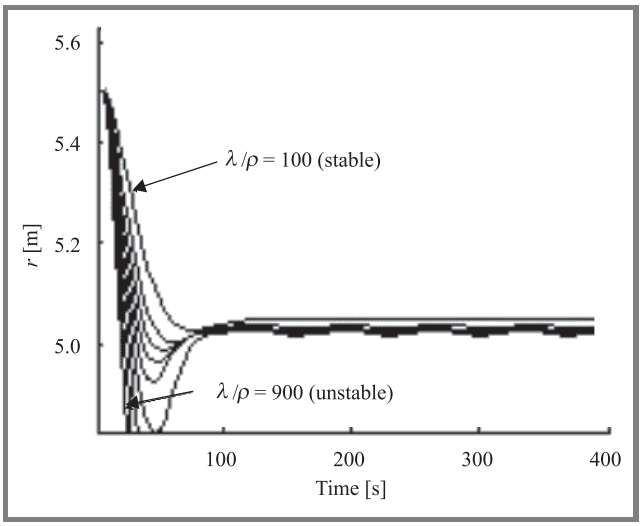

Fig. 5. Radial distance changes in time for different λ/ρ values (2 objects formation).

The control algorithm was tested for several values of control parameters. Controller efficiency as a function of time and a control parameter value is shown in Figs. 5 and 6.

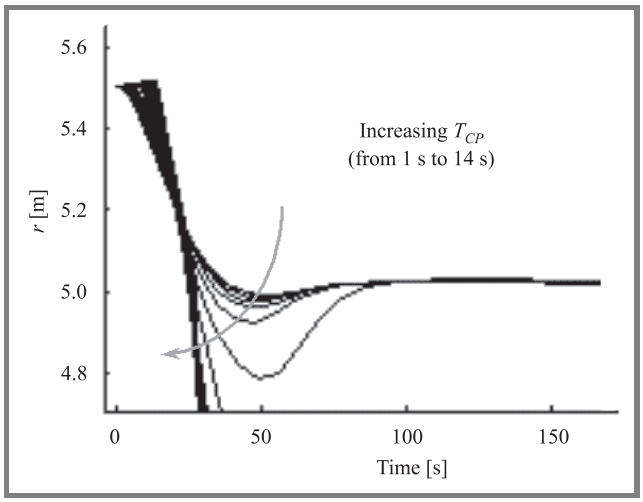

Fig. 6. Radial distance changes in time for different T_{CP} values (2 objects formation).

This example illustrates how the system returns to the nominal state when it starts from a configuration that is 10% larger than a nominal one (5 m distance of each satellite from the common centre of mass).
Figure 3 shows the change of the radial distance for different values of λ/ρ. This parameter represents a weighted combination of "penalty" parameters for displacement (λ) and control (ρ) errors; $\lambda/\rho = 0$ corresponds to the limit of infinitely expensive control. The instability at higher values of λ/ρ can be removed by decreasing the control step T_{CP}. Here, we use a discrete (realistic) control system, in which position measurements are taken and control variables actualised every T_{CP} seconds. As it is shown in Fig. 6, higher values of T_{CP} result in stability loss.

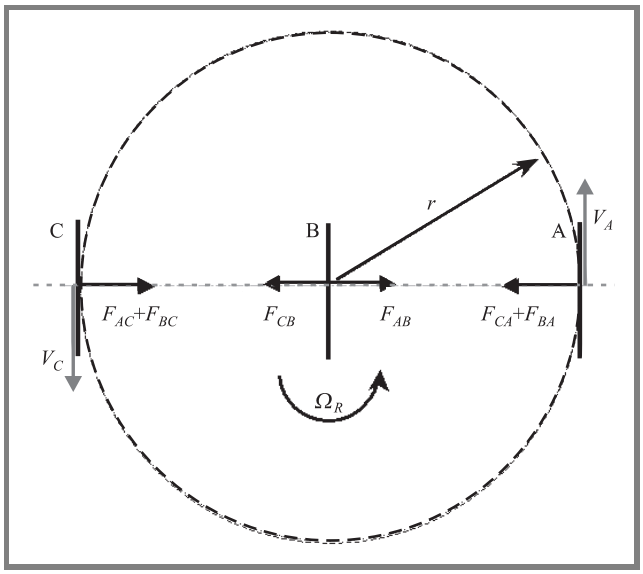

Fig. 7. Three rings on line – configuration view.

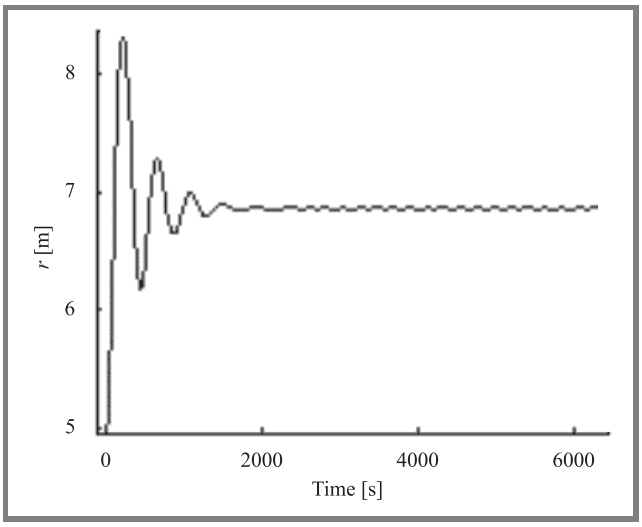

Fig. 8. Example of radial distance changes (r) in time for object A ($\lambda/\rho = 400$, 3 body system with controller).

A 3-body formation is a natural extension of the concept presented before. An example of the control performed for the 3-body linear configuration shown in Fig. 7 is presented (Fig. 8). All tests have been performed assuming that the formation is initially not so far from the nominal, equilibrium configuration.

3.2. Simple reconfiguration

Using the stability margin of a system with controller, we performed tests when intersatellite distance was gradually increased. In that case, we forced the controller to try to get

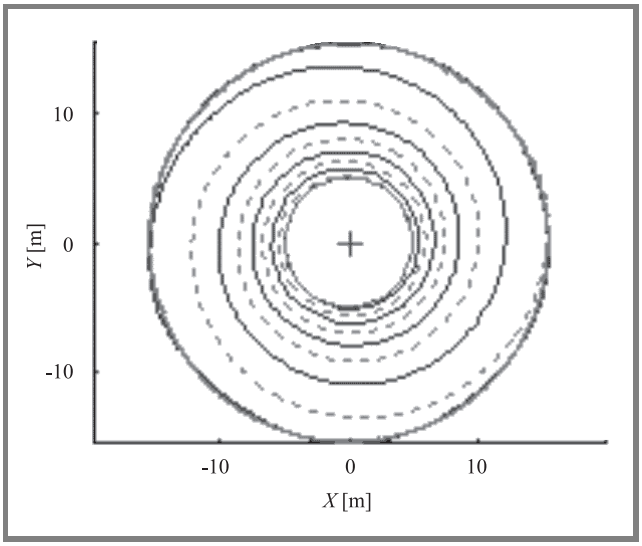

Fig. 9. Simulations with distance changing from 5 to 15 m – trajectories of 3 objects formation members in the plane of motion.

in each step a slightly increased target value by providing it with an artificial error signal. Using this method we made some successful simulations in both two- and three-body

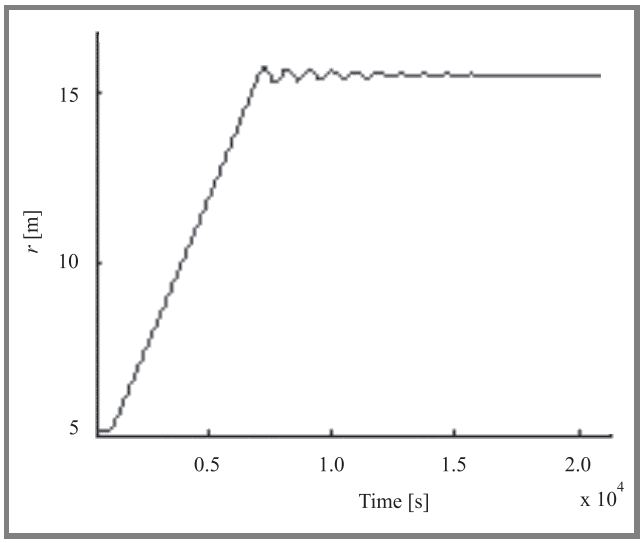

Fig. 10. Simulations with distance changing from 5 to 15 m – object A.

cases. Results of simulations with 3 coils are presented in Figs. 9 and 10. The cross in the centre of Fig. 9 represents the position of object B (see Fig. 7).

3.3. On orbit simulations

In analysing an electromagnetic formation on Earth orbit we neglect any forces but the first term of geopotential series (point mass). The comparison of uncontrolled motion, i.e., without magnetic forces – dotted line in Fig. 11, and trajectories with the control system acting (solid line in Fig. 11) shows that in second case the formation members can move on non-Keplerian, circular orbits, keeping a 5 m distance to the nominal (Keplerian) orbit. In other words: both objects stays at constant radial distances from the Earth that are 10 m apart. In-between a nominal orbit with 42 000 km radius is located.

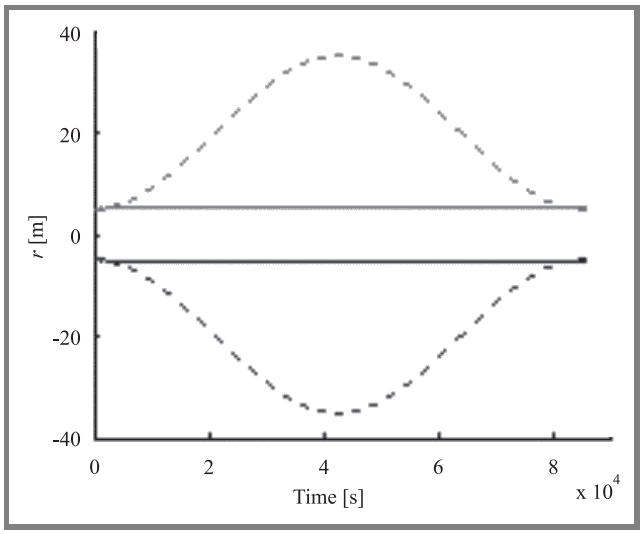

Fig. 11. On orbit simulations without (dotted line) and with (solid line) magnetic control system.

3.4. Comparison with interferometer missions requirements

The accuracy of the distance control can be found by calculating differences of resulting position with respect to the steady state value $r = f(t)$. For the analysed configurations the accuracy we found varies from about a few tenths of milimeter for a free flying formation case to a few centimeters in the in the Earth orbiting case. These values strongly depends on λ/ρ and T_{CP} parameters (Figs. 12 and 13). The results were obtained using a very simple model, hence many possible important factors were neglected.

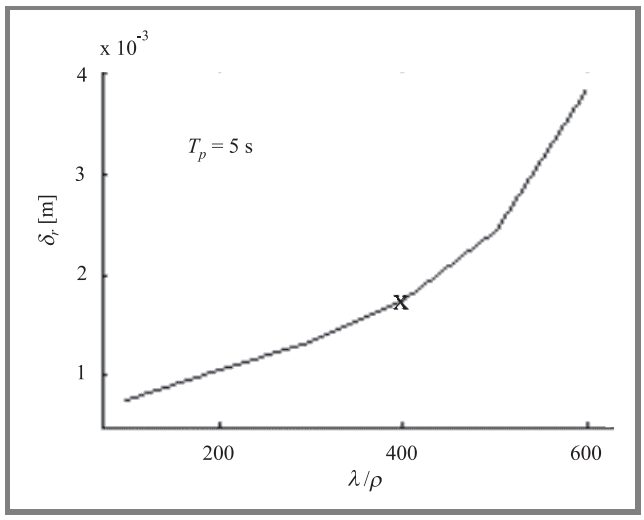

Fig. 12. Mean distance fluctuations in dependence on T_p parameter.

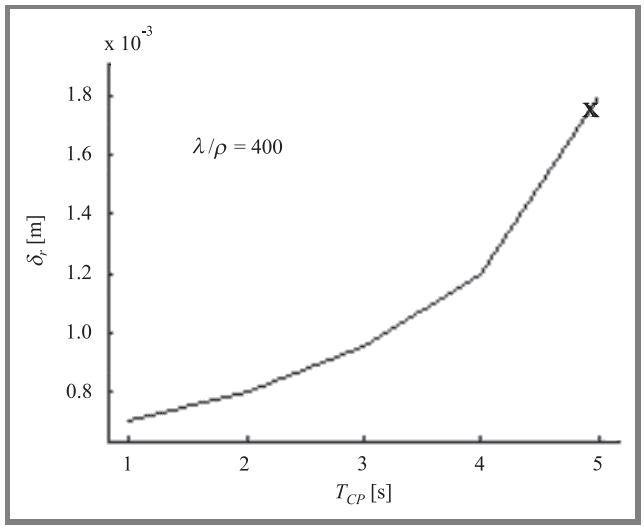

Fig. 13. Mean distance fluctuations in dependence on λ/ρ parameter.

The analysis of λ/ρ parameter impact on position accuracy shows that for small values the system is better stabilised (i.e., distance variations from the nominal position are smaller).
The accuracy obtained in simulations is still too small to fulfil requirements of the optical interferometry missions, but it could be good enough for longer wavelength missions.

4. Summary

In the paper, we presented results of simulations with controllers employing a single parameter (scalar control). Even such simple controller allows to obtain interesting results and works fine in 3-dimensional simulations. The comparison with interferometer missions requirements is not satisfying and shows that there is a need to investigate more advanced controlling and modeling concepts.

References

[1] E. M. C. Kong, D. W. Kwon, S. A. Schweighart, L. M. Elias, R. J. Sedwick, and D. W. Miller, "Electromagnetic formation flight for multisatellite arrays", *J. Spacecr. Rock.*, vol. 41, no. 4, 2004.

[2] M. Martin and S. Kilberg, "TechSat 21 and revolutionizing space missions using microsatellites", in *15th Conf. USU/AIAA*, Logan, USA, 2001.

[3] A. Wielders, B. Calvel, B. L. Swinkels, and P. D. Chapman, "Metrology concepts for a space interferometer mission: SMART-2", *Proc. SPIE*, vol. 4852, pp. 268–278, 2003.

[4] D. W. Miller, R. J. Sedwick *et al.*, "NIAC phase I final report: electromagnetic formation flight", Final Raport Massachusetts Institute of Technology, Dec. 2002.

[5] L. M. Elias, "Dynamics of multi-body space interferometers including reaction wheel gyroscopic stiffening effects: structurally connected and electromagnetic formation flying architectures". Ph.D. thesis, Massachusetts Institute of Technology, March 2004.

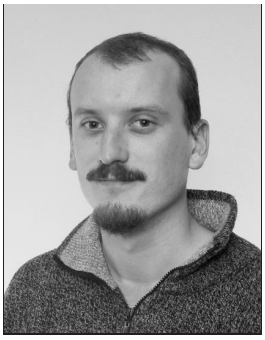

Roman Wawrzaszek was born in Koszalin, Poland, in 1977. He received his bachelor's and master's of science degrees from the Technical University of Koszalin, Poland, in 1998 in the digital telecommunication discipline. Currently he is a Ph.D. student in Space Research Center of the Polish Academy of Sciences (PAS) and his main research focus is on control, dynamics and technology of satellite formations systems. Other fields of his activities are: measurement systems, temperature sensors and software development.
wawrzasz@cbk.waw.pl
Space Research Centre
Polish Academy of Science
Bartycka st 18a
00-716 Warsaw, Poland

Marek Banaszkiewicz – for biography, see this issue, p. 53.

Paper

Interception of a free-rotating satellite: an autonomous rendezvous scenario

Karol Seweryn and Marek Banaszkiewicz

Abstract— The spacecraft's lifetime is often limited by reliability and redundancy of its components. Furthermore, serious restrictions on duration of spacecraft operations are posed by finite amount of fuel or cooling agent. It is also clear that once a satellite is launched, it is extremely difficult to replace/modify its hardware on the orbit. Future spacecraft missions, especially huge planetary orbiters, will require servicing support from autonomous unmanned satellites. In this paper we introduce and analyze a new scenario for interception of a free rotating satellite ion a Keplerian orbit. The scenario is divided into several stages to be executed by the servicing satellite: attitude determination of the target object; own motion planning; determination of the optimal target position and orientation before docking; controlled approach, i.e., decreasing of a range between satellites; orbiting of the servicing satellite around the target satellite; docking, i.e., radial degreasing of the intersatellite range till the satellites contact, while keeping constant the relative orientation between them. The control algorithm for the servicing satellite motion during its maneuvers is described. Finally, a few examples of satellite motion simulations according to the proposed scenario are presented.

Keywords— satellite rendezvous, autonomous control systems, docking maneuvers.

1. Introduction

Autonomous rendezvous is a very important element in the retrieval of space payloads (i.e., containerized harvest) or resupply of consumable resources (e.g., gases, fuel, and others) [1, 2]. The scenario of interception of a target satellite by a servicing spacecraft that is introduced in this study deals with a special situation. The target satellite is passive during the rendezvous maneuver, which means that communication between satellites does not exist, attitude control and active thrusters are not available. It corresponds to an event when the satellite is out of control. We assume that the target satellite mechanical parameters (i.e., inertia dyadic, mass) are known and that the satellite is equipped with markers [3, 4] as well as with a docking mechanism [6, 11]. In principle, it is possible to split the autonomous rendezvous into four different subproblems:

– determination of rotational states of both spacecraft by employing a sequence of momentarily orientations;
– optimization of motion during rendezvous with respect to consumed fuel, time of approach, accuracy and reliability of docking;
– planning and controlling the approaching maneuver;
– docking with the help of a robotic arm.

What concerns the spacecraft motion, we assume that initially the satellites follow each other on the same orbit, separated by a distance of 1 km and that the orbit is known with any required accuracy. The rotational motion of the servicing satellite is also known from its on-board attitude control system, but the orientation of the target satellite is to be determined by the vision system on servicing satellite during the rendezvous. Practically, a set of six parameters: three Euler angles and their derivatives have to be found for a given time.

2. Interception scenario

The passive spacecraft S_d is out of control and rotates freely in space, while moving on its approximately Keplerian orbit. The active satellite S_r (servicing spacecraft), should determine the rotational motion of the serviced object and then plan and execute the approach scenario. All operations should be performed autonomously and with minimal expenditure of fuel by the servicing satellite and with a high accuracy of touchdown. The rotational motion of the passive spacecraft is to be determined using a color markers [7].

We assume that S_r periodically (with a frequency of 10 Hz) takes images of S_d in order to identify a set of markers. Then, the onboard computer of S_r determines the six initial parameters of the S_d rotational motion employing a sequence of images. The obtained initial values (at $t = t_0$) are used to predict the future S_d motion. The S_d translational motion follows the simple Kepler equations in U_E frame. The S_r motion is described in the non-inertial U_{Ed} frame, while the control of S_r control will be realized in the orbital coordinate system U_{dorb}. Here, U_E is Earth-centered inertial coordinate system, U_{Ed} results from a parallel translation of U_E to the center of mass of S_d. Similarly, U_d is a S_d body fixed frame, and U_{dorb} is the orbital frame with its origin in the S_d.

The S_r motion is constrained by several factors. The first one is the condition that in the final phase of rendezvous, the relative motion of S_r in the U_d frame should be trans-

lational, the second one is a minimum difference between approaching and final velocity. Even before executing the approaching maneuver, the first approximation of the optimal solution can be found:

$$\begin{bmatrix} \vec{r}^{\,opt}_{\alpha 0,dorb} \\ \vec{v}^{\,opt}_{\alpha 0,dorb} \end{bmatrix}$$

$$= \min_{v} \left[\min_{r} \left[\begin{bmatrix} \left| \vec{r}_{\alpha 0,dorb;x}(t) \right| \\ \dfrac{d\vec{r}_{\alpha,dorb}(t)}{dt} - \vec{v}_{\alpha 0,dorb}(t) \end{bmatrix} \right] \right] \rightarrow t_{s\_opt} < t < t_{f\_opt}, \tag{1}$$

where r describes position vector in mentioned frame respectively, v – represents its time derivates in a specified time-range.

In the first step (Fig. 1), the translational part of motion can be planned, and later executed, by linking the initial

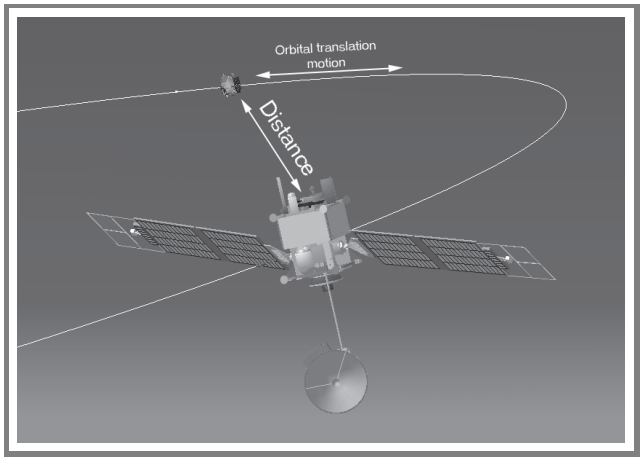

Fig. 1. First step of maneuver.

and final point Eq. (1) in the phase space. During the motion, new initial values of S_d motion are calculated first, then rotational motion is predicted and finally a new optimal solution is calculated from the condition of a minimum

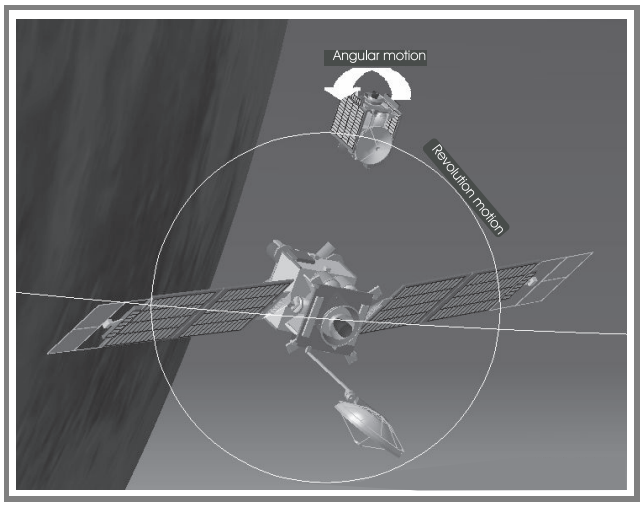

Fig. 2. Third step of maneuver.

difference between the new final state and the previous optimal solution Eq. (1).

In the next step, also the rotational motion is considered. The time dependence of Euler angles and angular velocity vector, as they change during the motion, can be derived from known initial and final angular positions and velocities. We follow the same approach as it was used in first step for planning the position and velocity change.

The third step (Fig. 2) is simply a synchronous orbital motion of S_r around S_d on a circle with a radius $|r_{\alpha 0,d}|$. We arbitrarily assume that half of the rotation cycle is executed before the docking operation is initiated.

In the fourth and final step (Fig. 3) S_r is decreasing its distance with respect to S_d. When observed from U_d (i.e., the coordinate system rotating with S_d), the motion of S_r is translational, i.e., the servicing spacecraft approaches S_r in radial direction. On the other hand, in U_{dorb} the trajectory is a spiral with an outer and an inner radii equal to $|r_{\alpha 0,d}|$ and $|r_{\alpha f,d}|$.

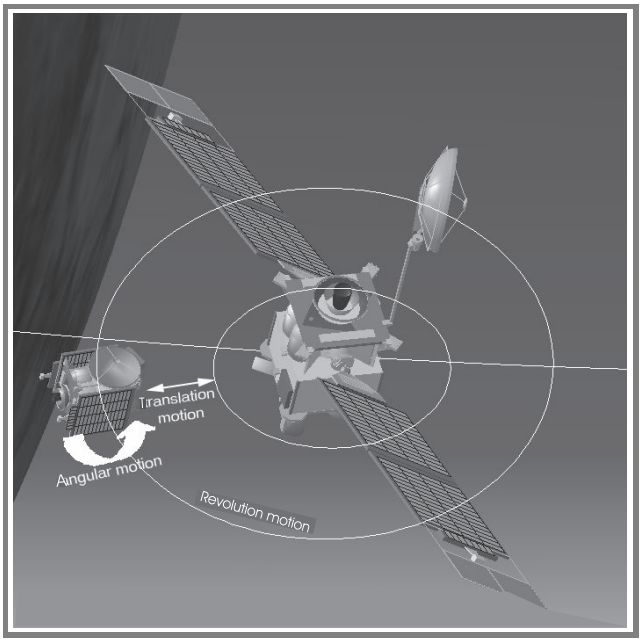

Fig. 3. Fourth step of maneuver.

The control system is taken from [5]. The mathematical description of the translational and rotational motion with a controlling term included is given by the expression (2) and (3). The numerical results have been performed using MATLAB, Simulink 6.0 and Aerospace Blockset 1.6 toolbox. This adds reliability to the proposed approach:

$$\ddot{r}_{\alpha} + \frac{\mu \cdot r_2}{|r_2|^3} = \frac{\mu \cdot r_1}{|r_1|^3} + \frac{F_c(t)}{m_S}, \tag{2}$$

$$I_S \dot{\varpi}_S + \varpi_S \times (I_S \cdot \varpi_S) = M_c(t), \tag{3}$$

where in Eq. (2) r_2 is the position of S_d in U_E, $r_{\alpha} = r_2 - r_1$ is the position of S_r in U_{Ed}, $F_c(t)$ – the controlling force

Table 1
Simulations parameters

Satellite	Initial orientation [rad]	Initial rate [rad/s]	Mass [kg]	Interia tensor [kg · m^2]	Total time of simulation [s]	Time for optimization $T\left((t\_\{sopt\},t\{fopt\}\right)$	Camera frequency [Hz]
Target (passive)	(0.5,0.01,0.2)	(0.3,0.2,0.1)	2366	diag(4069,12030,11029)	500	(260,370)	10
Service (active)	(0,π/4,0)	(0,0,0)	189	diag(13,38,35)			

of S_r motion, and in Eq. (3) ω is angular velocity of S_r, $M_c(t)$ – the controlling torque of S_r motion, m_s – mass of satellite S_r, and I_s – inertia dyadic of satellite S_r.

3. Simulation example and conclusions

The simulation results for a specific approach are presented in Fig. 4. The simulation includes all maneuvers considered in the scenario:

– translational motion;
– adjustment of rotational motion;
– orbiting over S_d;
– spiraling to a close distance.

The computations were performed using Runge-Kutta (ode45) procedure. The servicing and target satellites are in the same orbit: altitude 200 km with zero inclination and

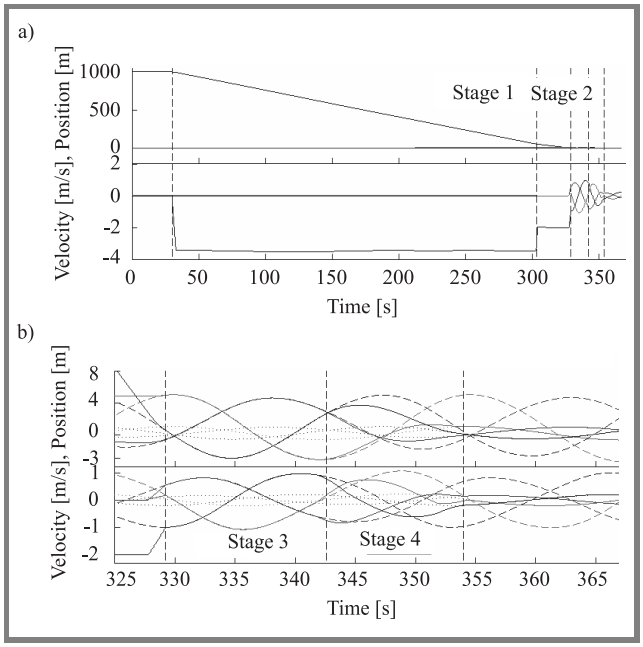

Fig. 4. Position and velocity of service satellite during approaching maneuver: (a) stages 1 and 2; (b) stages 3 and 4.

distance between satellites equal to 1 km. The simulation parameters are listed in the Table 1.

The servicing satellite (S_r), before starting the approaching maneuver, analyzes rotational motion of the target satellite (S_d) and determines its orientation [3, 4]. Then, it calculates the approaching trajectory and starts to realize it. In Fig. 5 the estimation error of Euler angles as determined by the S_r vision system is shown. During the maneuver, the final position is iteratively corrected.

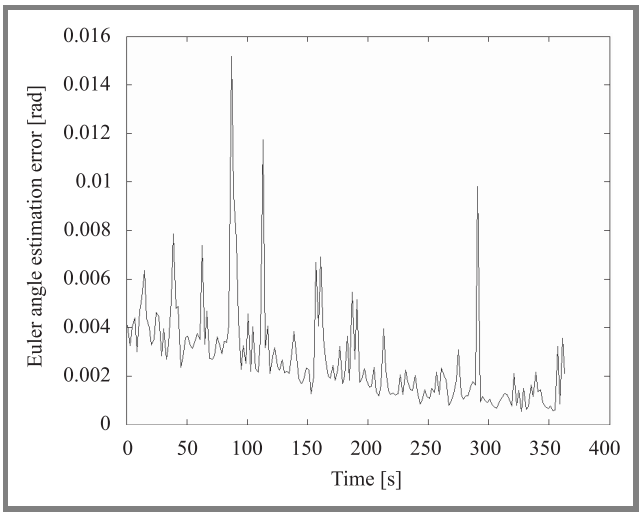

Fig. 5. Standard deviation of estimated error of Euler angles.

In Fig. 4 the trajectory and velocity during stage 1–4 is presented with fine resolution. The rendezvous position (in the end of stage 2) is optimal from the point of view of fuel consumption. In the stage 3, the position of (S_r) (solid line) with respect to the target satellite (dashed line) is constant and the distance between the object is equal to 5 m. In the stage 4, the spiral motion of S_r toward S_d is executed. In the rightmost part of the plot S_r (solid line) approaches the target satellite to a distance of 1 m (dotted line).

The plots in Fig. 6 show the corresponding result for the rotational motion. The solid line represents Euler angles (φ,θ,ψ) and angle-rate (p,q,r) of S_r, respectively, and the dotted line describes the same parameters for S_d. In the stages 3 and 4 these parameters are the same for both satellites. The obtained accuracy of the whole maneuver is about 6 cm.

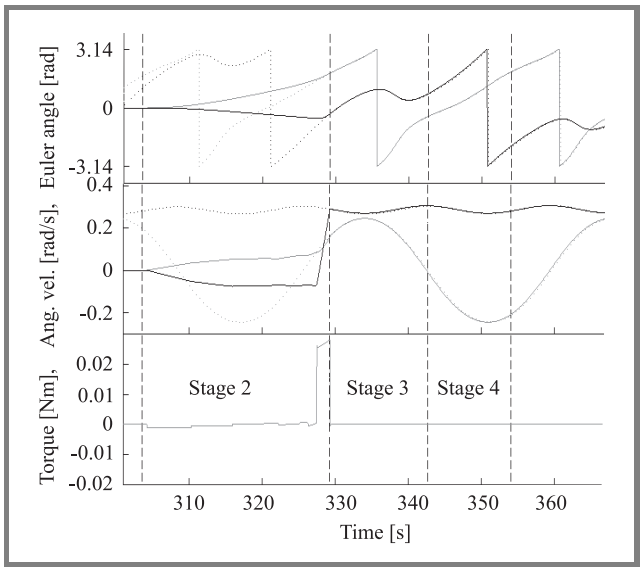

Fig. 6. Orientation and angular velocity of service satellite during approaching maneuver.

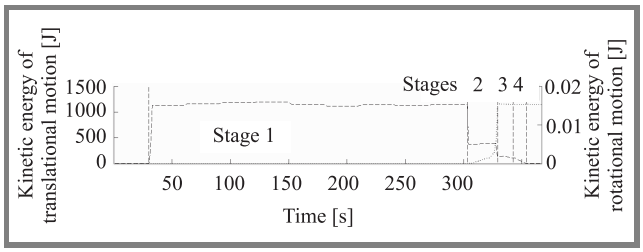

Fig. 7. Kinetic energy of translational (left axes) and rotational (right axes) motion.

The last plot (Fig. 7) presents the kinetic energy of S_r as it changes during the rendezvous. The right part (dotted line) corresponds to the rotational motion, while the left one to the translational motion (dashed line).

References

[1] E. M. Polites, "Technology of automated rendezvous and capture in space", *J. Spacecr. Rock.*, vol. 36, no. 2, pp. 280–291, 1999.

[2] I. Kawano *et al.*, "Result of autonomous rendezvous docking experiment of engineering test satellite – VII", *J. Spacecr. Rock.*, vol. 38, no. 1, pp. 105–111, 2001.

[3] C. J. Chi and H. McClamroch, "Automatic spacecraft docking using vision based guidance and control techniques", *J. Guid. Contr. Dynam.*, vol. 16, no. 2, pp. 281–288, 1993.

[4] N. G. Creamer *et al.*, "Interspacecraft optical communication and navigation using modulating retroreflectors", *J. Guid. Contr. Dynam.*, vol. 27, no. 1, pp. 100–106, 2004.

[5] F. Caccavale, C. Natale, and L. Villani, "Output feedback control of mechanical systems with application to spacecraft and robots", *J. Guid. Contr. Dynam.*, vol. 26, no. 2, pp. 273–281, 2003.

[6] P. Tchoryk Jr., A. B. Hays, and J. C. Pavlich, "A docking solution for on-orbit satellite servising: part of the responsive space equation", in *1st Resp. Space Conf.*, Redondo Beach, USA, 2003.

[7] D. P. Miller *et al.*, "Attitiude and position control using real time color tracking", in *Proc. Ninth Ann. Conf. Innov. Appl. Artif. Intell.*, Providence, USA, 1997.

[8] C. C. Liebe, K. Gromov, and D. M. Meller, "Toward stellar gyroscope for spacecraft attitiude determination", *J. Guid. Contr. Dynam.*, vol. 27, no. 1, pp. 91–99, 2004.

[9] R. S. Patera and G. E. Peterson, "Space vehicle maneuver method to lower collision risk to an acceptable level", *J. Guid. Contr. Dynam.*, vol. 26, no. 2, pp. 233–237, 2003.

[10] V. V. Beletskii, *Artificial Satellite Motion Relative to Its Center of Mass*. Moscow: Nauka, 1965 (in Russian).

[11] C. Y. Xia, P. K. C. Wang, and F. Y. Hadaegh, "Optimal formation reconfiguration of multiple spacecraft with docking and undocking capability", in *AIAA Guid. Navig. Contr. Conf.*, San Francisco, USA, 2005.

Karol Seweryn and **Marek Banaszkiewicz** – for biographies, see this issue, p. 53.

Paper

Feasibility study of the space synthetic aperture radar for the SSETI-ESMO project

Bartosz Dawidowicz and Krzysztof Kulpa

Abstract— The following paper presents the analysis of the feasibility study of the SAR radar for lunar space missions. The European Students Moon Orbiter (ESMO) project is conducted by the Students Space Exploration and Technology Initiative (SSETI) association. The phase A of this project is supported by the European Space Agency (ESA).

Keywords— SSETI, ESMO, feasibility study, space SAR radar.

1. Introduction

For many years space technology has been out of reach for many scientists or students. This situation was changed at the beginning of the 21st century, when in 2001, the European Space Agency (ESA)[1] Education Office founded the Student Space Exploration and Technology Initiative (SSETI)[2] association. The main objective of the SSETI association was to motivate the large number of students from European countries to participate in space projects and learn more about the space and science in general. The SSETI association is supported by ESA. This has enabled students participating in these projects to exchange information with experts from ESA and perform tests of the designed space components at the ESTEC Test Center Laboratory (Noordwijk, The Netherlands). Students are responsible for designing and manufacturing the whole spacecraft. Currently, there are two active SSETI space projects: European Student Earth Orbiter (ESEO) and European Student Moon Orbiter (ESMO). The paper presents the concept of the synthetic aperture radar (SAR) subsystem of the second project. This concept has been worked out by students from space synthetic aperture radar (SSAR) team, who have gained already practical experience with SAR technology, developing and implementing SAR algorithms and processing the recorded data from the airborne campaigns [12, 19]. The example of SAR image obtained from recorded data is presented in Fig. 1.

The involvement of students in working projects has the great educational impact. Nowadays many educational institutions intend to incorporate such projects into their teaching process. The description of another student educational radar project can be found in [15]. In that case students has designed the laboratory models of Doppler and SAR radar. Reading their paper, everyone can notice that this project gained their enthusiasm and helped them to enhance the educational experience.

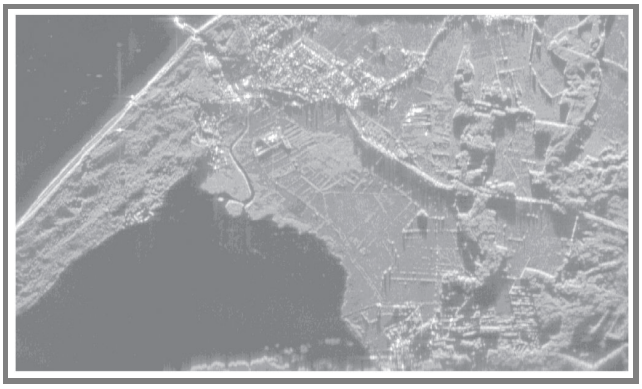

Fig. 1. Results of the SAR processing performed by the students: Łeba village (Poland).

2. The SSETI-ESMO

The ESMO satellite is going to be orbiting around the Moon and collecting the Moon surface 3D images. It will be treated as the reconnaissance platform, as well as a step towards the missions to other planets. The launch of the satellite is expected in 2010 year with the use of the Ariane 5 rocket. At the time being, there is no final decision about the ESMO payload. Several possibilities are taken into account. The basic SSETI-ESMO experiment plan consists of: reaching the Moon orbit, making of 2D/3D maps of the Moon surface using optical cameras, synthetic aperture radar in 2D mode and/or interferometric synthetic aperture radar (IfSAR) in 3D mode, making the Moon hight map using laser hight finder of LIDAR (light detection and ranging), the Moon magnetic field study and landing of student-made object at the Moon surface. The satellite in transportation phase should fit into the cylinder 1.5 m height and 1.5 m in diameter. The mass of the satellite should be below 300 kg. The weight of the SAR payload should not exceed the 20 kg. The whole ESMO mission should take 1 month.

To fulfill all the requirements, operational team has performed feasibility study on space SAR technology, collecting many different ideas described in open literature. The work has been started by analyzing the geometry of

[1]ESA, http://www.esa.int
[2]SSETI, http://www.sseti.org

the space borne SAR system. The comprehensive analysis of that problem can be found in [14]. In the second step, the fundamentals of the SAR technology for airborne and space applications have been reviewed. In the article [6] the basic description of radar system design and the limitations of the SAR radar swath width (coverage), range and azimuth resolution in function of radar velocity, antenna dimensions and pulse repetition frequency can be found. After wide analysis of above (and many others) articles and the construction of ESA and NASA SAR satellites, the students SSAR team proposed the ESMO SAR experiment plan. There are planned three stages of SAR image formation. In the first stage the Moon surface will be scanned by SAR/IfSAR radar, and the raw radar data will be stored on the board of the satellite. In the second stage the collected data should be transmitted to the data ground station on the Earth. In the last (third) stage, the final SAR image will be formatted off-line, after application of all required corrections (Fig. 2).

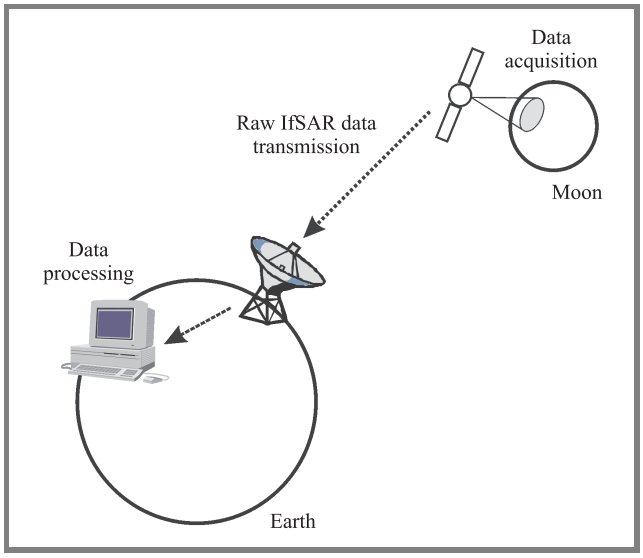

Fig. 2. The SSAR experiment plan.

The authors of this paper reviewed the state of art and the future trends in the spaceborne SAR technology. The design consideration about the key hardware blocks will be briefly discussed in Section 4.

3. The SAR, IfSAR technology

Synthetic aperture radar is an aircraft or spacecraft mounted sensor designed to obtain high-resolution radar images of the observed terrain by means of microwave radiation [9]. In this case of imaging, the radar is placed on moving platform. Radar pulses are aimed towards the Earth or another planet. The obtained image is a two dimensional estimate of the electromagnetic reflectivity of the mapped area. The resulting radar image is characterized by resolution in two directions: slant-range and cross-range. Slant-range refers to the range transversal to the path of flight, while cross-range refers to the range along the path of flight (see Fig. 3).

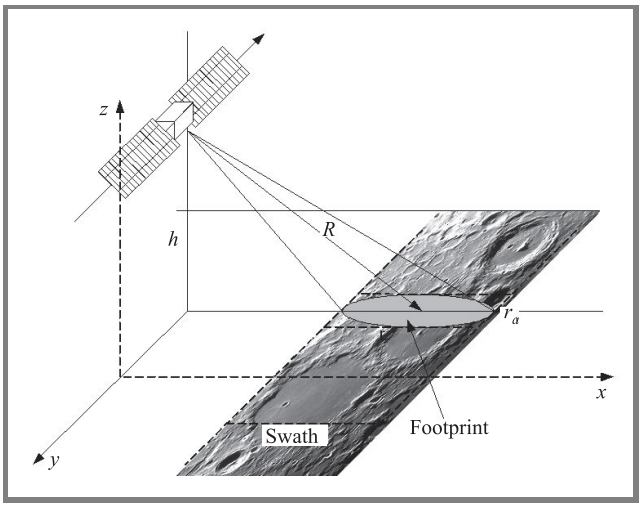

Fig. 3. The SAR geometry.

Fine slant-range resolution is obtained by transmission of frequency modulated (FM) pulses, a technique used in many different types of radars, not only in SAR. The slant-range resolution depends on the transmitted signal bandwidth, according to the following equation:

$$\delta_r = \frac{\mathrm{c}}{2B},$$

where: c – light velocity, B – transmitted signal bandwidth.

Cross-range resolution in SAR is obtained by coherent integration of the received signal, as the radar travels along the mapped area. The process of coherent integration can be thought of as the formation of the large antenna – the synthetic aperture. The theoretically achievable cross-range resolution is equal to the half of the real antenna aperture (antenna along-track length).

Both, slant-range resolution and cross-range resolution do not vary with the distance between the radar and the target. The process of SAR image formation can be divided into two consecutive stages: range processing and azimuth processing. These two steps correspond to resolution improvement in two different directions. The range processing (also called pulse compression) is realized by matched filtering of the received FM signal. The result of the pulse compression is a series of so called range profiles, which are used in further processing. This part of processing is relatively simple, because the parameters of the matched filter are independent of the platform movement and hence are invariant in time. The following step is the azimuth processing which is the essential part of SAR processing. Similarly as in pulse compression, the azimuth compression uses matched filtering. However, this time radar platform's movement strongly influences on the received signal. For this reason the matched filter has to be constantly adjusted to the changing situation. Since there is no navigation system providing that information with required accuracy,

the sophisticated motion compensation algorithms based on received signal are used. For high-resolution imaging, instead of using two single-dimensional filters, it is necessary to use more complicated 2-dimensional filter to mitigate the range-migration effects.

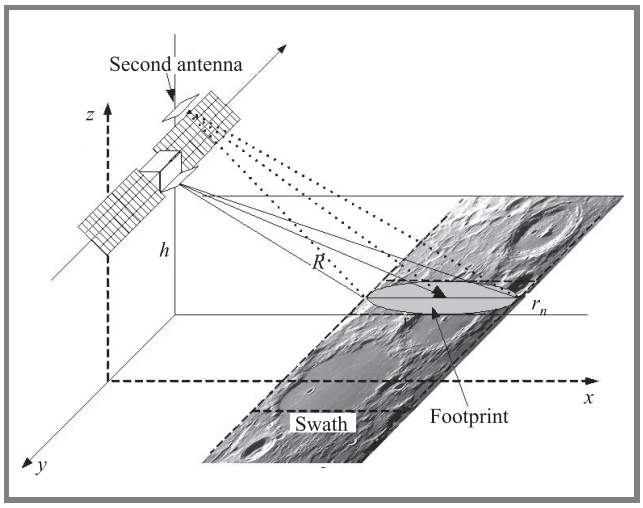

Fig. 4. The IfSAR geometry.

An extension of SAR technology is the IfSAR technology. Using IfSAR configuration (Fig. 4) 3D high resolution images can be obtained. The resulting 3D radar image can be characterized by the resolution in three directions: slant-range, cross-range and height. The IfSAR configuration consists of two receiving antennas so the same objects are observed from different angles. This causes a phase shift between the received signals which enables the height estimation of the observed objects [13].

4. Space SAR system considerations

The feasibility of designing and manufacturing of SAR radar for small satellite is limited by the available technology, including antenna technology, microwave transmitters' technology, digital signal processor (DSP) technology and others. Especially in this project, such technology must be available for student team. It is assumed that the temperature for the electronic components should be between –40°C to +85°C (industrial or military grade). The classical concept of space SAR system is presented in [2]. On the basis of the above mentioned concept, the SSAR team proposed the functional block diagram of the SAR radar (Fig. 5).

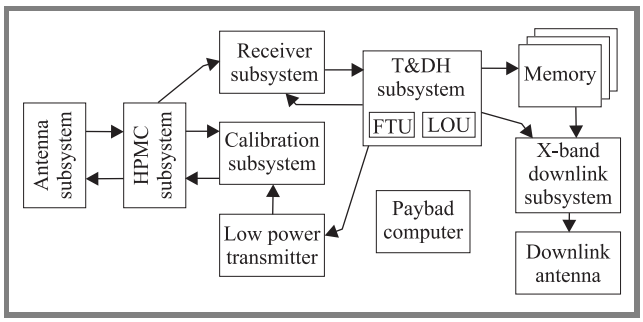

Fig. 5. The SAR radar block diagram. Explanations: FTU – formatter and timing unit, LOU – local oscillator unit.

The payload computer unit controls all aspects of payload operations. The high power microwave circuit (HPMC) provides the amplification of the radar signal from the LPT (for radar pulse transmission) or received by the antenna. Timing and data handling system (T&DH) provides very stable synchronization (master oscillator) of every SAR subsystem and formats the received raw data for storage in the on-board memory and transmission to the Earth. The key system blocks for every SAR radar are: antenna, microwave transmitter-receiver, memory storage devices and signal processing subsystem (performing calibration and image formation tasks).

4.1. Antenna subsytem

There are two main antennas technologies which can be taken into consideration: planar and dish antenna. The main advantage of the dish antenna is the ease of the manufacturing and simplicity. The main disadvantage is its weight and dimensions. The alternative concept is the usage of planar antennas. The planar antenna can be designed and manufactured in three technologies: waveguide, microstrip and as an active array of T/R modules. However, the fast development of the active antenna arrays enables new processing schemes in SAR technology [17]. The usage of such device in this project seams to be impossible because of the high costs of this technology. The usage of the waveguide or microstrip technology seems rather interesting, due to antenna low weight, low manufacturing costs and wide bandwidth.

4.2. Microwave amplifier (HPMC subsystem)

The authors of [1] deal with the problem of building a small (less than 120 kg) satellite with SAR radar on-board. The main conclusions are that manufacturing and building SAR radar for microsatellite is feasible, however its parameters (resolution) won't be comparable with big systems like ERS 1/2 or EnviSAT. The main advantage of such system would be low costs of obtaining satellite SAR images. The effective swath size would be about 3 km width (antenna aperture width about 2 m). Such satellite could operate at the altitude of 400–500 km, using the 300 W TWT (travelling wave tube) amplifier. The SSAR team performed similar studies taking into account technology available for the students at Warsaw University of Technology and the cost reduction. The main assumptions were as follows: X-band radar, 11 dB detection threshold, 12 dB of total hardware system loss, 0.7×1.5 m antenna aperture, 2.5 kHz pulse repetition frequency, 50 μs pulse time duration. The transmitted pulse power in the SAR mode for 30 km orbit, 60 km orbit, 120 km orbit height and

45° incidence angle were as follows: 10.3 W (1.2 W average), 82.4 W (9 W average), 659 W (72 W average). It appeared that the best solution for this student project is to use solid state amplifier. That limits the orbit to about 60 km, because of the maximum available transmitting power.

4.3. The SAR data compression

The SAR technology generates high amount of data. For example for the SAR radar analyzed in this article raw rate data transfer can be up to 10 Mbit/s for the 12 bit ADC (analog to digital converter) [10]. The study of the literature [23] and SSAR team research [10] showed that SAR data can be sampled using 8–12 bit ADC and than degraded to 1–4 bit representation using block adaptive quantization (BAQ) algorithm [21]. The example images obtained using 12 bits data and 1 bit data are presented in Figs. 6 and 7, respectively.

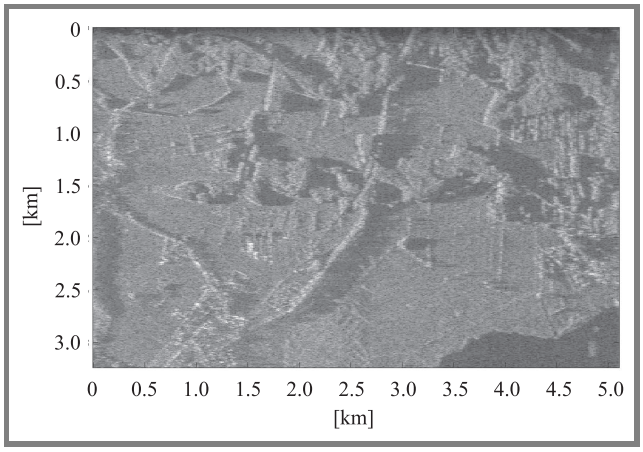

Fig. 6. The SAR image for 12 bit ADC.

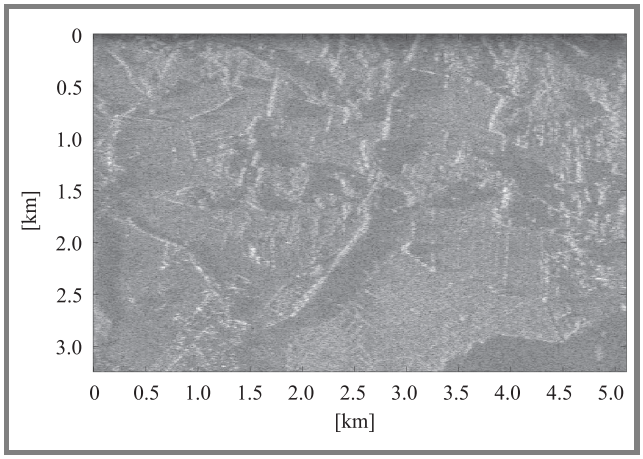

Fig. 7. The SAR image for 1 bit ADC.

Comparing these images (Figs. 6 and 7), it can be clearly seen that the image degradation is acceptable. More detailed analysis can be found in [10]. To simplify the hardware installed on the satellite, it is assumed that final image processing will be performed on the Earth, using PC's and software SAR processor developed by the SSAR team.

4.4. Data storage subsystem

The raw radar data must be stored on the board of SAR satellite prior to sending it to the Earth ground station. There are two reasons for this temporary storage – the satellite can scan the part of Moon invisible from the Earth and this same microwave system will be used both for SAR scanning and for data comunication. The fundamental information about designing data storage system for space application can be found in [16]. There are several candidates for mass storage in the outer space. It is possible to record data using hard disks, magnetic tapes, optical discs and solid stat memories (DRAM, EEPROM). After intensive analysis, the SSAR team has chosen 2 GB solid state memory for storing raw SAR radar data, photos and data from other measurements. To reduce the costs, the commercial off-the-shelf (COTS) memory components should be used. To enhance its reliability the redundancy and error detection and correction (EDAC) codes should be considered [4, 24]. SAR technology generates large amounts of data and requires high speed data bus (HSDB) to transfer them between transmitter/receiver system and processing and storage system. Very good comparison of data buses properties for space applications is given in [18]. It seems that the most adequate standard to use in the small/microsatellite are the Spacewire [22], and IEEE 1394. The idea of such network is described in [5]. These two buses are very compatible at the physical level and therefore can easily be combined. Analysis presented in that paper shows that the effectiveness of the IEEE 1394/Spacewire architecture can achieve the same fault tolerance capability as the IEEE 1394/I2C architecture with less redundancy. The components for building such network can be implemented in the field programmable gate array (FPGA) structure [11, 20].

The architecture of the processing and storage data system are shown in Fig. 8. It can be seen that the payload subsystems should be connected to the HSDB for fast data

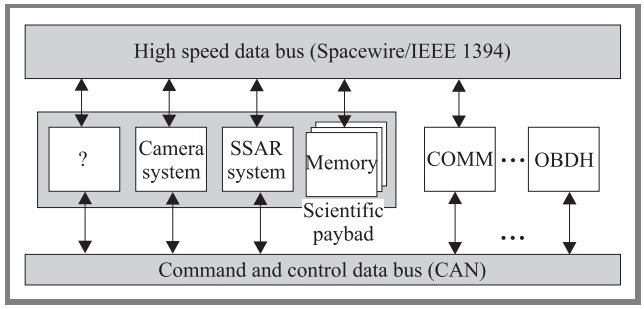

Fig. 8. Processing and storage architecture. Explanation: OBDH – on-board data handling.

exchange and storing in the on-board memory. For the cost and weight reduction, the hardware of the SAR and communication (COMM) systems can be partially combined together [7, 8].

4.5. The ESMO SAR satellite vision

After careful and detail analysis, the SSAR team proposed the first vision of the ESMO satellite (Fig. 9). This concept is similar to the one used for the TerraSAR-X [3] satellite. The shape of this satellite is compact and easy to manufacture. The number of moving parts is minimized. The other advantage is connected with the fact that for the certain height and width (during the transport, the satellite should fit in the specific cylinder) a prism has a bigger capacity than a cuboid.

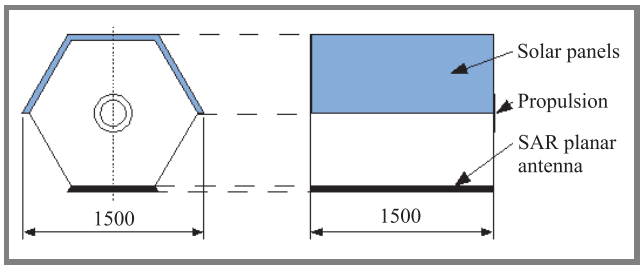

Fig. 9. The SSETI-ESMO satellite vision.

The main advantage of using non moving solar panels, is the simplification of the satellite design and reduction of the probability of system failure. However, during all satellite maneuvers, the precise position of the Sun must be taken into account. Especially during SAR scanning the ESMO satellite must be between the Sun and the Moon's surface. The feasibility of the IfSAR mode requires further studies. The main problem is that the second antenna must be equipped with deployable boom. The position and the baseline (length of the boom) between the two antennas have to be known precisely [17].

5. Conclusions

Analysis presented in this paper shows that building SAR radar for small lunar satellite is feasible. The SSAR team has the potential to design space SAR radar and develop the algorithms for SAR data processing. Students at the Warsaw University of Technology have the technical ability to design and manufacture the low frequency part of the system, specify the requirements for the microwave frontend and antenna, implement algorithms for space SAR system control and off-line processing of raw SAR data. The members of the SSAR team think that the state of art of electronic and software engineering technology enables the usage of some COTS components and industrial standards. This of course degrades the reliability of the system, but such solutions are used with success in many "low budget" space projects.

References

[1] J. P. Aguttes, "High resolution (metric) SAR microsatellite, based on the CNES MYRIADE bus", in *Proc. IEEE Geosci. Rem. Sens. Symp. IGARSS'01*, Sydney, Australia, 2001, vol. 1, pp. 224–226.

[2] A. Brand and Z. Mi, "Designing a spaceborne SAR for multi mode imaging", in *Proc. Electr. Comput. Eng., Canad. Conf. Digit. Obj. Ident.*, Calgary, Canada, 1996, vol. 1, pp. 17–20.

[3] S. Buckreuss, W. Balzer, P. Muhlbauer, R. Werninghaus, and W. Pitz, "The TerraSAR-X satellite project", in *Proc. Geosci. Remot. Sens. Symp. IGARSS'03*, Toulouse, France, 2003, vol. 5, pp. 3096–3098.

[4] G. C. Cardarilli, P. Marinucci, and A. Salsano, "Fault-tolerant solid state mass memory for satellite applications", in *Proc. IEEE Instrum. Meas. Technol. Conf.*, Ottawa, Canada, 1997.

[5] S. N. Chau, J. Smith, and A. T. Tai, "A design-diversity based fault-tolerant COTS avionics bus network", in *Proc. Depend. Comput. Pacific Rim Int. Symp.*, Seoul, Korea, 2001, pp. 35–42.

[6] A. Curie, "Synthetic aperture radar", *IEEE Electron. Commun. Eng. J.*, Aug. 1991.

[7] B. Dawidowicz, M. Piotrkowski, and T. Filipek, "Hardware system analysis for students space synthetic aperture radar (ESA SSETI-ESMO project)", in *Proc. XIV IEEE-SPIE Sig. Proces. Symp.*, Wilga, Poland, 2005.

[8] B. Dawidowicz, T. Filipek, M. Kuzniak, W. Kulka, M. Malanowski, M. Piotrkowski, and K. Kulpa, "Interferometric SAR for European Student Moon Orbiter", in *Proc. EuSAR 2006*, Dresden, Germany, 2006.

[9] B. Dawidowicz, M. Malanowski, G. Pietrzyk, M. Piotrkowski, V. Rakevich, and P. Samczyński, "Space synthetic aperture radar system analysis", in *Proc. STEC 2005*, Aalborg, Dennmark, 2005.

[10] B. Dawidowicz, K. Kulpa, M. Malanowski, and M. Piotrkowski, "The reduction of the SAR data transfer for the SSETI-ESMO project", in *Proc. KKRRiT Conf. 2005*, Kraków, Poland, 2005.

[11] L. Fanucci, A. Renieri, and P. Terreni, "VLSI design of a routing switch for the spacewire serial link standard", in *Proc. Electron. Circ. Syst. 2002*, Dubrovnik, Croatia, 2002, vol. 3, pp. 1103–1106.

[12] A. Gados, A. Gorzelanczyk, A. Jarzebska, M. Mordzonek, M. Smolarczyk, K. S. Kulpa, and B. Dawidowicz, "First Polish SAR trials", in *Proc. EUSAR 2004*, Ulm, Germany, 2004.

[13] A. Gromek, P. Jobkiewicz, and P. Samczyński, "Analysis of interferometric synthetic aperture radar on Moon orbiter", in *Proc. STEC 2005*, Aalborg, Dennmark, 2005.

[14] B. Himed, K. Y. Li, and S. U. Pillai, "Remote sensing using space based radar", in *Proc. NATO Adv. Sens. Secur. Appl.*, Il Ciocco, Italy, 2005.

[15] M. A. Jensen, D. V. Arnold, and D. E. Crockett, "System-level microwave design: radar-based laboratory projects", *IEEE Trans. Edu.*, vol. 43, no. 4, 2000.

[16] R. R. Katti, "Space data storage systems and technologies", *IEEE Trans. Magnet.*, vol. 30, no. 6, 1994.

[17] W. Keydel, "Perspectives and visions for future SAR systems", *IEE Proc. Radar Sonar Navig.*, vol. 150, no. 3, 2003.

[18] D.-Y. Kim, K.-H. Kwon, J.-W. Choi, J.-I. Lee, and H.-J. Kim, "Design of a new on-board computer for the new KOMPSAT bus", in *Proc. Aerosp. IEEE Conf. 2005*, Big Sky, USA, 2005, pp. 1–12.

[19] M. Malanowski "Multilook processing in unfocused synthetic aperture radar", in *Proc. XIV IEEE-SPIE Sig. Proces. Symp.*, Wilga, Poland, 2005.

[20] M. Nomachi, S. Ishii, Y. Kuroda, H. Nakamura, T. Sugimoto, and T. Takahashi, "A data readout system with high-speed serial data link for balloonborne X-ray detectors", in *Proc. Nucl. Sci. Symp.*, Rome, Italy, 2004, vol. 3, pp. 1478–1482.

[21] S. M. Parkes, "Data compression and spacewire", in *Proc. Geosci. Rem. Sens. Symp. IGARSS'99*, Hamburg, Germany, 1999, vol. 4, pp. 2267–2269.

[22] S. M. Parkes, "Spacewire: the standard", in *DASIA 1999 Conf.*, Lisbon, Portugal, 1999.

[23] V. Pascazio and G. Schirinzi, "Synthetic aperture radar imaging by one bit coded signals", *IEEE Electron. Commun. Eng. J.*, Febr. 1998.

[24] P. P. Shirvani, N. R. Saxena, and E. J. McCluskey, "Software-implemented EDAC protection against SEUs", *IEEE Trans. Reliab.*, vol. 49, no. 3, 2000.

Bartosz Dawidowicz was born in Warsaw, Poland. He graduated from Warsaw University of Technology (WUT), Poland, in 2004. He is the coordinator of the SSAR team in the SSETI-ESMO project. At the moment he is a Ph.D. student at WUT. During his research work at the university he is interested in developing algorithms for DSPs and FPGAs, performing Matlab simulations, and programming DSP processors and FPGAs (C, assembler, VHDL). For the last three years he has been processing real radar data (mainly in Matlab). His Ph.D. studies are focused on the STAP and PCL technologies. He is a Member of the IEEE and ESA SSETI.

e-mail: B.Dawidowicz@elka.pw.edu.pl
Institute of Electronic Systems
Warsaw University of Technology
Nowowiejska st 15/19
00-665 Warsaw, Poland

Krzysztof Kulpa was born in Warsaw, Poland. He graduated from Warsaw University of Technology (WUT), Poland, in 1981. He obtained Ph.D. in 1987 from WUT. He is the Head of Digital Signal Processing Laboratory at Warsaw University of Technology, Institute of Electronic Systems. In years 2003–2005 he was the Chairman of Poland Chapter of IEEE Signal Processing Society. His works are focused on radar technology, SAR and ISAR processing and PCL technology.

e-mail: K.Kulpa@elka.pw.edu.pl
Institute of Electronic Systems
Warsaw University of Technology
Nowowiejska st 15/19
00-665 Warsaw, Poland

Paper

Summary of SSETI Express satellite mission – gained experience

Karol Kardach and Damian Wydymus

Abstract— In the following paper we present the results of our input in the first of SSETI space missions: SSETI Express, the predecessor of ESEO mission, which we are currently working on, the experience we have gained from this project and how it can benefit us during the upcoming ESEO mission.

Keywords— spaceborne patch antennas, students satellite, SSETI.

1. Introduction

We represent a group of students from Wrocław University of Technology participating in the SSETI association. Student Space Exploration and Technology Initiative (SSETI) is a non-profit organization founded by the Education Office of the European Space Agency (ESA). Its objective is to create a network of students in order to design, build, launch and operate satellites and spacecraft.
This paper will focus on our team's commitment to SSETI Express satellite space mission, which is one of educational programs operated under the SSETI association, the experience we have gained through participating in this project and how the lessons learnt can benefit us during future missions.

2. The mission

The idea of SSETI Express mission came out from another project European Students Earth Orbiter (ESEO). As the students participating in SSETI projects are regular full time students who have their own classes and finals, working on SSETI projects is something they do after hours. The point is that making the ESEO satellite mission happen was taking so long that there has been an uncertainty whether the students working on this project will ever see the results of their work. Besides, there has been a need for testing of specific designs and concepts for the ESEO mission. And that is how the idea of SSETI Express came out.
One of the priorities of SSETI Express mission was speed – the plan was that the SSETI Express satellite will be made ready for launch out of the components we already had for ESEO mission, in the shortest time possible. But of course fast could not mean not-precise. There have been also several goals set for SSETI Express that were different from the ESEO mission. Besides the educational part, main goals of SSETI Express mission included:

- taking pictures of the planet Earth and sending them back to Earth;
- providing connectivity for radio amateurs in the UHF band and most significantly, because SSETI Express would be the first satellite ever to do it;
- taking up into space on its own board three other satellites – so called "cube-satellites" to be released later, when SSETI Express in space:
  - XI-V, designed by University of Tokyo (Japan);
  - UWE-1, by University of Würzburg (Germany);
  - Ncube-2, by Andoya Rocket Range (Norway).

The basic schedule outline of the SSETI Express mission was as follows:

- February/March 2004: start of the project;
- July 2004 – March 2005: building a test model (fit-check) and flight model integration;
- April – May 2005: testing of the satellite;
- July 2005: SSETI Express ready for shipment to Plesetsk space center;
- 27th of September 2005: launch date.

Our task in SSETI Express mission was to design a telecommunication subsystem for the satellite along with AMSAT UK. In particular, we were responsible for the following components:

- low gain antennas (LGAs) for S-band shown in Fig. 1, including:
  - internal back shielding boxes, protecting other electronic devices onboard the satellite against electromagnetic interference caused by antenna back radiation;
  - external protective caps for the antennas;
- transceiver enclosure with integrated microwave antennas divider (Fig. 2);
- microwave cabling with clamps holding the cables inside satellite structure (Fig. 2).

During the testing phase carried out in Poland as well as in ESTEC (European Space Technology and Research Center, Noordwijk – The Netherlands) and in Saab Ericsson

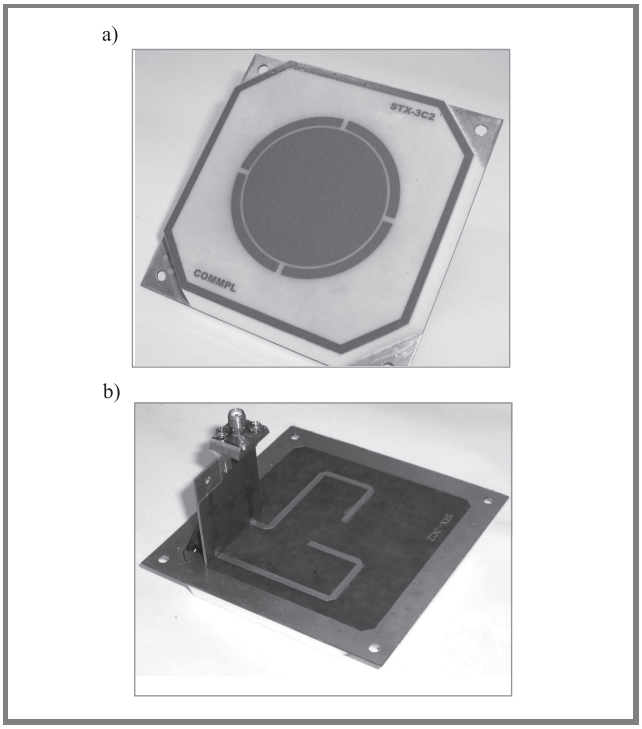

Fig. 1. The antenna: top (a) and bottom (b) views.

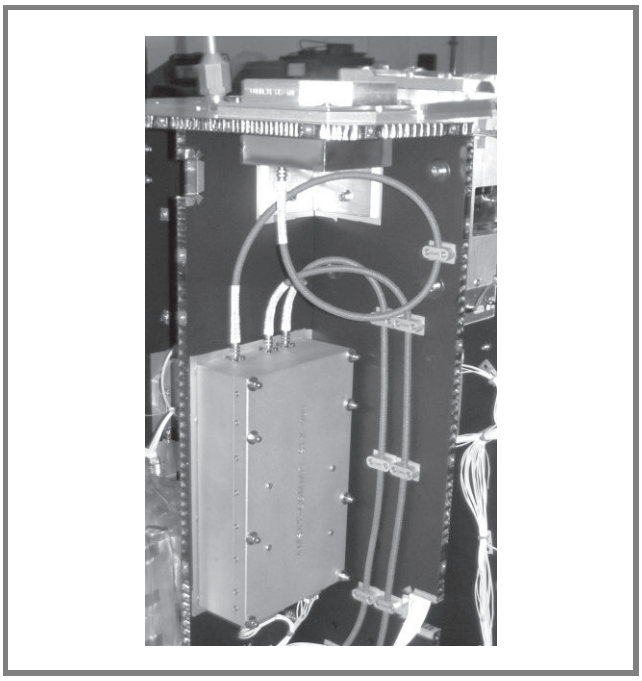

Fig. 2. Transceiver enclosure with power divider and fixed microwave cables.

Space (Sweden) it turned out that our components attained good characteristics and values of specific parameters. LGAs which weighted only 46 g ($100 \times 100 \times 10$ mm) each had 7 dBi of gain, while exhibiting an excellent right handed circular polarization (RHCP) values in wide range of elevation angle. Return loss of each antenna stayed above 25 dB in the operating band.

Our microwave divider delivered superior values of its parameters as well: return loss above 20 dB and isolation above 25 dB – over the full operating band in both cases.

Besides that, members of our team have built our own ground station for the purpose of receiving signals from the SSETI Express satellite. The ground station is capable of operating in both SSETI Express satellite bands: UHF – 437.250 MHz and S-band – 2401.835 MHz. Currently after the failure of the electrical power subsystem of the SSETI Express satellite, the ground station is receiving signals from cube-sats that SSETI Express has taken up into space on its board.

3. Lessons learnt

While working on the SSETI Express project we had an undisputed opportunity to improve our skills in several fields, pertaining to both technical issues and interpersonal skills. In particular, we can say that the most important issues are related to:

- team work,
- managing of work,
- cooperating on the international level,
- exchange of information.

In order to achieve success as a team it is critical that all the individuals working on the project should understand they should put aside their personal ambitions and realize what a team work is in order to be effective.

First of all, responsibilities and tasks should be clearly defined and assigned to specific members of the team, so it is clear who is responsible for what, in case somebody falls behind.

Since it is a student project and people come and people go it is important that the rotation of people be balanced – fresh brains mean new ideas, however it takes time before newbies gain necessary knowledge and it takes time to pass on the knowledge from the more experienced team members. Information flow is the key. Especially because it is an international project we have noticed that for work to be more efficient it is critical that there is a flawless flow of information both between members of one team and between teams from different universities.

When it comes to technical issues, we would mention the following:

- Internal communication must be clearly described to avoid protocol incompatibilities between onboard subsystems of the satellite. The entire telecommunication subsystem shall be described in a single, separate document (i.e., this approach protects from data type incompatibilities during the process of exchanging the data between systems).
- Housing – high frequency chain should be always very well separated from other chains to avoid interference of any kind.

- Redundancy can significantly increase device reliability, if the design is done in a proper way. A method of detecting malfunctions and switching algorithms must be prepared with the highest attention. We find important that the redundancy systems are not overbuilt and too complicated.
- Receiver – both primary and secondary receivers should work simultaneously because their switching in case of a failure of the active one would be impossible.
- Transmitter – redundancy of the transmitter should also be ensured in case of a failure. Switching could be realized on command from the ground station.
- Planning of placement of cables should be arranged in close collaboration with people responsible for harnessing, to let us choose the optimal solution.
- All connectors should be checked in detail with appropriate cables before applying them for temperature cycles, pressure and vibration tests to avoid disconnection.
- Electronic devices aboard satellite must be resistant to effects caused by ionizing radiation (i.e., hopping of bits) and electrostatic discharges. Also they should work in a wide range of temperatures.

We took our lesson from the SSETI Express mission and we try to apply what we have learnt to the ESEO project we are currently working on.
In addition, we put bigger emphasis on communication between teams, trying to work out every single detail and issue. We make sure that every team is being represented during all the chats that we hold on regular basis. To improve communication and information flow we also decided to go for additional chats – specific subjects and subsystems oriented.
As for the internal group improvements, we decided – again for a better information flow which is the key – that every new member of our team will from now on have his own individual tutor to guide him and introduce him to the project and the particular tasks he will be working on, from the general view to the very details.
We meet more often in person to discuss details of proposed technical solutions.
We also pay more attention to previously considered maybe not so relevant details while working on the documentation, since it is the main source of information about our subsystem for the other groups.
Since there had been problems with overheating of the S-band transmitter during the SSETI Express mission we now pay way more attention to temperature-related specifications and issues related to overheating of devices. So now, while working on ESEO we have even invited a group of heat dissipation specialists to help us solve possible overheating problems.
And finally we try to develop our whole telecommunication subsystem according to standards set forth by The Consultative Committee for Space Data Systems (CCSDS) that guarantee a proper functioning of devices that have been used.
Concluding, we hope that we will benefit from the experience gained throughout the SSETI Express mission and that it will help us in designing better telecommunication subsystems for the ESEO mission that we are currently working on and the upcoming European Student Moon Orbiter (ESMO) mission.

References

[1] Student Space Exploration and Technology Initiative (SSETI), http://sseti.net

[2] SSETI COMM PL, Wrocław University of Technology, http://sseti.pl

Karol Kardach was born in Wrocław, Poland, in 1979. He is a student of Wrocław University of Technology and Scholar at Universidad de Las Palmas de Gran Canaria. Currently pursuing towrds his M.Sc. degree in telecommunications to be obtained from Wrocław University of Technology in April 2007. In his scientific research he focuses on spaceborne satellite networks and satellite telecommunication protocols. His interests also include biometrics and voice recognition and verification as well as voice encoding and transmission techniques.
e-mail: KarolKardach@hotmail.com
Institute of Telecommunications, Teleinformatics, and Acoustics
Wrocław University of Technology
Wybrzeże Wyspiańskiego st 27
50-370 Wrocław, Poland

Damian Wydymus was born in Częstochowa, Poland, in 1982. He received a M.Sc. degree in electronics and telecommunications from Wrocław University of Technology, Wrocław, Poland, in 2006. Currently he is carrying studies towards the Ph.D. degree at Wrocław University of Technology. His scientific interests include feeding networks for antenna arrays, spaceborne microvave components and high power applications of microvawe fields.
e-mail: damian.wydymus@pwr.wroc.pl
Institute of Telecommunications, Teleinformatics, and Acoustics
Wrocław University of Technology
Wybrzeże Wyspiańskiego st 27
50-370 Wrocław, Poland

Paper

Building distributed ground station system with radio amateurs

Marcin Stolarski and Wiesław Winiecki

Abstract— The paper concerns radio amateur satellites that are built by international student teams. For contacting a satellite, a single ground station is usually used. In this configuration and with the satellite on the low Earth orbit (LEO), teams have contact only for about 40 minutes per day. If the satellite has service for radio amateurs, they use it for 20 hours per day. A lot of them have connection to Internet. This is a big difference. In this paper, is shown how they can use the radio amateur transceivers and antenna systems in order to build ground stations network named distributed ground station system (DGSS). Frequencies, types of modulations, calculation of power budge, and the ways to control amateur stations by the Internet are also shown. These are essential procedures, because radio amateurs have their standards and habits. Finally a proposal of implementation dedicated DGSS system for radio amateurs with and without use of APRS network is put forward. Distributed ground station is one of the experiments on PW-Sat satellite, which is being build on the Warsaw University of Technology.

Keywords— space technology, satellite communications, radio amateurs.

1. Introduction

The connection between Earth and the satellite is usually made via one ground station. Only in special situations and for a particular mission, stations situated all around Earth are being used. But this solution is much more expensive, which is not acceptable in amateur space missions, for example in AMSAT [1] programme. On the other hand, a single ground station has restricted range, which depends on the position of ground station and a satellite's orbit. Because of this the greater part of the mission does not have contact with the satellite, which in turn causes the reduction of the amount of data transmission between Earth and the satellite. A lot of radio amateurs have proper devices for radio amateur satellite communication and Internet connection. If they would like to cooperate, the communication through most of the orbit would be possible. In this article, the results of mathematical analysis carried out with author's software named distributed ground station system (DGSS) calculator will be shown. This software simulates optical visibility between the satellite and a ground station [2–5], and calculates parameters like free space loss (FSL) [3, 4] or bit error rate (BER) [3]. It can also calculate position of a satellite due to Keplerian elements [2–5].

2. Single ground station analysis

In Figs. 1 and 2 one can see an analysis of a single ground station radio-wave range for International Space Station (the orbit of 370 km has been chosen to emphasise the differences shown later in the paper).

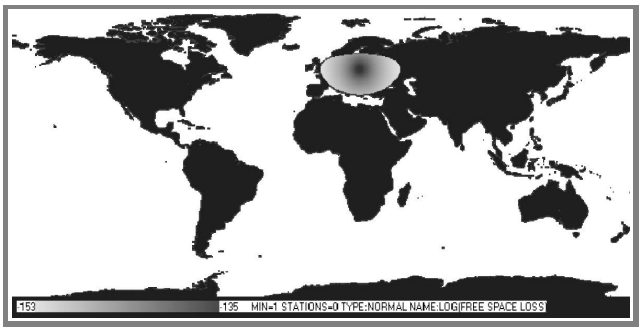

Fig. 1. Free space loss [dB].

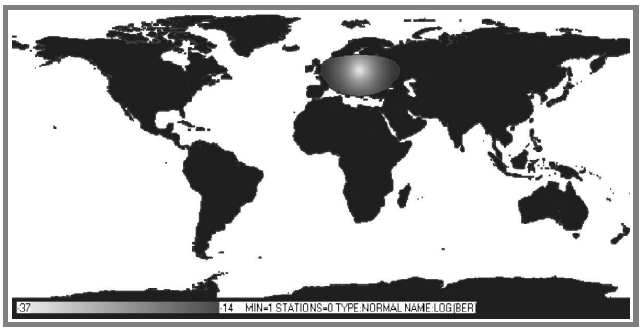

Fig. 2. Bit error rate.

Figure 1 shows FSL (Eq. (1)) in relation to distance between the satellite and a ground station for frequency $f = 433$ MHz in the optical horizon:

$$FSL\ [\mathrm{dB}] = 10 \log \left(\frac{4\pi R}{\lambda}\right)^2, \tag{1}$$

$$\lambda = \frac{\mathrm{c}}{f}, \tag{2}$$

where: R – distance, c – speed of light.

Beyond the horizon FSL is assumed to be equal to ∞. Next, the bit error rate (Eq. (3)) was calculated on the basis of FSL:

$$BER = \frac{1}{2} e^{\frac{SN\ [\mathrm{dB}]\, B}{-2BR}}, \tag{3}$$

$$\begin{aligned} SN\ [\mathrm{dB}] = & \\ & + TX\_power\ [\mathrm{dBw}] \\ & + TX\_gain\_ant \\ & + RX\_gain\_ant\ [\mathrm{dBi}] \\ & - FSL\ [\mathrm{dB}]. \end{aligned} \tag{4}$$

For the calculation the following parameters have been established: frequency shift keying (FSK) modulation, bit rate $BR = 1200$ bit/s, canal bandwidth $B = 7$ kHz, power of transmitter 5 W, gain of transmitter antenna 0 dBi, gain of receiver antenna 6 dBi. The calculated *BER* was between 10^{-14} and 10^{-32}.

3. Distributed ground station system analysis

The automatic position reporting system (APRS) [6, 7] is used by a lot of radio amateurs. Its job is to send the radio station position via radio to the APRS network. A typical APRS station can receive packets from other stations via radio and forward them via radio or the Internet.
In one week the activity of around 14 000 stations may be observed (Fig. 3), and the amount of data transferred by Internet servers is close to 250 MB per day. Most of it is generated in USA and the European countries (Fig. 4). APRS stations function also in other parts of the word. If the range of the satellite at 370 km would be simulated (Fig. 5), it could be seen that a satellite will be able to communicate with the APRS net in most of the areas.

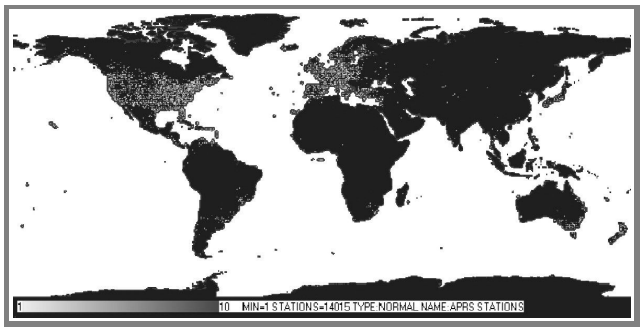

Fig. 3. The APRS stations.

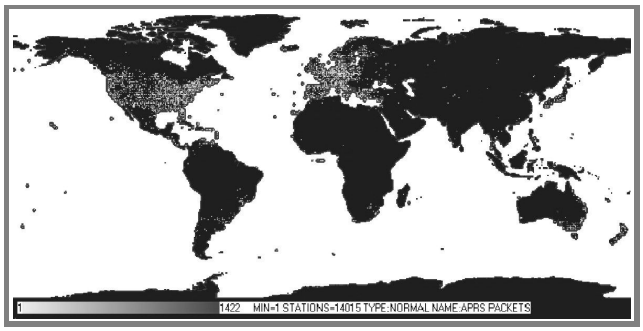

Fig. 4. The APRS packets.

Over USA and the EU the number of APRS stations within the range of the satellite exceeds 600. The results of theoretical *FSL* (Eq. (5)), assuming that the received energy will be summed, are visible in Fig. 6:

$$FSL_T\ [\mathrm{dB}] = 10 \log \left(\sum_{i=1}^{n} 10^{\frac{FSL_i\ [\mathrm{dB}]}{10}} \right). \tag{5}$$

In comparison with *FSL* of a single ground station, the *FSL* here is lower by about 25 dB.

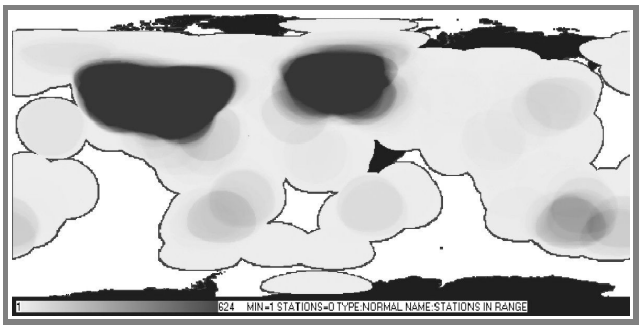

Fig. 5. Stations in range.

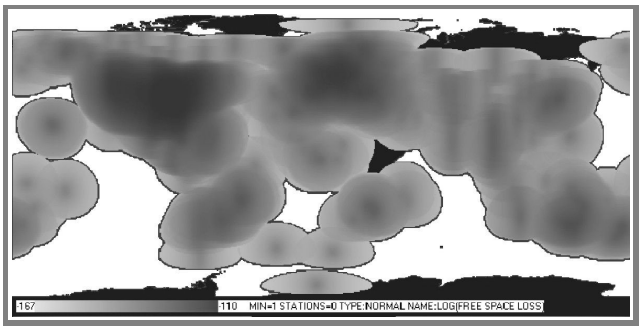

Fig. 6. Theoretical free space loss [dB].

Because it is rather impossible to connect all the antennas to a single receiver, the author proposes to carry out a comparative analysis of the received packets. The first idea is to compare *BER* of all the stations within a range, and chose the packet for the lowest one. This method will ensure keeping *BER* (Eq. (6)) between 10^{-4} and 10^{-36} (Fig. 7):

$$BER_{\mathrm{MIN}} = \min_{i=1}^{n} (BER_i). \tag{6}$$

A more advanced solution is also possible. The author's second proposition is to send raw data to the server, which would make the comparative analysis through voting between particular bits of particular packets. With the large number of stations we get a large number of

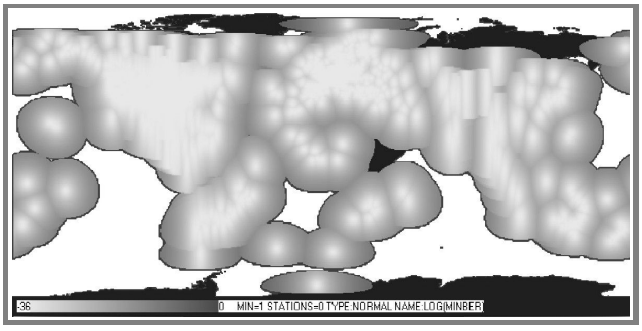

Fig. 7. Minimal bit error rate.

Fig. 8. Bit error rate.

packets to compare, which allows reducing *BER* (Eq. (7)) up to 10^{-30792} (Fig. 8):

$$BER_0 = \prod_{i=1}^{n} BER_i \,. \tag{7}$$

With such low *BER* one can considerably reduce the power of a transmitter, or increase transmission speed to the point where it would be possible to receive the packets with *BER* not higher than 10^{-4} on a given area. This would allow reducing the power on the satellite or increasing the amount of transmitted data.

4. Automatic position reporting system

The empirical verification of the proposed methods of reducing *BER* could be performed in the APRS net. There are different kinds of communications transmitted via this net. The first one contains the geographical situation of a station and some additional information, for instance the speed of the vehicle on which a station in located. The second kind of packets is telemetry. Its main use is transmitting information from weather stations, but any other kind of information can also be transmitted. The third kind of communications is short messages.

The packets of the first two kinds are broadcasted to all units of the APRS net. The amount of packets sent via radio is territorially restricted on account of radio wave link capacity. The full stream of data may be received via Internet.

The messages are being sent in a different manner. The messages are of two kinds. The first one is the bulletins, which are sent to all stations. The second one is private messages, which are sent to specific recipients.

The APRS net sends this kind of messages for re-transmitting to all stations connected to the Internet. If one of the stations hears the station of the addressee on a radio port within a specific period of time (usually 30 min), the re-transmission of the message via the radio port goes through. When the addressee receives the message, he sends a confirmation message to the sender.

This way of communication is not 100% successful, but it is sufficient for radio amateurs. It is also used for communication with radio amateur satellites [1]. However, it has some flaws. While the system enables receiving telemetry from the satellite when it is within the range of the net, sending messages to the satellite via the net is virtually impossible. When the satellite is, for instance, over USA, it is within the range of over 600 stations, and if all of them re-transmit the message to the satellite at once (because they all heard the satellite within the last 30 min) the packets will collide in the radio wave and such packet will not be received correctly. Because of this, transmission to the satellite is possible only when it is directly over the main ground station.

The author proposes to solve this problem by providing radio amateurs with special client software. Such a client would receive the re-transmission packet by a separate channel, which would allow for the message to be transmitted only to the chosen station.

The second problem concerns the legal aspects of working with the APRS net. The national and international regulations demand that transmissions via radio amateur systems be overt (not encoded). This makes a satellite vulnerable to an unauthorised access of other radio amateurs.

The author proposes to carry out the authorisation by means of an electronic signature. Every message to the satellite would be signed electronically by the operation team and the satellite would only accept the commands signed in this way. Still, there is a risk of a signed message being intercepted and re-transmitted again by an unauthorised sender. To eliminate this risk, the addition of an incremented counter to the message is proposed, which would allow eliminating the already used packets.

5. Distributed ground stations system

In order for the experiment to take advantage of all the possibilities of a diffused packet analysis, the author proposes to construct a system of a diffused ground station. Such a system would make use of a couple of subsystems.

The DGSS elements are:

- Local ground station for a direct communication with a satellite in case of unavailability of the distributed system.
- Remote control ground station also known as virtual ground station [8]. The system would allow for a remote managing of a radio amateur station through the remote turning of radio amateur antennas and altering the radio frequency.
- Distributed client server communications system for collecting raw data from the station in order to process it later. The packets to be send to a satellite would be sent in a return channel. This system would assess the quality of data (it would foresee *BER* on the basis of the location of a station and a satellite). It would also decide which station would be most suitable for sending the packets to a satellite

(on the basis of the quality of the received packets and theoretical capabilities resulting from a mathematical model).

- Packet voting system (PVS) for comparing many packets (even the damaged ones) received simultaneously by many stations (parallel receiving system). Eventually, the correct packets with the information from a satellite would be received.
- Remote control console is a panel for receiving the decoded telemetry of a satellite with PVS, and creating the packets with commends for a satellite.

6. Summary

The author presented a new method of space communication, which uses a parallel data reception from the satellite and proposed a subsequent analysis in order to reduce *BER* with mathematical methods. The calculation results show a great improvement of transmission when using a parallel reception. A practical verification of the method could be carried out using APRS communication with certain modifications, which would allow further improvement of *BER*. The experiment is planned as a part of space mission PW-Sat [9], which consist in the Warsaw University of Technology sending a small satellite in order to check a possibility of bringing satellites from the orbit by using aerodynamic resistance at the orbit.

References

[1] AMSAT, http://www.amsat.org

[2] "Orbital mechanics with MATLAB". Documents describes an interactive MATLAB script named npoe.m, http://www.cdeagle.com/ommatlab/npoe.pdf

[3] M. O. Kolawole, *Satellite Communication Engineering*. New York: Marcel Dekker, 2002.

[4] D. J. Bem, *Telewizja satelitarna*. Warszawa: Wydawnictwo SIGMA NOT, 1992 (in Polish).

[5] J. A. Magliacane, "PREDICT: a satellite tracking/orbita prediction program", http://www.qsl.net/kd2bd/predict.html

[6] APRS International, www.aprs.org

[7] APRS Poland, www.aprs.pl

[8] S. Bernier and M. Barbeau, "A virtual ground station based on distributed components for satellite communications", in *15th Ann. AIAA Conf. Small Satell.*, Logan, USA, 2001.

[9] G. Niemirowski, "Cubesat microsatellite with balloon", in *56th Int. Astronaut. Congr.*, Fukuoka, Japan, 2005.

Marcin Stolarski was born in Warsaw, Poland, in 1976. He received the M.Sc. degree in computer science at the Warsaw University of Technology, Poland, in 2004. He is currently a Ph.D. student at the same university. His research interests and work are related to space technology, focusing on communication systems, distributed networks and fault tolerant systems. He is a member of the Student Space Engineering Scientific Group and works in space projects like SSETI ESEO Satellite, PW-Sat and YES2. He is the author and co-author of many documents concerning space systems.
e-mail: M.Stolarski@elka.pw.edu.pl
Institute of Radioelectronics
Warsaw University of Technology
Nowowiejska st 15/19
00-665 Warsaw, Poland

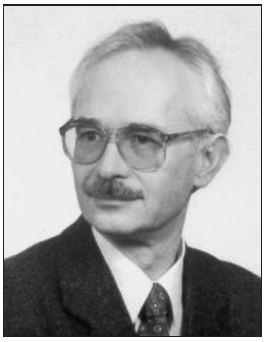

Wiesław Winiecki received his M.Sc., Ph.D. and D.Sc. degrees from the Faculty of Electronics, Warsaw University of Technology, Poland, in 1975, 1986 and 2004, respectively. Since 1975 he has been with the Institute of Radioelectronics of that university, now as a Professor. Since the beginning of his professional carrier he has been involved in the activities of the group on computer-aided measurements concerning the hardware and software for measuring systems. His main field of activity has been focused on virtual instruments and distributed measuring systems. He is the author or co-author of four books and over 120 scientific publications. Head of the Computer-Aided Measurement Laboratory; member of the Measuring Systems Section of the Metrology and Instrumentation Committee, Polish Academy of Science; President of the Polish Society for Measurement, Automatic Control and Robotics POLSPAR; and member of IEEE.
e-mail: w.winiecki@ire.pw.edu.pl
Institute of Radioelectronics
Warsaw University of Technology
Nowowiejska st 15/19
00-665 Warsaw, Poland

Paper

Microwave radiometry in monitoring and emergency mapping of water seepage and dangerously high groundwaters

Anatoly M. Shutko, Alexander Haldin, Vladimir Krapivin, Evgenij Novichikhin, Igor Sidorov, Yurij Tishchenko, Roland Haarbrink, Georgi Georgiev, Rumiana Kancheva, Hristo Nikolov, Tommy Coleman, Frank Archer, Paolo Pampaloni, Simonetta Paloscia, Anatoly Krissilov, and Adriano Camps Carmona

Abstract— Detailed and geo-referenced maps identifying the locations of saturated and dry levees can be produced using microwave radiometric measurements from a light aircraft or helicopter, and integrated with GPS for positioning and orientation. The development of synergetic remote sensing technology for raised groundwater and seepage detection by the joint use of microwave and optical data along with GIS databases is an effective and most contemporary way of supporting risk assessment and facilitating disaster prevention and management. In this paper we present a remote sensing microwave technology for monitoring and detection of areas of water seepage through irrigation constructions, levees and dykes as well as for revealing areas with dangerously high groundwater level. The possibility for emergency response mapping, integrated with GPS and GIS data, facilitates the risk assessment and management services. The passive microwave radiometry (PMR) is based on spectral measurements in the millimetre to decimetre range of wavelengths. Compared to other remote sensing techniques, such as colour and infrared photography, thermal images and lidar, PMR is the only technology taking measurements under the earth's surface and therefore is very well suited for water seepage and underground water monitoring in a fast and reliable way.

Keywords— remote sensing, passive microwave radiometry, soil moisture, water seepage, risk assessment.

1. Multilateral agreement

Multilateral agreement on collaboration in the field of remote sensing of the Earth has been developed on the initiative of Prof. Anatoly Shutko between the following institutions:

- Institute of Radioengineering and Electronics (IRE), Russian Academy of Sciences (RAS), Moscow and Friazino, Russia;
- Microwave Radiometer Mapping Company (Miramap) – a Dutch ESA ESTEC Startup Company, Noordwijk, the Netherlands;
- Solar-Terrestrial Influences Laboratory (STIL), Bulgarian Academy of Sciences (BAS), Sofia, Bulgaria;
- Centre for Hydrology, Soil Climatology and Remote Sensing (HSCaRS), Alabama A&M University (AAMU), Huntsville, USA;
- Institute of Applied Physics (IFAC), National Research Council (CNR), Florence, Italy;
- Institute of Market Problems and Econo-Ecological Studies (IMPEES), National Academy of Sciences of Ukraine (NASU), Odessa, Ukraine;
- Politechnical University of Catalunya (UPC), Barcelona, Spain.

Among the issues of collaboration are:

- developing technologies for water seepage detection through levees and dykes;
- joint use of microwave, optical and other remote sensing devices;
- developing joint scientific projects;
- conducting research, experiments and teaching.

2. Fields of application

Following are the main application fields of the project activities:

- multispectral and multitemporal remote sensing monitoring of land covers from mobile platforms and aircrafts;
- hydrology [1, 2, 3];
- agriculture [4];
- forestry [5];
- ecology [6];
- risk assessment, emergency monitoring (levees and dams damage, flooding, etc.) [6].

3. Goals

The goal of the planed work is to create a powerful centralized information and management service by developing and adapting to the real environments of a new geoinformation monitoring system (GIMS) for land surface and water areas monitoring. The GIMS approach has been developed at the Institute of Radioengineering and Electronics, Russian Academy of Sciences (IRE RAS) [7, 8]. It is based on the joint use of the following constituents:

– remotely sensed microwave and optical data;

– *in situ* measurements;

– geographic information system (GIS) and other available database information;

– mathematical modeling of the spatial-temporal variations of land covers biophysical parameters.

Thus the efforts will be focused on the creation of new geoinformation technologies based on the combined use of GIS with measurement and modeling results in accordance with the formula: GIMS = GIS + measurements + models. Final products will include information about:

– soil moisture;

– depth to shallow water table;

– vegetation biomass;

– contours of water seepage through levees;

– contours of flooding;

– contours of areas with destroyed drainage;

– cloudiness;

– rainfall;

– melting: freezing conditions;

– contours of water pollution in the outflow zones, river deltas, lakes and harbors;

– risk assessment and emergency monitoring of situations associated with these phenomena.

4. Expected results

The main expected result of the project will be the development of advanced synergetic methods for microwave and optical remote sensing of land covers. Their utilization along with GIS knowledge-based information will permit the creation of GIMS, will increase data informational content and improve the possibility for emergency situations predicting and mitigating.

5. Approach

Among the various remote sensing instrumentation used in environmental studies microwave and optical systems can be implemented for investigation of vegetation type and biomass, soil moisture, dryness index, depth to shallow water table and buried objects location. Compared to other remote sensing techniques, such as color and infrared photography, thermal images and lidar, microwave radiometry is the only one taking measurements under the earth's surface and therefore is very well suited for levee and hydrological parameters monitoring in a fast and reliable way.

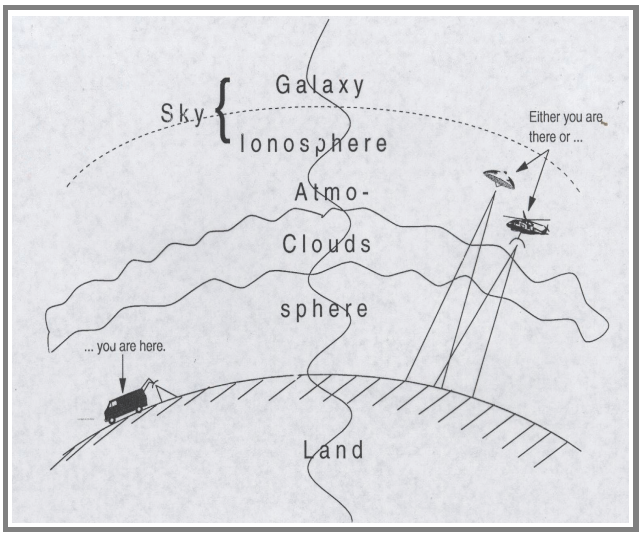

Fig. 1. Different sources of microwave radiation.

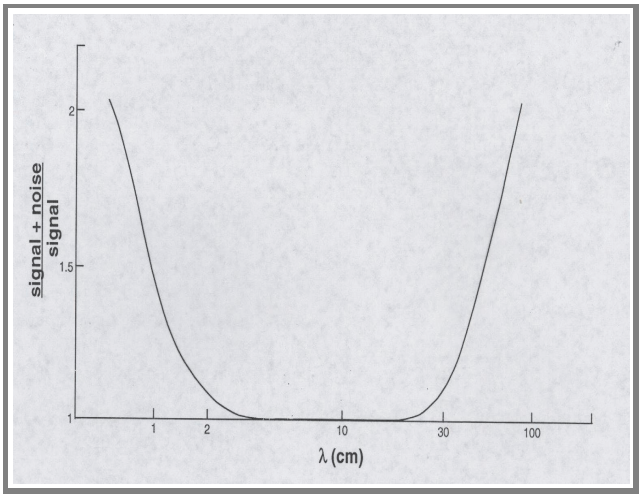

Fig. 2. Microwave windows of transparency.

Passive microwave radiometric systems record the naturally emitted radiation in the centi- to decimetric wavelength range. Different sources of microwave radiation are shown in Fig. 1. Investigations of water and land surfaces are performed in the 0.8–2.0 cm to 18–30 cm spectral bands. Within these bands, land surface and water radiation is

Fig. 3. Field and airborne microwave experiments.

primarily a function of the free water content in soil, but it is also influenced by other parameters, such as vegetation above-ground biomass, shallow groundwater, salinity and temperature of open water. The sensitivity of microwave measurements to these factors depends on the wavelength.

Least influenced by different sources of "radio noise" is the 2-cm to 21-cm wavelength band (Fig. 2). At wavelengths shorter than 0.8 cm, the surface radiation is considerably influenced by the atmosphere (water vapour, clouds, rain). At wavelengths longer than 21 cm, the surface radiation is affected by the ionosphere, galaxy radiation, and technical communication facilities. Agricultural vegetation is practically transparent at wavelengths longer than 21 cm. At shorter wavelengths the microwave radiation is a function of canopy type and biomass.

Optical sensors provide information about, vegetation type and state, soil humus content and erosion, contours of water bodies, floods, cloudiness, etc. Analysis of some experimental studies reveals the high potential and advantage of fusing microwave and optical remote sensing data. To find the best ways of advantageous synergetic use of microwave and optical remote sensing devices with due regard to a prior knowledge-based GIS information will be the main GIMS objective of this project.

6. Microwave radiometers

Through laboratory, field and airborne experiments (Fig. 3) it has been documented [1–4, 7, 8] that the passive microwave radiometers, and processing/retrieval algorithms developed at the IRE RAS are feasible to determine the listed below soil, water and vegetation related parameters:

- surface soil moisture;
- underground moistening;
- depth to a shallow water table (down to 2 m in humid areas and down to 3–5 m in arid/dry areas);
- located on the surface and shallowly buried metal objects of a reasonable size under dry ground conditions;
- contours of water seepage through hydrotechnical constructions (levees, dams, destroyed drainage systems, different kinds of leaks);
- biomass of vegetation above water surface or wet ground;
- temperature increase of land, forested and volcano areas;

– changes in salinity/mineralization and temperature of water surfaces;

– water surface pollution, oil slicks on water surfaces;

– on-ground snow melting;

– ice on water surfaces, roads and runways.

The operating range and errors of some land cover features retrieval are given in Table 1.

Table 1

Range and errors of land cover parameters retrieval

Parameter	Operating range	Maximum absolute error
Soil moisture content [g/cc]:	0.02–0.5	
– vegetation biomass less than 2kg/m^2		0.05
– vegetation biomass more than 2 kg/m^2		0.07
Depth to shallow water table [m]:		0.3–0.6
– humid, swampy areas	0.2–2	
– dry arid areas, deserts	0.2–5	
Plant biomass [kg/m^2]	0–3	0.2
Water salt and pollutant concentration [ppt]	1–300	1–5

7. Participants' resources

Following are today's participants and their currently available resources:

- **Institute of Radioengineering and Electronics, Russian Academy of Sciences, Russia**:

  – a set of microwave radiometric sensors consisting of three non-scanning radiometers, operating at the wavelengths of 6, 18 and 21 cm, a three-channel scanning radiometer operating at the wavelengths of 0.8, 2 and 5.5 cm and a twin-beam 21 cm radiometer (Tables 1, 2 and 3, Fig. 4);

  – software for surface soil moisture assessment (Fig. 5);

  – software for detecting areas with high groundwater level and water seepage through levees (Fig. 6);

  – data acquisition system;

  – data mapping software.

Fig. 4. Scanning microwave radiometer inside a fixed-wing aircraft.

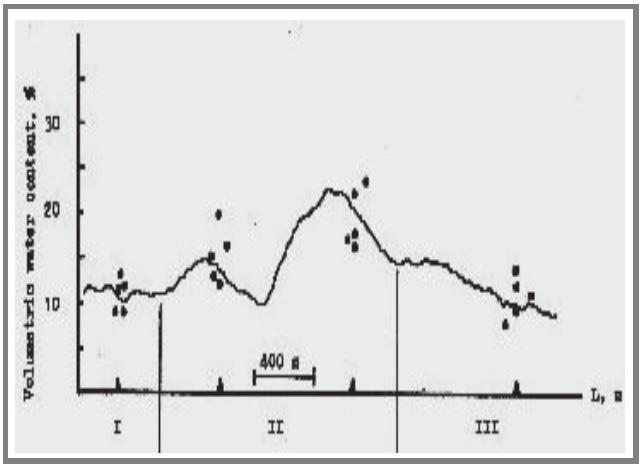

Fig. 5. Soil moisture from airborne microwave (—) and ground-truth measurements (•) along a transact with different soil types (I-III).

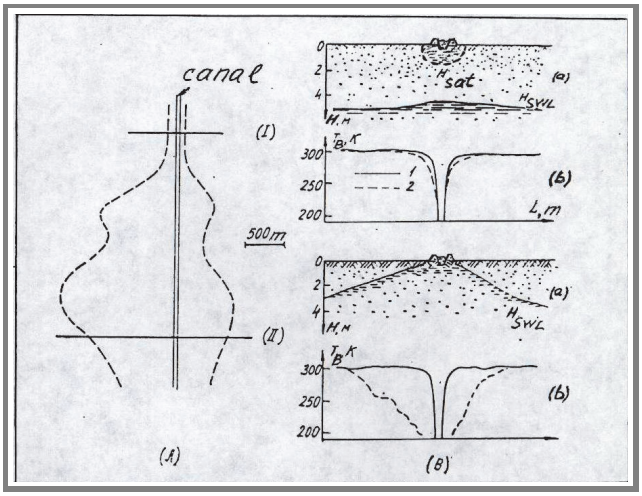

Fig. 6. Seepage/leakage detection through levees/dikes.

Table 2
Technical characteristics of the scanning
(H – height above ground)

Frequency [GHz]	Wavelength [cm]	Band	Pixels/scan	Resolution	Mode
37	0.8	Ka	32	0.04 · H	Scanning
15.2	2	X	16	0.08 · H	Scanning
5.5	5.5	C	6	0.13 · H	Scanning
1.4	21	L	2	0.65 · H	Twin-beam

Table 3
Parameters of twin-beam radiometers

Parameter	Scanning system
Ground swath	1.3 · H
Power consumption	300 W
Power supply	27 V_{DC}
Aircraft mounting hole	50 cm
Weight	130 kg

- **Microwave Radiometer Mapping Company (Miramap), the Netherlands**:
  - light aircraft (Fig. 7);
  - avionics;
  - geodetic global positioning system (GPS) receiver;
  - flight management system;
  - portable digital optical colour camera Axis 2100 to be used for tracking on-ground objects and for use of optical data along with microwave radiometric data.

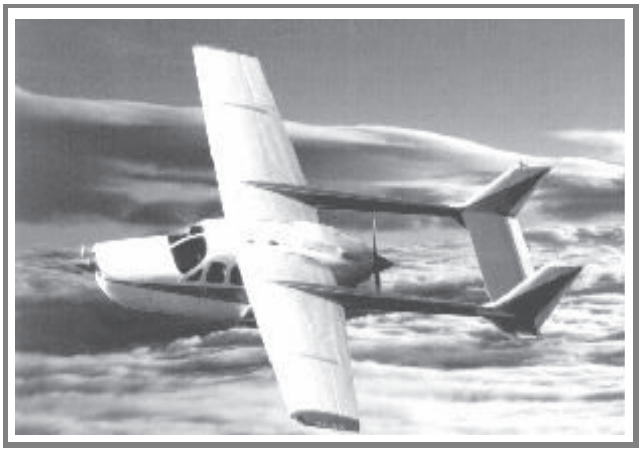

Fig. 7. Aircraft operation: Skymaster.

- **Solar-Terrestrial Influences Laboratory, Bulgarian Academy of Sciences, Sofia, Bulgaria**:
  - optical spectrometer;
  - data processing algorithms.
- **Centre for Hydrology, Soil Climatology and Remote Sensing, Alabama A&M University, Huntsville, USA**:
  - unmanned helicopter (Fig. 3);
  - data interpretation.
- **Institute of Market Problems and Econo-Ecological Studies, National Academy of Sciences of Ukraine, Odessa, Ukraine**:
  - hosting autumn 2005 experiments.
- **Institute of Applied Physics, National Research Council, Florence, Italy**:
  - thematic data interpretation.
- **Polytechnical University of Catalunya (UPC), Barcelona, Spain**:
  - thematic data interpretation.

8. Conclusions

There exists a fundamental background for bringing together an international team of experts ready to conduct research, development, application and teaching in microwave radiometry for soil surface and underground moisture investigations as well as in optical spectrometry for soil-vegetation land covers assessment. The added-value of the collaboration will be the implementation of advanced technologies based on data fusion for such important and urgent tasks as the detection of areas of water seepage through irrigation constructions, levees and dykes and the revealing of areas with dangerously high groundwater level. It is our belief, that this collaboration will provide a beneficial impact on research, application and teaching in the field of remote sensing technologies and their operational use.

Acknowledgment

The collaborating partners are thankful to all sponsoring institutions for their support of the scientific research concerning such an important emergency related problem. The paper was prepared also in the frameworks of the contract between the Russian and Bulgarian Academies of Sciences *Development of New Technologies in Aerospace Remote Sensing of the Earth* and under the support of the NSFB contract NZ-1410/04.

References

[1] A. M. Shutko, "Remote sensing of soil moisture and moisture related parameters by means of microwave radiometry: instruments, data, and examples of application in hydrology", in *Land Surface Processes in Hydrology, Trials and Tribulations of Modeling and Measuring*, S. Sorooshian, H. V. Gupta, and J. C. Rodda, Eds. Berlin: Springer, 1997, pp. 263–273.

[2] T. J. Jackson, A. Y. Hsu, A. Shutko, Yu. Tishchenko, B. Petrenko, B. Kutuza, and N. Armand, "Priroda microwave radiometer observations in the Southern Great Plains: 1997 hydrology experiment", *Int. J. Rem. Sens.*, vol. 23, no. 2, pp. 231–248, 2002.

[3] F. A. Mkrtchan, E. Reutov, A. Shutko, K. Kostov, M. Michalev, N. Nedeltchev, A. Spasov, and B. Vichev, "Experiments in Bulgaria for determination of soil moisture in the top one-meter using microwave radiometry and a priori information", in *Proc. IGARSS'88 Int. Symp.*, Edinburgh, UK, 1988, pp. 665–666.

[4] S. P. Golovachev, E. A. Reutov, A. A. Chukhlantsev, and A. M. Shutko, "Experimental investigation of microwave emission of vegetable crops", *Izvestia VUZ'ov, Radiofizika*, vol. 32, pp. 551–556, 1989 (in Russian; English Translation: *Univ. Dig., Radiophys. Quant. Electron.*).

[5] P. Pampaloni, "Microwave radiometry of forests", *Wav. Rand. Med.*, vol. 14, pp. S275–S298, 2004.

[6] R. B. Haarbrink and A. M. Shutko, "Airborne passive microwave radiometry for emergency response", in *Proc. 1st Int. Symp. Geo-Inform. Disas. Manag.*, Delft, the Netherlands, 2005.

[7] A. M. Shutko, A. A. Haldin, E. P. Novichikhin, A. A. Milshin, S. P. Golovachev, A. G. Grankov, V. G. Mishanin, T. J. Jackson, B. J. Logan, G. B. Tilley, E. W. Ramsey III, and H. Pirchner, "Microwave radiometers and their application in field and aircraft campaigns for remote sensing of land and water surfaces", in *Proc. IGARSS '95 Int. Symp.*, Florence, Italy, 1995, pp. 734–735.

[8] B. Kutuza, A. Shutko, V. Pliushchev, E. Ramsey III, B. Logan, S. DeLoach, A. Haldin, E. Novichikhin, I. Sidorov, and G. Nelson, "Advantages of synchronous multispectral SAR and microwave radiometric observations of land covers from aircraft platforms", in *Proc. EUSAR 2000*, Germany, Munich, 2000.

Anatoly Mikhailovich Shutko, Prof., Ph.D., Head of Laboratory, Institute of Radioengineering and Electronics, Russian Academy of Sciences, 141190 Moscow region, Fryazino, Acad. Vvedenskogo Sq. 1, Russia, phone: (495) 702-9588, fax: (495) 702-9572, research Professor at HSCaRS AAMU, and Assoc. Prof. at STIL-BAS, e-mail: ashutko@ms.ire.rssi.ru. Scientific interests: Earth observation, multispectral remote sensing of the environment, development and implementation of radiophysical methods for soil moisture assessment, microwave radiometry, development of a geoinformation monitoring system and advanced technologies for remote sensing.

Alexander Alexandrovich Haldin, Dr., Head of Department, Special Design Bureau at the Institute of Radioengineering and Electronics, Russian Academy of Sciences, Russia, 141190 Moscow region, Fryazino, Acad. Vvedenskogo Sq. 1, phone: (495) 526-9133, fax: (495) 702-9572, e-mail: ahaldin@sdb.ire.rssi.ru. Scientific interests: design and construction of remote sensing instruments.

Vladimir Fedorovich Krapivin, Prof., Ph.D., Head of Department, Institute of Radioengineering and Electronics, Russian Academy of Sciences, Russia, 141190 Moscow region, Fryazino, Acad. Vvedenskogo Sq. 1, fax: (495) 702-9572, e-mail: vfk@ms.ire.rssi.ru. Scientific interests: development and application of a geoinformation monitoring system technology for remote sensing.

Evgenij Pavlovich Novichikhin, Ph.D., Head of Laboratory, Institute of Radioengineering and Electronics, Russian Academy of Sciences, Russia, 141190 Moscow region, Fryazino, Acad. Vvedenskogo Sq. 1, phone: (495) 702-9588, fax: (495) 702-9572, e-mail: epnov@ms.ire.rssi.ru. Scientific interests: remotely sensed data processing and interpretation.

Igor Sidorov, Dr., Head of Laboratory, Radio Corporation "VEGA", Russia, Moscow, Kutuzovski prospekt, e-mail: igor_sidorov@mail.ru. Scientific interests: active and passive microwave radiometry, SAR, data processing, remote sensing.

Yurij Grigorievich Tishchenko, Assoc. Prof., Ph.D., Head of Department, Institute of Radioengineering and Electronics, Russian Academy of Sciences, Russia, 141190 Moscow region, Fryazino, Acad. Vvedenskogo Sq. 1, phone: (495) 702-9588, fax: (495) 702-9572, e-mail: tishchen@ire.rssi.ru. Scientific interests: development and application of radiophysical methods for Earth remote sensing, optical and microwave data processing and interpretation, information technologies in land cover monitoring.

Roland B. Haarbrink, Dr., Dutch ESA ESTEC Startup Company Miramap (Microwave Radiometer Mapping Company), Managing Director Keplerlaan 1, P.O. Box 299 2200 AG Noordwijk, the Netherlands, web: www.miramap.com. Scientific interests: Earth remote sensing, light aircraft equipment for land cover monitoring, sensor fusion, digital photogrammetry, microwave radiometry, GPS, GIS.

Georgi S. Georgiev, Dr., Remote Sensing Department, Solar-Terrestrial Influences Laboratory (STIL), Bulgarian Academy of Sciences (BAS), Bulgaria, 1113 Sofia, Acad. G. Bonchev bl. 3, phone: (359) 2 979-3353, fax: (359) 2 8700 178, e-mail: gsgsgs@abv.bg. Scientific interests: design and construction of remote sensing devices, telecommunications, wireless network technologies for scientific and industrial applications.

Rumiana H. Kancheva, Assoc. Prof., Ph.D., Solar-Terrestrial Influences Laboratory, Remote Sensing Department, Bulgarian Academy of Sciences, Bulgaria, 1113 Sofia, Acad. G. Bonchev bl. 3, phone: (359) 2 979-3353, fax: (359) 2 8700 178, e-mail: rumik@abv.bg. Scientific interests: Earth remote sensing, soil and vegetation assessment, agroecology, advanced data processing tools, information extraction algorithms.

Hristo S. Nikolov, Dr., Solar-Terrestrial Influences Laboratory, Remote Sensing Department, Bulgarian Academy of Sciences, Bulgaria, 1113 Sofia, Acad. G. Bonchev bl. 3, phone: (359) 2 979-3353, fax: (359) 2 8700 178, e-mail: hristo@stil.bas.bg. Scientific interests: Earth remote sensing, soil and vegetation assessment, image processing, neural networks, data fusion.

Tommy Coleman, Prof., Ph.D., Soil Science Department Director, Centre for Hydrology, Soil Climatology and Remote Sensing, Alabama A&M University (HSCaRS AAMU), NASA research centre, Room 207 Carver Complex Thomas Wing, P.O. Box 1208, Alabama A&M University Normal, AL 35762, Huntsville, USA, phone: (256) 372 4192, fax: (256) 372 5429, e-mail: tcoleman@aamu.edu, web: http://saes.aamu.edu/. Scientific interests: soil studies, remote sensing, optical and microwave radiometry, and land covers assessment.

Frank Archer, Dr., research Assistant, Centre for Hydrology, Soil Climatology and Remote Sensing, Alabama A&M University (HSCaRS AAMU), Room 209 Carver Complex Thomas, Wing P.O. Box 1208 Alabama A&M University Normal, AL 35762, Huntsville, USA, web: http://saes.aamu.edu/. Scientific interests: remote sensing technologies, microwave radiometry, soil studies.

Paolo Pampaloni, Dr., Ph.D., Head of Research Laboratory, Institute for Applied Physics "Nello Carrara" (IFAC), National Research Council (CNR), Florence, Italy, Via Madonna del Piano, 10 I-50019 Sesto Fiorentino (FI), web: http://www.ifac.cnr.it/index-e.php. Scientific interests: remote sensing technologies, microwave radiometry application in soil, vegetation and snow cover assessment.

Simonetta Paloscia, Dr., Institute for Applied Physics "Nello Carrara" (IFAC), National Research Council (CNR), Florence, Italy, Via Madonna del Piano, 10 I-50019 Sesto Fiorentino (FI), web: http://www.ifac.cnr.it/index-e.php. Scientific interests: active and passive remote sensing of soils and vegetation, data thematic interpretation for land covers assessment.

Anatoly Krissilov, Dr., Institute of Market Problems and Econo-Ecological Studies (IMPEES), National Academy of Sciences of Ukraine (NASU), Foreign Relations Department, 54 Volodymyrska st, 01601, Kyiv-30, Ukraine, phone: (044) 235 2239, e-mail: VictorK@o1405.paco.net, web: http://www.nas.gov.ua

Adriano Camps Carmona, Dr., Polytechnical University of Catalunya (UPC), Department of Signal Theory and Communications DESPATX 016 Campus NORD – Edif. D4 C. JORDI GIRONA, 1-3 08034 Barcelona, Spain, web: http://www.tsc.upc.edu/eng/. Scientific interests: remote sensing technologies, data processing and thematic interpretation, land covers assessment.

Paper

Modeling of mixed traffic for mobile cellular network

Imdadul Islam, Jugal Krishna Das, and Siddique Hossain

Abstract— The most convenient way of presenting one- or two-dimensional offered traffic in a network by Markovian chain to evaluate quality of service (QoS). Pictorial presentation of chain becomes very complicated for three dimensional traffic case, required for voice data integrated service/mixed traffic of mobile cellular network; hence application of cut or node equations become a cumbersome job. This paper proposes a model of three-dimensional traffic in a network for both unlimited and limited user case. Here direct analytical method is introduced instead of Markovian chain to achieve traffic parameters.

Keywords— quality of service, Markovian chain, time and call congestion, probability states and voice data integrated network.

1. Introduction

In teletraffic engineering two different cases of traffic, i.e., limited and unlimited users are prevalent. Both types of traffic and their combination could be modeled using state transition diagram/Markovian chain, to reveal different probability states of offered traffic and their transition based on average arrival and termination rate like in [1–5]. After modeling the chain, cut or node equations are applied to achieve relation between different probability sates. Finally each probability state is normalized by dividing it by entire sample space.

A good example of multi-dimensional traffic is mobile cellular network where two different arrivals, i.e., new originating call and handoff arrival traffic are prevalent, summarized in [6–9]. Of course, bandwidth (BW) of either traffic is same since both are voice signals. If there is a provision of another offered traffic of different bandwidth, say video/text/image data is added to conventional mobile cellular system like voice data integrated network of [10, 11].

Three-dimensional traffic model of this paper would be consistent with voice data integrated service and could be an useful tool for a network planar to estimate performance of his network.

Here the concept of two-dimensional traffic is adopted to achieve generalized equation of probability state and blocking probability for three-dimensional traffic case. Section 2 of the paper reveals theoretical analysis of three-dimensional traffic, Section 3 proposes mathematical modeling of 3D traffic, Section 4 depicts the results of previous sections and finally Section 4 concludes the entire paper.

2. Mixed traffic model

Let us now consider a three-dimensional Markov process where any probability state $P_{u,v,w}$ reveals that a cell is occupied by u voice calls of new arrival, v packet/data calls and w handover voice calls. Assuming the bandwidth of data call is $h \geq 2$ times wider than that of voice call. State transition chain of three-dimensional mixed traffic is shown in Fig. 1 based on general packed radio services (GPRS) network of [13], birth-death process of IS-95 handoff of [14] and multimedia traffic of [15].

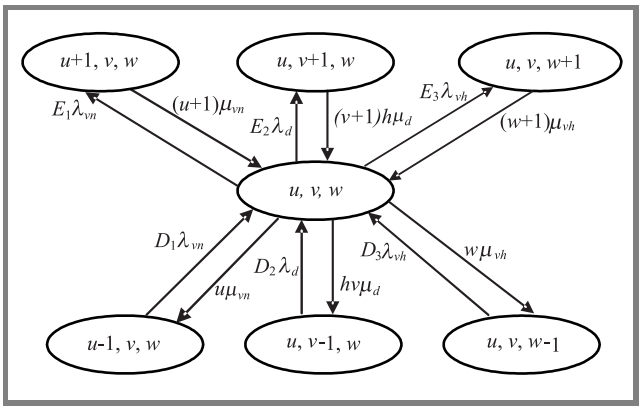

Fig. 1. State transition diagram for mixed traffic.

Entire set of probability states of the transition diagram is

$$S = \left\{ (u,v,w) \middle| 0 \leq v + vh + w \leq n, 0 \leq u \leq n, 0 \leq v \leq \left\lfloor \frac{n}{h} \right\rfloor \text{ and } 0 \leq w \leq n \right\}, \tag{1}$$

where $\lfloor x \rfloor$ is a floor function.

For all valid states:

$$\sum_{(u,v,w)\in S} P(u,v,w) = 1\,, \tag{2}$$

where S is the set of valid probability states.

Several states are unreachable, based on following six conditions:

$$D_1 = \begin{cases} 1;\ u-1+hv+w \leq n-1 \quad \text{and} \quad (u-1,v,w) \in S \\ 0;\ \text{otherwise} \end{cases}, \tag{3}$$

$$D_2 = \begin{cases} 1;\ u+h(v-1)+w \le n-h \quad \text{and} \quad (u,v-1,w) \in S \\ 0;\ \text{otherwise} \end{cases}, \tag{4}$$

$$D_3 = \begin{cases} 1;\ u+hv+w-1 \le n-1 \quad \text{and} \quad (u,v,w-1) \in S \\ 0;\ \text{otherwise} \end{cases}, \tag{5}$$

$$E_1 = \begin{cases} 1;\ u+hv+w \le n-1 \quad \text{and} \quad (u+1,v,w) \in S \\ 0;\ \text{otherwise} \end{cases}, \tag{6}$$

$$E_2 = \begin{cases} 1;\ u+hv+w \le n-h \quad \text{and} \quad (u,v+1,w) \in S \\ 0;\ \text{otherwise} \end{cases}, \tag{7}$$

$$E_3 = \begin{cases} 1;\ u+hv+w \le n-1 \quad \text{and} \quad (u,v,w+1) \in S \\ 0;\ \text{otherwise} \end{cases}. \tag{8}$$

Now the sum of the probabilities of complete occupation of channels in Eq. (12) gives call blocking probability based on [12]:

$$B = \sum_{C \in \left\{(u,v,w) \middle| u+hv+w=n,\ 0 \le u \le n,\ 0 \le v \le \left\lfloor \frac{n}{h} \right\rfloor,\ 0 \le w \le n \right\}} P(u,v,w). \tag{9}$$

Let us now apply node equation at (u,v,w) of Fig. 1:

$$\begin{aligned} & P_{u,v,w}\{E_1\lambda_{vn} + E_2\lambda_d + E_3\lambda_{vh} + u\mu_{vn} + hv\mu_d + w\mu_{vh}\} \\ &= P_{u+1,v,w}(u+1)\mu_{vn} + P_{u,v+1,w}(v+1)h\mu_d \\ &\quad + P_{u,v,w+1}(w+1)\mu_{vh} + P_{u,v,w-1}D_3\lambda_{vh} \\ &\quad + P_{u,v-1,w}D_2\lambda_d . \end{aligned} \tag{10}$$

Any probability state could be determined from a set of such linear equations at different nodes.

3. Proposed traffic model

It would be a laborious job to determine quality of service (QoS) or probability states of the network from a series of node equations like Eq. (10). In this section an alternate model is proposed to determine normalized probability states or QoS directly. One of the convenient ways of presenting two-dimensional traffic is in triangular matrix form, where corresponding terms of the following two series of A_1 and A_2 (A_1 and A_2 are the offered traffic of $M/M/n$ case) are multiplied:

$$1,\ \frac{A_2}{1!},\ \frac{A_2^2}{2!},\ \frac{A_2^3}{3!},\ \ldots,\ \frac{A_2^{n-2}}{(n-2)!},\ \frac{A_2^{n-1}}{(n-1)!},\ \frac{A_2^n}{n!}$$

$$1,\ \frac{A_1}{1!},\ \frac{A_1^2}{2!},\ \frac{A_1^3}{3!},\ \ldots,\ \frac{A_1^{n-2}}{(n-2)!},\ \frac{A_1^{n-1}}{(n-1)!},\ \frac{A_1^n}{n!}.$$

For limited trunk case, only the probability states, $P_{x,y}$ satisfying the condition $x+y \le n$ (n is the total number of channels) will remain in the table, form a triangular matrix. Diagonal elements the table/matrix will be the complete occupied states and sum of those states in normalized form gives the call blocking probability the network.

Now rows of the triangular matrix for n channels network would be like:

$$\begin{aligned} & \left(1 \quad \frac{A_2}{1!} \quad \frac{A_2^2}{2!} \quad \frac{A_2^3}{3!},\ \ldots,\ \frac{A_2^{n-2}}{(n-2)!} \quad \frac{A_2^{n-1}}{(n-1)!} \quad \frac{A_2^n}{n!}\right) \\ & A_1\left(1 \quad \frac{A_2}{1!} \quad \frac{A_2^2}{2!} \quad \frac{A_2^3}{3!},\ \ldots,\ \frac{A_2^{n-2}}{(n-2)!} \quad \frac{A_2^{n-1}}{(n-1)!}\right) \\ & \frac{A_1^2}{2!}\left(1 \quad \frac{A_2}{1!} \quad \frac{A_2^2}{2!} \quad \frac{A_2^3}{3!},\ \ldots,\ \frac{A_2^{n-2}}{(n-2)!}\right) \\ & \vdots \\ & \frac{A_1^{n-3}}{(n-3)!}\left(1 \quad \frac{A_2}{1!} \quad \frac{A_2^2}{2!} \quad \frac{A_2^3}{3!}\right) \\ & \vdots \\ & \frac{A_1^n}{n!}. \end{aligned}$$

Therefore complete set of occupied states (utilization of n channels), i.e., diagonal elements of the matrix are:

$$\frac{A_2^n}{n!},\ \frac{A_2^{n-1}}{(n-1)!}A_1,\ \frac{A_2^{n-2}}{(n-2)!}\frac{A_1^2}{2!},\ \ldots,\ \frac{A_2^3}{3!}\frac{A_1^{n-3}}{(n-3)!},\ \ldots,\ \frac{A_1^n}{n!}.$$

The normalized form of sum of complete occupied states is given as

$$\therefore\ S = \frac{\sum_{r=0}^{n} \frac{A_1^r}{r!}\frac{A_2^{n-r}}{(n-r)!}}{\sum_{p=0}^{n} \frac{A_1^p}{p!}\sum_{q=0}^{n-p}\frac{A_2^q}{q!}}. \tag{11}$$

Each element of the matrix is divided by the entire sampling space to achieve normalized probability states and blocking probability would be the sum of normalized completely occupied states shown in Eq. (11). Probability states of three-dimensional unlimited user's traffic with offered traffics, A_x, A_y and A_z erlangs of equal bandwidth could be presented like triangular matrix of two-dimensional traffic taking any single traffic like A_z as a parameter shown in Fig. 2. Here the states corresponding to complete utilization of channel are depicted with shaded block on right side for number of channel $n = 4$; of course all the states are shown here before normalization.

Now sum of complete utilized states in normalized form, i.e., blocking probability is derived as:

$$B(A_x,A_y,A_z,n) = \frac{\sum_{p=0}^{n} \frac{A_z^p}{p!}\sum_{r=0}^{n-p}\frac{A_x^r}{r!}\frac{A_y^{n-r-p}}{(n-r-p)!}}{\sum_{p=0}^{n} \frac{A_z^p}{p!}\sum_{r=0}^{n-p}\frac{A_x^r}{r!}\sum_{s=0}^{n-r-p}\frac{A_y^s}{s!}}. \tag{12}$$

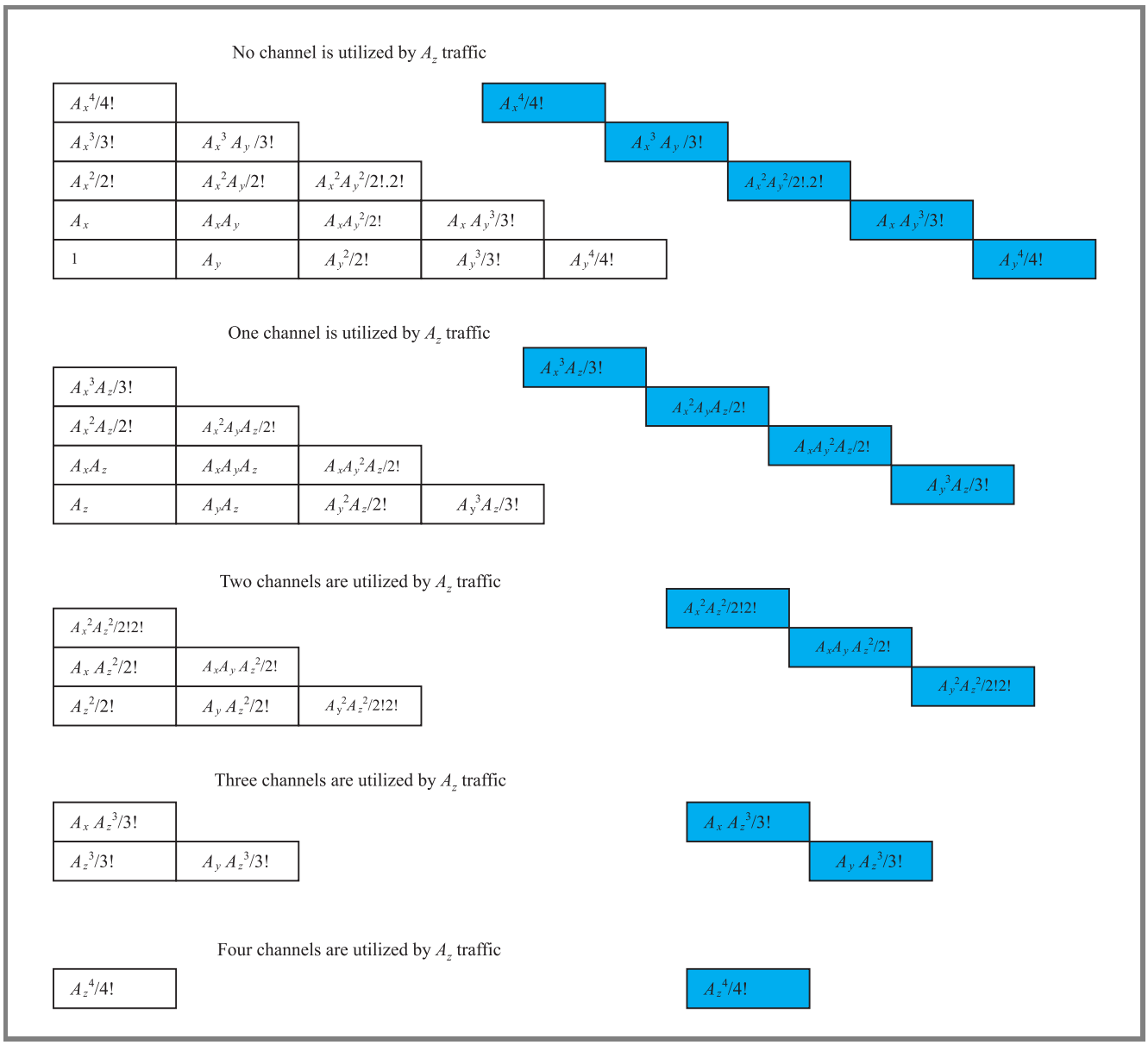

Fig. 2. Probability states of 3D traffic with complete utilization states before normalization ($n = 4$).

Probability states of Fig. 2 could be shown more explicitly in three-dimensional plain like Fig. 3, where each shaded state indicates complete utilization of channels by combination of traffic A_x, A_y and A_z. Arrows in z direction indicates blocking states of A_z traffic.

For non-uniform bandwidths above equations have to be modified according to the bandwidth of offered traffic A_x, A_y and A_z. Before going to mathematical derivation, let us assume that bandwidth of A_z traffic is twice wider than that of A_x or A_y. Now probability states of Fig. 3 would be modified like Fig. 4, where number of probability states are greatly reduced. Observing the trend of change of Figs. 3 and 4 would help us to derive generalized equation of probability state for non-uniform bandwidth traffic.

Let us consider a case when bandwidth of A_z traffic is h times greater than that of A_x or A_y of course bandwidth of A_x and A_y are equal. Blocking probability of Eq. (12) now would be modified like follows:

$$B(A_x,A_y,A_z,n,h) = \frac{\sum_{p=0}^{\Omega} \frac{A_z^p}{p!} \sum_{i=0}^{h-1} \sum_{r=0}^{\phi} \frac{A_x^r}{r!} \frac{A_y^{\phi-r}}{(\phi-r)!}}{\sum_{p=0}^{\Omega} \frac{A_z^P}{p!} \sum_{i=0}^{n-hp} \frac{A_x^i}{i!} \sum_{j=0}^{\phi} \frac{A_y^j}{j!}}, \quad (13)$$

where $\Omega = \lfloor n/h \rfloor$ and $\phi = n - i - hp$ and $\phi \geq 0$.

Limited user's traffic is applicable to small networks like a micro/pico cell of a mobile cellular network with low offered traffic, cell of a wireless local loop (WLL)

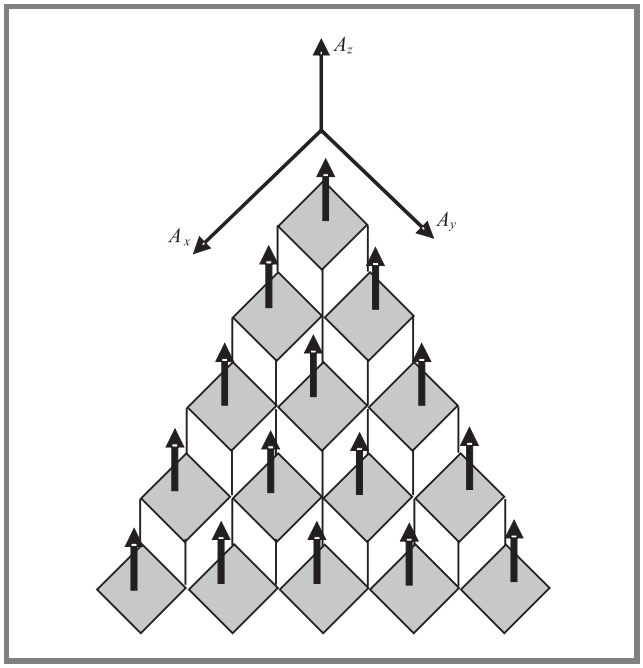

Fig. 3. Entire probability states in 3D plain for uniform BW ($n = 4$).

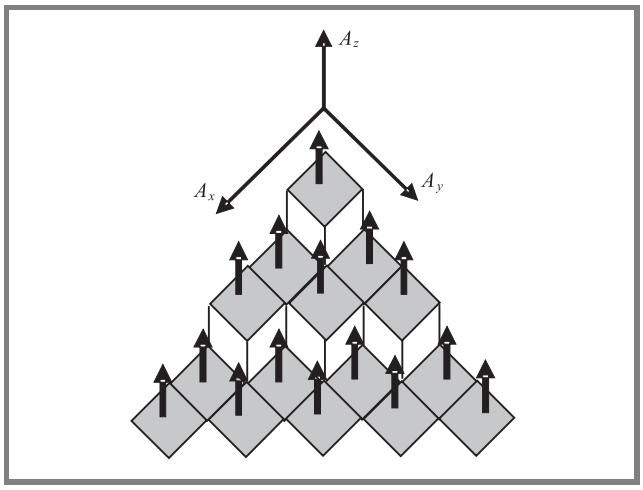

Fig. 4. Entire probability states in 3D plain for twice BW of A_z traffic ($n = 4$).

of rural area, pico net of Bluetooth, etc. For limited user case any probability state for uniform bandwidth would be like one shown below, based on Engset's traffic model of [18]:

$$P_{r,q,p} = \frac{\binom{N}{p} A_z^p \binom{M}{r} A_x^r \binom{O}{q} A_y^q}{\sum_{p=0}^{n} \binom{N}{p} A_z^p \sum_{r=0}^{n-p} \binom{M}{r} A_x^r \sum_{s=0}^{n-r-p} \binom{O}{s} A_y^s}, \qquad (14)$$

where M, O and N are the numbers of users for A_x, A_y and A_z traffic. Of course A_x, A_y and A_z are now considered as traffic intensity per user.

Probability of time congestion, i.e., percentage of total observation period, when the network remains blocked is derived based on papers [18, 19], like:

$$B_T = \frac{\sum_{p=0}^{n} \binom{N}{p} A_z^p \sum_{r=0}^{n-p} \binom{M}{r} A_x^r \binom{O}{n-r-p} A_y^{n-r-p}}{\sum_{p=0}^{n} \binom{N}{p} A_z^p \sum_{r=0}^{n-p} \binom{M}{r} A_x^r \sum_{s=0}^{n-r-p} \binom{O}{s} A_y^s}. \qquad (15)$$

Probability of call congestion, i.e., percentage of lost call is derived as

$$B_c = \frac{\sum_{p=0}^{n} (N-p) \binom{N}{p} A_z^p \sum_{r=0}^{n-p} (M-r) \binom{M}{r} A_x^r (O-n+r+p) \binom{O}{n-r-p} A_y^{n-r-p}}{\sum_{p=0}^{n} (N-p) \binom{N}{p} A_z^p \sum_{r=0}^{n-p} (M-r) \binom{M}{r} A_x^r \sum_{s=0}^{n-r-p} (O-s) \binom{O}{s} A_y^s}. \qquad (16)$$

For non-uniform traffic, Eqs. (15) and (16) can be modified according to the trend of Eqs. (12) and (13). Equations (12), (13), (15) and (16) reveal performance of a network in context of QoS.

4. Results and discussions

The number of complete occupied states by A_z traffic (shaded states) is 15 in both Figs. 3 and 4. In Fig. 3 the length of sample space is 35 but that of Fig. 4 is only 21; hence blocking probability of A_z traffic would be greater in the second case ($h = 2$) for the same number of channels. This phenomenon is depicted graphically in Figs. 5 to 7, where call blocking probability is varied against A_x, A_y for a fixed value of A_z as parameters. Values of A_x/A_y is varied from 0 to 5 erl with $h = 1, 2, 3$, $A_z = 2$ erl and $n = 14$. For limited user case call and time congestion are plotted in similar way varying A_x/A_y

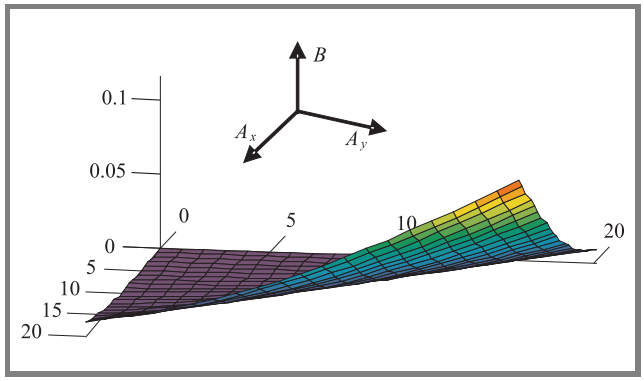

Fig. 5. Variation of blocking probability against A_x and A_y for a fixed value of A_z ($h = 1$, $A_z = 2$, $n = 14$).

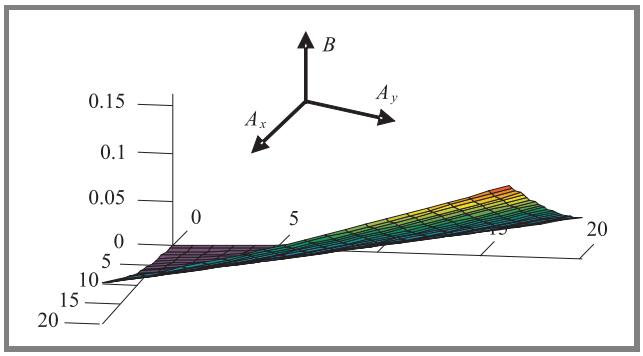

Fig. 6. Variation of blocking probability against A_x and A_y for a fixed value of A_z ($h = 2$, $A_z = 2$, $n = 14$).

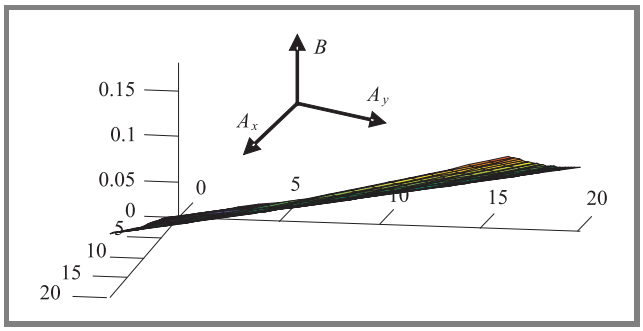

Fig. 7. Variation of blocking probability against A_x and A_y for a fixed value of A_z ($h = 3$, $A_z = 2$, $n = 14$).

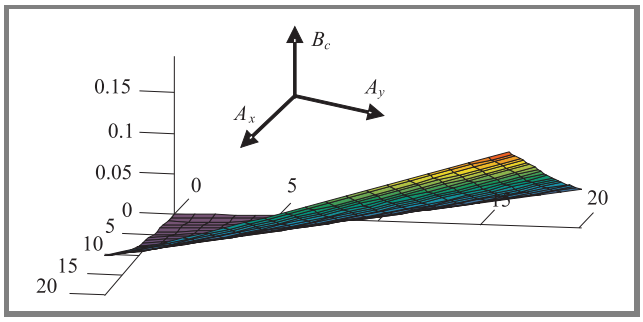

Fig. 8. Variation of call congestion against A_x and A_y for a fixed value of A_z ($h = 1$, $M = 100$, $N = 100$, $O = 100$, $n = 14$, $A_z = 0.05$ erl/user).

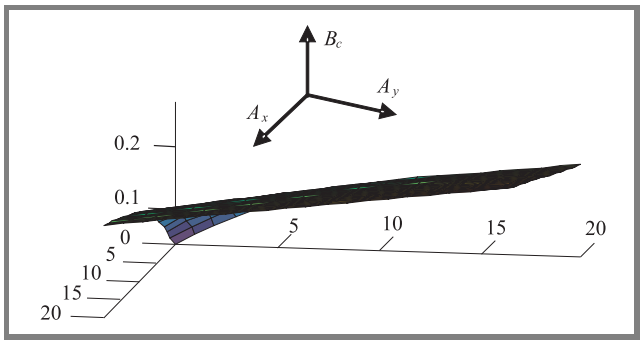

Fig. 9. Variation of call congestion against A_x and A_y for a fixed value of A_z ($h = 3$, $M = 100$, $N = 100$, $O = 100$, $n = 14$, $A_z = 0.05$ erl/user).

from 0 to 0.05 erl/user, with $h = 1$ and 3, $M = 100$, $N = 100$, $O = 100$, $n = 14$, $A_z = 0.05$ erl/user. Comparison of Figs. 8 and 9 or Figs. 10 and 11 reveals the same impact of h like unlimited users case.

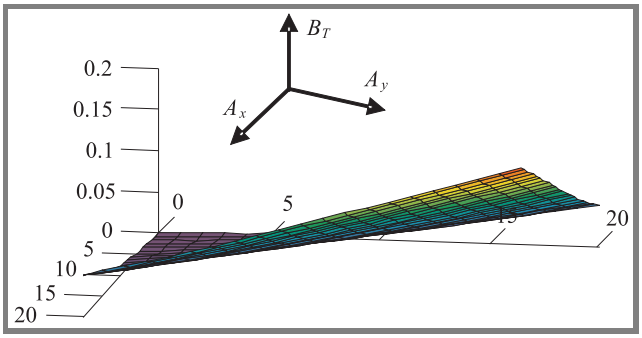

Fig. 10. Variation of time congestion against A_x and A_y for a fixed value of A_z ($h = 1$, $M = 100$, $N = 100$, $O = 100$, $n = 14$, $A_z = 0.05$ erl/user).

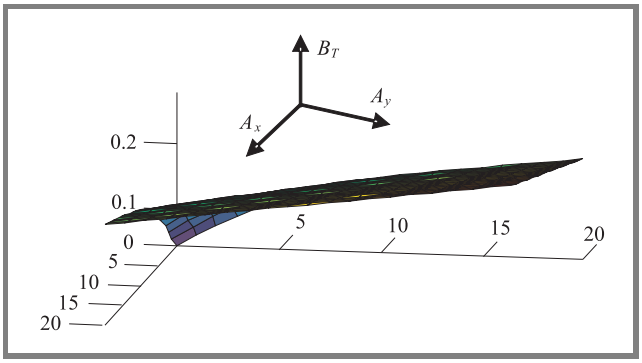

Fig. 11. Variation of time congestion against A_x and A_y for a fixed value of A_z ($h = 3$, $M = 100$, $N = 100$, $O = 100$, $n = 14$, $A_z = 0.05$ erl/user).

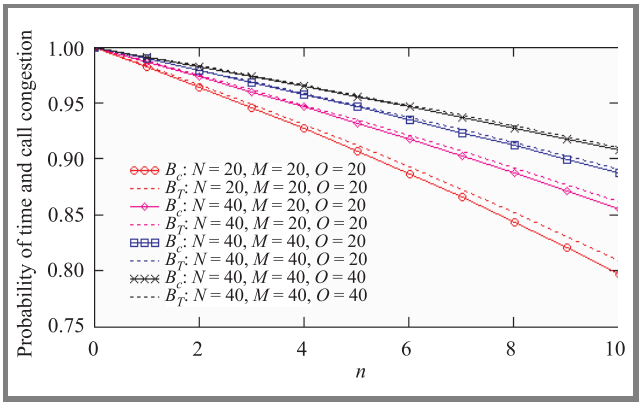

Fig. 12. Comparison of time and call congestion against number of channel (n).

Figure 12 makes a comparison of time and call congestion probability, where dotted lines are represent time and solid lines represent call congestion probability taking, $M = N = O = 20$ and $M = N = O = 40$. Here the num-

ber of users is lowered to visualize distinct separation between time and call congestion. All the graphs in this paper show very high blocking probabilities because of taking large offered traffic compared to number of channels. In real life environment, however, the number of channels would be selcted based on offered traffic and required QoS, using Eqs. (12), (13) and (15), (16). We have expected before that the entire analysis presented here can be done using three-dimensional Markovian chain, node equation and inverse matrix technique to solve the linear node equation like described in [20–23] but the analysis would be very complicated in comparison to our model.

5. Conclusion

This paper proposes a mathematical model of analyzing 3D limited and unlimited user's traffic of dissimilar bandwidth. All the graphs shown in this paper (Figs. 5–12) yield a logical result. Combination of limited and unlimited user's traffic even different call admission schemes like "duel threshold bandwidth reservation", "dynamic partition" could be done quite comfortably based on concept of the paper.

References

[1] J. Mar and J. P. Huang "Traffic performance analysis of integrated dual-band cellular radio network", *IEE Proc. Commum.*, vol. 147, no. 3, pp. 180–186, 2000.

[2] G. D. Morley and W. D. Grover, "Strategies to maximize carried traffic in dual-mode cellular systems", *IEEE Trans. Veh. Technol.*, vol. 49, no. 2, pp. 357–366, 2000.

[3] G. M. Galvan-Tejada and J. G. Gardiner, "Theoretical blocking probability of SDMA", *IEE Proc. Commum.*, vol. 146, no. 5, pp. 303–306, 2000.

[4] M. I. Islam and S. Hossain, "An analytical model of performance analysis of SDMA system of low dense traffic network", *WSEAS Trans. Commun.*, issue 2, vol. 3, Apr. 2004.

[5] S. M. Ross, *Introduction to Probability Models*. San Diego: Academic Press, 2001.

[6] B. Jabbari and W. F. Fuhrmann, "Traffic modeling and analysis of flexible hierarchical cellular networks with speed-sensitive handoff strategy", *IEEE J. Selec. Areas Commun.*, vol. 15. no. 8, pp. 1539–1548, 1997.

[7] M. I. Islam and S. Hossain, "An analytical model of traffic performance of mobile cellular network in underlay overlay cell system", in *6th Int. Conf. Comput. Inform. Technol. ICCIT*, Dhaka, Bangladesh, 2003, pp. 230–234.

[8] P. Fitzpatrick, Ch. S. Lee, and B. Warfield, "Teletraffic performance of mobile radio networks with hierarchical cells and overflow", *IEEE J. Selec. Areas Commun.*, vol. 15. no. 8, pp. 1549–1557, 1997.

[9] K. L. Yeung and S. Nanda, "Channel management in micro/macro cellular radio systems", *IEEE Trans. Veh. Technol.*, vol. 45, no. 4, pp. 14–23, 1996.

[10] M. Mahdavi, R. M. Edwards, and S. R. Cvetkovic, "Polycy enhancement of traffic in TDMA hybrid switched integrated integrated voice/data cellular mobile communications systems", *IEEE Commun. Lett.*, vol. 5, no. 6, pp. 242–244, 2004.

[11] B. Li, L. Li, B. Li, and X.-R. Cao, "Call admission control for voice/data integrated cellular networks: performance analysis and comparative study", *IEEE J. Selec. Area Commun.*, vol. 22, no. 4, pp. 706–718, 2004.

[12] S. Zachary, "On blocking in loss networks", *Adv. Appl. Prob.*, vol. 23, pp. 355–372, 1991.

[13] P. Lin and Y.-B. Lin, "Channel allocation for GPRS", *IEEE Trans. Veh. Technol.*, vol. 50, no. 2, pp. 375–387, 2001.

[14] D.-J. Lee and D.-H. Cho, "Performance analysis of channel borrowing handoff scheme based on user mobility in CDMA cellular systems", *IEEE Trans. Veh. Technol.*, vol. 49, no. 6, pp. 375–387, 2000.

[15] Q. Huang, S. Chan, K.-T. Ko, and M. Zukerman, "An enhanced handoff control scheme for multimedia traffic in cellular networks", *IEEE Commun. Lett.*, vol. 8, no. 3, pp. 195–197, 2004.

[16] P. Srisukpibul, "Traffic measurement on a cellular mobile network". Master thesis, Division of Telecommunications, AIT, Bangkok, Thailand, 1997.

[17] M. I. Islam and S. Hossain, "A proposed 2-D queuing model of PCT-I traffic", in *6th Int. Conf. Comput. Inform. Technol. ICCIT*, Dhaka, Bangladesh, 2003, pp. 114–118.

[18] _____, "Analysis of two dimensional limited source and mixed traffic model for a BTS of small mobile cellular network", in *6th Int. Conf. Comput. Inform. Technol. ICCIT*, Dhaka, Bangladesh, 2001, pp. 190–196.

[19] D. Bear, *Principle of Telecommunication Traffic Engineering.* London: Peter Peregrinus, June 1980.

[20] M. I. Islam and S. Hossain, "Impact of channel reservation on call blocking and forced termination in mobile cellular network", *Jahangirnagar Univ. J. Sci.*, vol. 26, pp. 123–132, 2004.

[21] _____, "Theoretical modeling of traffic of multilayer cell of 3G mobile cellular network", in *Proc. Conf. TENCON 2004*, Chiang Mai, Thailand, 2004.

[22] M. I. Islam and S. Hossain, "Analysis of SDMA PCT-II traffic for duplicated first case a theoretical study", in *Int. Conf. Wirel. Commun. Netw. Mob. Comput.*, Wuhan, China, 2005,pp. 423–426.

[23] M. I. Islam and S. Hossain, "A new call admission control in 3G mobile cellular network", in *8th Int. Conf. Adv. Commun. Technol. 2006*, Phoenix Park, Republic of Korea, 2006, http://www.icact.org

Imdadul Islam has completed his B.Sc. engineering in electrical and electronic engineering from Bangladesh University of Engineering and Technology, Dhaka, in 1993 and M.Sc. engineering from the same institute in 1998. Now he is perusing Ph.D. at the department of CSE, J.U., Dhaka, in the field of teletraffic engineering. He worked as an Assistant Engineer in Sheba Telecom (Pvt.) Ltd. (a joint venture company between Bangladesh and Malaysia, for mobile cellular and WLL), from Sept. 1994 to July 1996. He has very good field experiences in installation of radio base station and switching center for WLL. He is now working as an Associate Professor, at the Department of Computer Science and Engineering, Jahangirnagar University, Savar, Dhaka, Bangladesh. His research field is network traffic, OFDMA, WCDMA and array antenna

system. He has more than fifity papers in national and international journal and conference proceedings.
e-mail: imdad22000@yahoo.com
Department of Computer Science and Engineering
Jahangirnagar University
Savar, Dhaka, Bangladesh

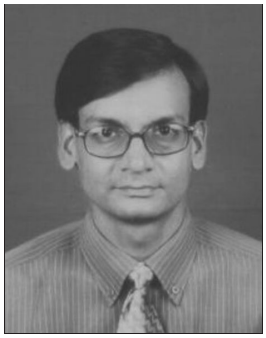

Jugal Krishna Das was born in Shariatpur in 1964. He received his M.Sc. and Ph.D. in computer engineering from Donetsk Technical University of Ukraine in 1989 and 1993, respectively. He joined as a lecturer at the Department of Electronics and Computer Science, Jahangirnagar University in 1994 and now serving as a Professor at the Department of Computer Science and Engineering of the same university. His research interests are in mobile ad hoc network and distributed system.
e-mail: drdas64@yahoo.com
Department of Computer Science and Engineering
Jahangirnagar University
Savar, Dhaka, Bangladesh

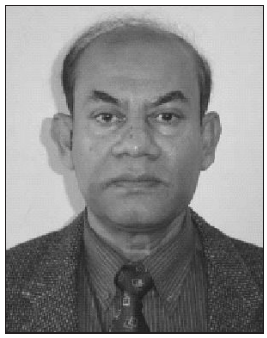

Siddique Hossain is the senior most Professor of Department of Electrical and Electronic Engineering, Bangladesh University of Engineering and Technology, Dhaka. He has more than 34 years of teaching, research and administrative experience both at home and abroad. Worked as the Head, EEE Department, Head, CSE Department, Dean, EEE Faculty and Director, BUET Computer Centre. He worked as a visiting faculty member of more than ten universities. He is a Senior Member of IEEE and was engaged as Chief of IEEE in Bangladesh in 1997–1998. He is interested in the field of computers and communication engineering, 3G mobile communication, wideband code division multiple access (WCDMA) for universal mobile telecommunication system (UMTS), etc. He has more than 40 publications in national, international journals and conference proceedings.
e-mail: sdq@eee.buet.ac.bd
Department of Electrical and Electronic Engineering
Bangladesh University of Engineering and Technology
Dhaka, Bangladesh